Env-antibody coevolution identifies B cell priming as the principal bottleneck to HIV-1 V2 apex broadly neutralizing antibody development

Rumi Habib[1,2]*, Ryan S. Roark[3,4]*, Hui Li[1]*, Andrew Jesse Connell[1]*, Michael P. Hogarty[1], Kshitij Wagh[5], Shuyi Wang[1], Lorie Marchitto[1], Ashwin N. Skelly[1], John W. Carey[1], Kirsten J. Sowers[1], Kasirajan Ayyanathan[1], Samantha J. Plante[1], Frederic Bibollet-Ruche[1], Younghoon Park[1], Colby J. Agostino[2], Ajay Singh[1], Christian L. Martella[1], Emily Lewis[1], Juliette M. Rando[1], Neha Chohan[1], Jinery Lora[1], Wenge Ding[1], Mary S. Campion[1], Chengyan Zhao[1], Weimin Liu[1], Yingying Li[1], Xuduo Li[1], Bo Liang[1], Rohan Roy Chowdhury[1], Khaled Amereh[1], Elizabeth Van Itallie[5], Zizhang Sheng[3], Amrit R. Ghosh[6], Katharine J. Bar[1], Wilton B. Williams[5], Kevin Wiehe[5], Kevin O. Saunders[5], Robert J. Edwards[5], Derek W. Cain[5], Mark Lewis[7], Facundo D. Batista[6], Dennis R. Burton[8], Raiees Andrabi[1], Daniel W. Kulp[2], Barton F. Haynes[5], Bette Korber[9], Lawrence Shapiro[3,4], Peter D. Kwong[3,4], Beatrice H. Hahn[1], George M. Shaw[1]†

[1]Departments of Medicine and Microbiology, Perelman School of Medicine, University of Pennsylvania, Philadelphia, PA 19104, USA.

[2]Vaccine and Immunotherapy Center, The Wistar Institute, Philadelphia, PA 19104, USA

[3]Aaron Diamond AIDS Research Center, Vagelos College of Physicians and Surgeons, Columbia University, New York, NY 10032, USA

[4]Department of Biochemistry and Molecular Biophysics, Columbia University, New York, NY 10027, USA

[5]Duke Human Vaccine Institute, Duke University School of Medicine, Durham, NC 27710, USA

[6]Departments of Microbiology and Immunology, Harvard Medical School and the Ragon Institute of MGH, MIT and Harvard, Cambridge, MA 02139, USA

[7]Bioqual, Inc., Rockville, MD 20850, USA

[8]Department of Immunology and Microbiology, The Scripps Research Institute, La Jolla, CA 92037, USA

[9]New Mexico Consortium, Los Alamos, NM 87545, USA

*These authors contributed equally to this work.

†Corresponding author. Email: shawg@pennmedicine.upenn.edu

Abstract

Broadly neutralizing antibodies (bNAbs) are rarely elicited during HIV-1 infection. To identify obstacles to bNAb development, we longitudinally studied 122 rhesus macaques infected by one of 16 different simian-human immunodeficiency viruses (SHIVs). We identified V2 apex as the most common bNAb target and a subset of Envs that preferentially elicited these antibodies. In 10 macaques, we delineated Env-antibody coevolution from B cell priming to bNAb development. Antibody phylogenies revealed permissive developmental pathways guided by evolving Envs that contained few mutations in or near the V2 apex C-strand, which were a sensitive indicator of apex-targeted responses. The absence of such mutations reflected a failure in bNAb priming. These results indicate that efficiency of B cell priming, and not complexities in Env-guided affinity maturation, is the primary obstacle to V2 apex bNAb elicitation in SHIV-infected macaques and identify specific HIV-1 Envs to advance as novel vaccine platforms.

Introduction

A primary objective of HIV-1 vaccine design is the reproducible elicitation of broadly neutralizing antibodies (bNAbs) to the HIV-1 envelope (Env) glycoprotein. This is a challenging goal as potent bNAbs are rarely elicited during HIV-1 infection and generally require years to develop (*1-7*). A major question in the fields of HIV-1 immunology and vaccinology is why some individuals develop bNAbs and others do not. While several correlates of bNAb induction have been identified, including viral load, CD4 T cell count, superinfection, viral diversity, length of infection, integrity of the Env glycan shield, and Env genealogy (*6-12*), the mechanistic bottlenecks underlying the stochasticity in bNAb development during HIV-1 infection remain unknown. Here we provide evidence that in the case of V2 apex bNAbs, priming of germline B cells capable of bNAb development is the rate-limiting step.

HIV-1 bNAbs in humans target one of six canonical epitope sites that are generally conserved across the global diversity of HIV-1 strains and subtypes. These include the V2 apex, V3-glycan high mannose patch, CD4-binding site (CD4bs), silent face (SF), gp120/gp41 interface region including the fusion peptide (FP), and the membrane-proximal external region (MPER). Surface exposed glycans targeted by Fab-dimerized Abs represent an additional set of bNAb epitopes (*13-16*). bNAbs targeting each of these sites exhibit properties that reflect the unique obstacles to antibody access inherent to the heavily glycosylated viral Env trimer as well as underlying features of the human B cell immunoglobulin gene repertoire (*13-15*). The most common bNAb epitope specificity in people living with HIV-1 is the V3-glycan high mannose patch, followed by V2 apex (*4, 6, 17*). In rhesus macaques (RMs) infected with chimeric simian-human

immunodeficiency viruses (SHIVs) expressing HIV-1 Env ectodomains (*18, 19*), the relative frequency of different bNAb epitope specificities is unknown.

A mechanistic understanding of bNAb elicitation in people living with HIV-1 and in SHIV-infected monkeys can guide vaccine design in multiple ways. First, the inference of authentic bNAb unmutated common ancestors (UCAs) by B cell lineage tracing can provide important antibody sequence information, structures and molecular reagents that are essential for immunogen design as they comprise representative examples of B cell receptors that effective priming immunogens must engage (*15, 20*). UCAs inferred with high confidence from deep longitudinal immunoglobulin sequence datasets closely represent authentic bNAb UCAs, whereas inferred germline (iGL) inferences that revert only gene-templated antibody regions are invariably confounded by uncertainty at non-templated V-D and D-J junctions. Second, tracing viral evolution can identify Env immunotypes that bind bNAb UCAs and lineage intermediates and then guide antibody affinity maturation along desired pathways (*21-26*). Third, the identification of shared features among different UCAs of a bNAb class and their evolved progeny can inform both immunogen design and clinical trial assessment by defining success criteria for priming and boosting B cell lineages that possess bNAb potential. Finally, studies of Env-antibody coevolution can point to obstacles or rate-limiting steps in bNAb development during the course of infection, and by inference, following vaccination (*20-24*). To address these issues, we analyzed V2 apex bNAb development in a prospective cohort of 122 SHIV-infected RMs to understand why such antibodies are so rarely elicited during infection, and how they might be more efficiently induced by vaccination.

SHIV-infected RMs are a favorable model to study bNAb development. The model allows for regular and controlled sampling of blood and lymphoid tissues as well as an analysis and comparison of Env-antibody coevolution that results from the same Env replicating in multiple outbred animals, some of which develop bNAbs and others that do not (*27*). We can thus look for shared patterns of B cell priming and antibody evolution leading to breadth, and at the same time, identify patterns of Env evolution driving that breadth. We previously showed that V2 apex bNAbs from SHIV-infected RMs exhibit striking structural homology to prototypic human V2 apex bNAbs (*27*, *28*). In the present report, we use next-generation sequencing (NGS) of B cells and single genome sequencing (SGS) of plasma virion RNA to define Env-antibody coevolution leading to bNAb development, beginning with Env engagement of the naïve germline B cell followed by sequential rounds of affinity maturation resulting in neutralization breadth and potency. We estimate when each bNAb lineage precursor B cell was triggered, infer with high confidence the precise heavy and light chain sequences of these UCAs, and identify intermediate stage antibodies on the path toward neutralization breadth. Simultaneously, we identify and characterize candidate Envs that were likely responsible for initial B cell priming along with Env escape variants that guided B cell lineage maturation to full breadth and potency. Finally, we augment these results with analysis of data from human cohort studies of HIV-1 infection to identify generalizable features, bottlenecks, and "rules" of V2 apex bNAb induction applicable to both humans and rhesus.

Results

V2 apex is the most common bNAb target in SHIV-infected RMs

Most HIV-1 infections are established by a single transmitted/founder (T/F) virus (*29*). Because of the extraordinary genetic diversity of HIV-1, nearly every infected individual acquires a unique strain. This, along with the fact that most infections do not lead to bNAb development, has made identifying any particular Env as a promising vaccine candidate challenging. Nonetheless, Trkola and colleagues found neutralization breadth to be associated with certain donor-recipient transmission pairs in a cohort of epidemiologically linked HIV-1 infections, leading to the concept of "bNAb imprinting Envs" (*7*). In support of this concept, we found that certain HIV-1 Envs that had elicited V2 apex, V3-glycan, and CD4bs bNAbs in several human study participants induced the same antibody specificities in RMs when expressed as SHIVs, with the molecular patterns of Env-antibody coevolution in these monkeys recapitulating those found in humans (*27, 30*). These findings led us to postulate that certain HIV-1 Envs may have a propensity for eliciting particular bNAb specificities, a hypothesis that we formally examine in the current study.

The SHIV model is uniquely poised to evaluate the concept of bNAb imprinting since it allows for the infection of multiple RMs with SHIVs expressing the same Env. In the present study, we infected 122 rhesus macaques with SHIVs bearing any one of 16 different primary HIV-1 Envs (*18, 19*) and followed them for up to six years (mean of 2 years, median of 1.7 years) for the development of neutralization breadth (**table S1**). The Envs selected for SHIV construction were chosen based on criteria that we hypothesized might increase the probability that they would elicit bNAbs. This included Envs that in humans induced bNAbs targeting V2 apex, V3 glycan, or CD4bs epitopes (*12, 27*); Envs that were previously shown to bind germline-reverted V2 apex bNAb precursors (*31-35*); Envs that corresponded to T/F sequences from acutely-infected human

participants (*29*); and Envs that represented all major HIV-1 group M subtypes (*18*, *19*). All 122 macaques became persistently infected with setpoint plasma virus loads of 10^2-10^7 vRNA/ml (geometric mean = 1.4×10^4 vRNA/ml) (**table S1**). Seven SHIV-infected RMs experienced rapid disease progression and died or were euthanized within months of infection because of opportunistic infections, AIDS-related malignancies or generalized wasting (**table S1**). Each of these monkeys had extremely high setpoint plasma viral loads (~10^7 vRNA/ml) with no detectable anti-SHIV antibody responses as assessed by ELISA, western immunoblot and neutralization assays. This rapid progressor phenotype is similar to that reported for a subset of SIVmac-infected monkeys (*36*, *37*). Rapid progressor animals were deemed unevaluable for bNAb induction but served as valuable controls for Env sequence evolution in the absence of adaptive immune selective pressure. Of the remaining RMs, 115/115 (100%) developed autologous, strain-specific NAbs with 50% plasma inhibitory dilution (ID_{50}) titers against the infecting SHIV strain ranging from 1:24-1:120,000 (geometric mean = 1:750), generally within 3-6 months of infection (**table S1**).

Twenty-five of 115 (22%) monkeys developed neutralization breadth defined as ID_{50} titers of ≥1:80 against two or more members of an 18-strain tier 1B/2 heterologous virus panel (**Fig. 1A, table S1**). Epitope specificity was confirmed by differential neutralization against heterologous viruses containing site-directed mutations in canonical bNAb epitopes, by EMPEM analysis of heterologous virus-antibody binding, or by isolation of bNAb mAbs followed by cryoEM structural analysis as previously described (**fig. S1**) (*27*, *28*, *30*). We chose a low threshold for neutralization breadth combined with a stringent threshold for bNAb epitope confirmation to ensure sensitive detection of canonical bNAb lineages. We did this because a similarly wide

range in neutralization breadth and potency would be expected in polyclonal responses to candidate vaccines where the summation of narrow but potent bNAb responses could contribute significantly to clinical protection (*38-41*). Based on these criteria, we identified 18 RMs with V2 apex bNAbs, four with V3 glycan high mannose patch bNAbs, two with silent face bNAbs and one each with FP and CD4bs bNAbs (**Fig. 1A**). One RM developed two distinct bNAb lineages targeting both V2 apex and FP. If we increased the stringency of the definition of neutralization breadth to require ID_{50} titers of ≥1:80 against four or more members of the 18-strain virus test panel, then eight, three, one, one and one monkeys had confirmed V2, V3, SF, FP and CD4bs bNAbs respectively, or 13/115 (11.3%) overall (**table S1**). This frequency of verified bNAbs in SHIV-infected RMs ranging from 11-22% is generally similar to that observed in people living with HIV (*4*, *6*).

Identification of HIV-1 Envs with a predilection for V2 apex bNAb induction

V2 apex bNAbs were elicited by SHIVs Q23.17 (5 of 10 RMs), CH505 (7 of 20 RMs), CAP256SU (2 of 9 RMs), T250 (2 of 6 RMs) and Ce1176 (2 of 5 RMs) but by none of the other 11 SHIVs (**Fig. 1A**). This uneven distribution of bNAb elicitation indicated a significant association between particular Envs and V2 apex bNAb elicitation (Fisher's Exact Test, p=0.011). Monte Carlo repeated random sampling also indicated that the restriction of V2 apex bNAb elicitation to five SHIVs was highly significant ($p < 0.0001$, see Supplemental Text). Interestingly, the particular Envs that elicited V2 apex bNAbs — Q23.17, CH505, T250, CAP256, ZM233 and WITO — were significantly enriched (16 of 54 versus 2 of 61; $p = 0.0002$, Fisher's Exact Test; see **Fig. 1B**) among a group Envs previously shown to bind or be neutralized by germline-reverted human V2 apex bNAbs (*31-35*).

Maximum neutralization breadth in the plasma was not significantly different among RMs with different bNAb specificities, with V2, V3, CD4bs, FP, and SF bNAbs achieving 50%, 61%, 63%, 32%, and 50% breadth, respectively, against the 18-virus panel ($p > 0.05$ by Kruskal-Wallis test followed by Dunn's multiple comparisons test) (**Fig. 1C**). Similarly, the potency of heterologous neutralization was not different for V2, V3, CD4bs, FP and SF bNAbs with median geometric mean reciprocal plasma ID_{50} titers of 102, 92, 152, 139 and 77, respectively ($p > 0.05$ by Kruskal-Wallis test followed by Dunn's multiple comparisons test) (**Fig. 1D**). There was also no overall difference in the time to the first detection of heterologous neutralization among the different bNAb specificities ($p > 0.05$ by Kruskal-Wallis test followed by Dunn's multiple comparisons test) (**Fig. 1E**), although V2 apex bNAbs developed significantly faster in RMs infected by SHIVs Q23.17 and CH505 compared to all other monkeys (42 weeks and 44 weeks vs 99 weeks, $p = 0.02$ and $p = 0.01$ by Kruskal-Wallis test followed by Dunn's multiple comparisons test) (**Fig. 1F**). Altogether, these findings indicated that certain Envs exhibited an enhanced predilection for inducing V2 apex bNAbs, with Envs Q23.17 and CH505 standing out for their ability to quickly and reproducibly elicit these antibodies.

B cell lineage tracing identified 12 new V2 apex bNAb UCAs with shared features

Essential features of mature human and rhesus V2 apex bNAbs include their long, negatively charged CDRH3s and unique CDRH3 topologies, which enable the antibodies to penetrate Env's dense apical glycan canopy and engage positively charged C-strand residues (*27, 28, 31, 42-45*). Key questions in the field of germline-targeted immunogen design are how closely do V2 apex

bNAb UCAs resemble their affinity-matured bNAb progeny, what distinguishes authentic bNAb UCAs from similarly appearing antibodies that lack the potential to affinity mature to acquire breadth and potency, and what design features must immunogens possess to selectively prime authentic bNAb germline precursors? For humans, only two authentic V2 apex bNAb UCAs have been inferred (*23, 46*), and for rhesus, none have been identified. Thus, to elucidate key features common to a much larger number of such precursors, we lineage-traced the maturation pathways of 12 rhesus V2 apex bNAbs. Previously, Roark and colleagues (*27, 28*) isolated mature bNAb mAbs from these monkeys and determined their immunogenetic and structural features (**Table S2)**. Here we used next generation sequencing (NGS) of IgG+ memory B cells sorted from multiple timepoints beginning soon after SHIV infection through the time of bNAb isolation to sequence immunoglobulin V(D)J gene mRNA and identify bNAb lineage members (**Fig. 2A**). Lineage members were identified based on similarity to mature bNAb heavy and light chain sequences (*28*), and their UCAs and lineage intermediates were determined by phylogenetic inference. This was done using a combination of SONAR (*47*) and IgDiscover (*48, 49*) analyses, which allowed for the assignment of V(D)J alleles not present in published rhesus immunoglobulin gene databases. UCA heavy and light chains were inferred independently and subsequently paired to generate a complete antibody sequence. Importantly, this B cell lineage tracing strategy enabled us to infer germline UCA sequences, including their non-templated residues, with high confidence (**fig. S2A**). Altogether, from ten RMs, we determined 5,461,808 unique IgG+ memory BCR sequences, 651,218 unique IgM+/IgD+ naïve BCR sequences, and inferred 12 high-confidence bNAb UCAs (**Fig. 2A and fig S2A**). In addition, we reanalyzed previously reported longitudinal B cell NGS datasets for human participants PC64 (*46*) and CAP256 (*23*) to re-infer their UCAs. While our inference of the PCT64 UCA was identical to

that previously published, our inference of the CAP256-VRC26 UCA differed from the previously published UCA by two amino acids in the CDRH3 D-gene templated region (**fig. S2B**).

Because of frequent monthly sampling following SHIV infection, BCR sequences with very low levels of somatic hypermutation compared with the inferred bNAb UCA could be identified in every monkey (**fig. S3**). An example of the UCA inference for the V033-a lineage is shown in **Figure 2B**. The V033-a lineage was of particular interest because it gave rise to one of the broadest and most potent of all rhesus V2 apex bNAbs, and because it affinity-matured rapidly and with low somatic hypermutation (3.5-7.8% in the heavy chain) (**Figs. 2C** and **3A**) (*28*). In RM V033, a week 4 post-infection memory B cell NGS sequence was identified that exhibited 100% nucleotide sequence identity with the germline monkey-specific V, D, and J genes. Two NGS sequences from memory B cells 8 weeks post-infection bore two and three nucleotide changes, respectively, compared to the week 4 sequence. One of these mutations in the D-J non-templated region was nonsynonymous and corresponded to a positively selected codon where mutations continued to accumulate through to the mature bNAb sequences. This mutational pattern, together with 199 additional lineage sequences spanning weeks 4-20 (**fig. S4**), lent high confidence to the UCA heavy chain inference depicted in **Figure 2B**. As bNAb lineage members were first detectable at week 4 but were not detectable in B cells sampled prior to SHIV infection, the V033 bNAb lineage must have been primed soon after SHIV infection but before week 4. We could also identify heavy chain sequences from the 5695-b and T646-a lineages that exhibited 100% identity to germline genes in peripheral blood memory B cells from SHIV-CH505 infected RMs 5695 and T646 at weeks 12 and 16 post-infection, respectively (**figs. S2**

and S3). For each of the remaining nine V2 apex bNAb lineages, we identified BCR sequences that had very few heavy and light chain mutations compared with monkey-specific germline alleles (**fig. S3**). In each case, these sequences coalesced phylogenetically to unambiguous heavy and light chain sequences. Thus, for all 12 bNAb lineages we could infer high confidence UCAs.

Rhesus V2 apex bNAb UCA CDRH3s exclusively utilized the IGHD3-15*01 gene and ranged from 23-27 amino acids in length (**Fig 2C**). This CDRH3 length was slightly shorter than that of five human bNAbs ranging from 25-37, a difference that was not statistically significant (**Fig 2C**). Two of the 12 rhesus V2 apex bNAb lineages, 6561-a and V031-a, contained small CDRH3 insertions of one and two amino acids, respectively (**Fig. 2C**). Therefore, all rhesus lineages acquired their necessarily long CDRH3s during VDJ recombination rather than from insertions during affinity maturation. From these results and others (**Fig. 2C** and B.H.H. and R.A., unpublished), we inferred a minimum CDRH3 length for canonical V2 apex bNAbs to be 22-23 amino acids. This is consistent with findings by Kwong and colleagues who showed that the human mAb 2909, which targets the V2 apex C-strand but can only neutralize N160-glycan deficient viruses, is limited in its neutralization potential because its 21 residue CDRH3 is too short to penetrate the apical glycan shield of most heterologous Envs (*50*). Rhesus bNAb lineages exhibited relatively low levels of SHM, ranging from 3.5% (V033-a.07 and 41328-a.03) to 17.9% (6561-a.15), consistent with shorter maturation pathways compared to bNAbs targeting other epitopes (**Fig. 2C**).

To evaluate how the CDRH3s of rhesus V2 apex bNAbs compared with CDRH3 features in the naïve rhesus and human B cell repertoires, we analyzed ~650,000 unique IgM+ naïve B cell receptor sequences from 10 RMs that made V2 apex bNAbs (**Fig. 2A**). Naïve B cells were analyzed to minimize bias from clonal expansions and somatic hypermutation following antigen exposure. Rhesus naïve B cell CDRH3s were normally distributed with a mean CDRH3 length of 13.6, a result that is slightly lower than the mean length of 14.8 for human CDRH3s (*51*) (**Fig. 2D**). In our analysis, rhesus B cells with CDRH3 lengths ≥ 23 comprised less than 1% of B cells, while the modal rhesus bNAb UCA CDRH3 length of 25 constituted only 0.16% of the naïve repertoire. Rhesus naïve B cell CDRH3 charge was similarly normally distributed around a net charge of 0 (**Fig. 2E**). Rhesus V2 apex bNAb UCA CDRH3s, however, all had negative charges ranging from -2 (V031-a, found in 9% of B cells) to -6 (RHA1 and 5695-b, found in 0.04% of B cells) (**Fig 2E**). Less than 1% of naïve rhesus B cell CDRH3s exhibited the modal net charge of -4. Thus, the low frequency of naïve B cells with bNAb features contributes to the infrequency of V2 apex bNAb elicitation in both monkeys and humans. Together, the results indicate that V2 apex bNAb CDRH3s acquire their key features of length and charge during VDJ recombination rather than during affinity maturation, consistent with the interpretation that priming of B cells with these features is a rate-limiting step for V2 apex bNAb elicitation.

Env-Antibody coevolution in RM V033 leading to neutralization breadth

We next sought to examine steps in bNAb development that followed UCA activation and ultimately led to breadth and potency. We did this first by investigating the V2 apex bNAb lineage V033-a, which exhibited one of the earliest, broadest, and most potent bNAb activities in the cohort. We then extended this analysis to all 12 bNAb lineages to look for generalizable

features. RM V033 was infected with SHIV-Q23.17 and rapidly acquired neutralization breadth detectable in plasma as early as 12 weeks post-infection and approximately 10 weeks (range 8-12 weeks) post-priming of the bNAb lineage UCA (**Fig. 3A**). Neutralization reached 68% breadth on our 18-virus panel with a geometric mean heterologous plasma ID_{50} titer of 1:250 by 24 weeks post-infection (**Fig. 3A**) (*28*). One of the bNAb mAbs isolated from the week 24 time point of V033 exhibited 37% neutralization breadth on an extended 208 virus panel with a geometric mean IC_{50} titer of 0.6 µg/ml (*28*). This rapid acquisition of breadth and potency within a timeframe desirable for a vaccine makes the developmental pathway of the V033-a bNAb lineage an instructive example. We used longitudinal B cell sequencing to infer the maturation pathway of this bNAb lineage, and SGS to characterize coevolving Env escape mutations that selected for affinity maturation and breadth development.

The V033-a.UCA neutralized the infecting SHIV-Q23.17 at an IC_{50} of 106 µg/ml (**Fig. 3A**). Sensitivity of a primary HIV-1 Env to UCA binding and neutralization is unusual, and this finding combined with the very early priming of the V033-a.UCA <4 weeks post-SHIV infection, suggested that the SHIV-Q23.17 Env and not an evolved derivative served as the priming "immunogen." Analysis of plasma viral RNA sequences from week 4 showed the Env quasispecies to be extremely homogenous (99.85% identical, **Fig. 3B** and **fig. S5A**), supporting the conclusion that the WT Q23.17 Env primed the V033-a lineage. A phylogenetic tree of V033-a heavy chain sequences constructed using IgPhyML (*52, 53*) (**Fig. 4A**) revealed an early bifurcation in bNAb evolution followed by convergent evolution leading to as few as 12 key amino acid substitutions in the heavy chain that were critical to neutralization breadth and potency (**Fig 4B,** V033-a.07). V033-a lineage intermediates, designated V033-a.I1 – V033-a.I6,

shared increasing numbers of these substitutions and demonstrated progressive increases in neutralization potency against the infecting SHIV-Q23.17 strain, beginning with an IC_{50} of 106 ug/ml for the UCA and ending at 0.002 ug/ml for the mature V033-a.01 bNAb (**Fig. 3A)**. This 50,000-fold increase in neutralization potency against SHIV-Q23.17 was accompanied by corresponding increases in apparent binding affinity for the Q23.17 Env trimer (unmeasurable for V033-a UCA, 195 nM for V033-a.I1, and 4 nM for V033-a.01) (**fig. S6**). These increases in apparent binding affinity and neutralization potency for the autologous Q23.17 Env were accompanied by corresponding increases in breadth and potency against heterologous viruses, recapitulating the pattern of breadth acquisition detected in the plasma (**Fig. 3A**). For example, just two heterologous viruses in the screening panel (BG505 and BJOX0020000) were neutralized by V033-a.I2 and these two viruses were also neutralized by plasma at week 12 post-infection (**Fig. 3A**). V033-a.I4 neutralized seven heterologous viruses in the panel, and six of these were neutralized by week 16 plasma. Ten viruses in the panel were neutralized by the mature bNAb V033-a.01, and all 10 were neutralized by week 24 plasma. Thus, the full developmental pathway of neutralization breadth in RM V033 plasma was recapitulated by the heavy chain sequences depicted in **Figure S6** and represented in V033-a.I1- V033-a.I6 and the mature bNAb mAb V033-a.01. Neutralization analysis of a 119-virus panel (*28*) indicated a strong association between resistance to V033-a.01 and presence of the N130 glycan ($p < 0.0001$, Fisher's exact test, **fig. S7**). Thus, N130 restriction limited the overall neutralization breadth of the V033-a.01 bNAb.

To elucidate the earliest events in V033 Env-antibody coevolution following priming and how they impacted antibody affinity maturation, we created individual site-directed mutations in the

V033 bNAb UCA heavy and light chains corresponding to positively selected mutations observed in memory B cell immunoglobulin sequences and in mature bNAb mAbs (**Fig. 3E and fig. S4**). Each of 19 mutations individually conferred to the bNAb UCA between 1.5- and 20-fold increases in neutralization potency against the autologous SHIV-Q23.17, with an average increase of 7-fold (**Fig. 3E**). The mutation conferring the largest increase in neutralization potency was an F100jL (Kabat numbering) mutation in the CDRH3 D-J non-templated region. This mutation was under strong positive selection as indicated by its high prevalence just 4 weeks after the expanding lineage first became detectable (**fig. S4)**. A structural explanation for this early, strongly selected mutation was provided by a cryoEM structure of the V033-a.I1 antibody in complex with a Q23.17 SOSIP trimer, where modeling showed a progressive accommodation of Env K168 by mutations at F100j from Phe to Leu to Ser (**fig. S8**). The fact that each of the 19 V033 bNAb UCA mutations appeared independently or in unique combinations and showed enhanced neutralization potency against the Q23.17 Env suggests that there was minimal epistasis in the selection of these mutations and in further affinity maturation of the bNAb lineage. This lack of epistasis and the absence of indels in the bNAb lineage contributed to the permissive maturation pathways that we observed leading rapidly to neutralization breadth. These findings, together with the stepwise >10,000-fold increase in neutralization potency between the V033-a.UCA and V033-a.01 mature bNAb for the infecting Q23.17 strain (**Fig. 3D**), predicted that the Q23.17 Env as a nonreplicating immunogen might prime and boost the initial steps in B cell affinity maturation of this lineage sufficiently to result in neutralization of homologous and heterologous viruses — a prediction borne out in a V033 UCA KI mouse model described in a companion manuscript (*54*).

To examine how SHIV-Q23.17 Env evolution selected for bNAb lineage affinity maturation in RM V033, we performed SGS of gp160 Env sequences spanning 24 weeks of infection (**Fig. 3B and fig. S5A).** V033 bNAbs developed maximally in plasma within the first 24 weeks, during which time strongly selected mutations in the replicating plasma virus quasispecies were limited to just a few positions in Env. Some of these mutations (R308H, K460E, D461G/N, N463H, V464E, T533A) corresponded to autologous, strain-specific NAb or cytotoxic T cell escape or fitness reversions (**fig. S5**, and see Supplementary Text), and likely did not contribute to bNAb development. Mutations in the V2 apex C-strand at residues 170 and 171 and in the V2 carboxy-terminus (V2′) at residue 187 (**Fig. 3B**) contributed directly to bNAb affinity maturation by providing a stepwise affinity gradient for evolving bNAb lineage B cells (**Fig. 3C**). While the V033-a.UCA was able to neutralize the wildtype Q23.17 Env, it was unable to neutralize any of the C-strand or V2′ escape variants. Intermediates I1-I6 developed increasing neutralization potency for N187S and N187S + K171R variants, as well as to the N160 glycan KO variant N160K (**Fig. 3D**). Once full plasma breadth developed by week 24 post-infection, the predominant Env variant in the virus quasispecies (Q170R+K171R+N187S) showed complete escape from neutralization by the coevolving bNAbs, presumably limiting their further affinity maturation (**Fig. 3B-D**). These findings suggest a model wherein within-host Env escape mutations selected for more mature V033-a bNAb lineage members that can tolerate those residues in heterologous viruses, a capacity that conferred increasing neutralization breadth as the V033 bNAb lineage matures (see Supplemental Text). In sum, V033-a bNAb ontogeny followed a rapid and simple evolutionary pathway driven solely by the priming Q23.17 Env and three mutations in or near the V2 apex C-strand. Altogether, these findings support the conclusion that priming was the rate limiting step in V033-a bNAb elicitation.

Common features of Env-antibody coevolution leading to V2 apex bNAbs

In RM V033, bNAb maturation followed multiple independent evolutionary trajectories leading to the acquisition of breadth. The isolated bNAb mAbs, despite their divergent pathways of development, acquired a limited set of 12-21 convergent amino acid substitutions that were positively selected by affinity for the evolving Env quasispecies (**fig. S4 and Fig. 4B**). To explore the generalizability of these findings to other rhesus V2 apex bNAbs, we constructed phylogenetic trees of eight of the remaining bNAb lineages. We hypothesized that population bottlenecks in phylogenetic trees might reflect potential barriers to affinity maturation and acquisition of neutralization breadth. Conversely, multiple independent maturation trajectories leading to bNAbs without such bottlenecks would suggest less restrictive pathways, similar to that in RM V033 (*55*, *56*).

In most monkeys, we found multiple permissive mutational pathways for primed naïve B cells leading to neutralization breadth (**Fig. 4A**). In RMs V033, 6561, 40591, 41328, and 44715. as in the human subject PC64, we found mature bNAb mAbs distributed throughout the respective heavy chain sequence trees. In each case, the most recent common ancestor (MRCA) to the broadly neutralizing mAbs in each tree was located close to the UCA, indicating divergence of the lineages into two or more distinct sublineages shortly after priming but each leading successfully to neutralization breadth (**Fig. 4A**). Antibodies from the distinct clades acquired positionally convergent but often chemically distinct mutations that resulted in neutralization breadth **(Fig. 4B)**. This finding suggested multiple permissive diverging pathways to breadth,

indicating that the majority of V2 apex bNAb UCAs were able to evolve diverse solutions to epitope recognition (**Fig. 4A)**.

Trees with late MRCAs were indicative of phylogenetic bottlenecks that immediately preceded the development of bNAbs (*21, 57*). These were observed for two lineages: V031-a and 42056-a (**fig. S9A**). The bottleneck in the V031-a lineage coincided with the acquisition of a two-amino acid CDRH3 insertion immediately preceding the acquisition of breadth in the plasma, suggesting that this insertion was a key event in the maturation of this lineage (**fig. S9A**). We deleted this insertion in V031-a bNAb mAbs and found that neutralization breadth was eliminated (**fig. S10**). A very similar result was reported for a CD4bs targeted bNAb lineage in another SHIV-infected monkey (*30*). The other V2 apex bNAb lineage that acquired a CDRH3 insertion, 6561-a, did so twice independently, suggesting strong positive selection (**Fig. 4A**). Members of the 42056-a lineage that exhibited heterologous Env binding and neutralization breadth also clustered tightly in a small section of the tree distinguished by acquisition of a set of three disfavored mutations (**fig. S11**) (*58*). For the 5695-b and RHA1 lineages, an intermediate phenotype was observed, with divergence into multiple clades occurring closer to the base of the tree but not as early as for the lineages described above (**fig. S9B**). From this analysis we conclude that potential bottlenecks to bNAb development did occur in a subset of lineages but B cell evolution readily overcame these obstacles. Thus, for most V2 apex bNAb lineages, once a naïve germline B cell with potential for breadth was primed, evolutionary bottlenecks did not substantially hinder their development.

To gain insight into what Envs triggered V2 apex bNAb UCAs, we examined the reactivity of rhesus bNAb UCAs to autologous and heterologous Envs. As observed with other HIV-1 bNAb UCAs (*25*), the majority of rhesus UCAs failed to neutralize any T/F Env tested. The V033-a and V031-a lineage UCAs were exceptions, showing neutralization of the autologous Env Q23.17 at an IC_{50} of 106µg/ml and 183µg/ml respectively (**fig. S12A**). In these RMs, T/F V1V2 sequences comprised the majority of Env sequences detected in the plasma preceding the emergence of the bNAb lineages (**Fig. 3B** and **fig. S13**). In contrast, in most other animals, the emergence of bNAbs occurred at timepoints when Envs bearing T/F V1V2 sequences were undetectable in plasma (**fig. S13**). These findings suggest that in these RMs, the priming event for bNAb lineages necessarily involved exposure to evolved viral variants rather than the original T/F Env. Examples of this included N130 glycan deletion in the CH505 plasma virus quasispecies of RMs T279, T646, 5695, 5593, 6070, and T277 (**fig. S14**) and additional V1V2 changes in other monkeys (**fig. S13**), all occurring prior to V2 apex bNAb induction. Still other examples included the 6070-a and T646-a UCAs that were unable to neutralize any primary Env but were able to neutralize multiple N160-glycan knockout viruses (**fig. S12B**). Interestingly, N160-glycan deficient Envs were detectable in the plasma of 6070 and T646 monkeys prior to the triggering of the respective bNAb lineages (**figs. S15 and S16**). An emerging theme in this study and others (*21, 30, 46, 59-63*) is that evolution of viral variants, including those with glycan deletions near canonical bNAb epitope supersites, is associated with enhanced bNAb lineage priming.

We next asked what Env mutations were responsible for positive selection of V2 apex bNAb lineage breadth following priming. Longitudinal SGS of the circulating plasma viral quasispecies in the 18 monkeys with V2 apex bNAbs demonstrated strong positive selection at residues 166-

171 (**Fig. 5 and fig. S17**). Env residues 166-171, which comprise the N-terminus of the C-strand and two residues immediately preceding it (**Fig 5A**), constitute critical peptide contacts for all canonical V2 apex bNAbs thus far described (*27, 28, 31, 42-45, 64-66*). For brevity, we include residues 166 and 167 together with 168-171 when referring to the C-strand. In 16/18 RMs with V2 apex bNAbs, selection for complete (or near complete) escape occurred at the C-strand (**Fig. 5B and fig. S17**). In the other two monkeys, RMs 42056 and 6729, C-strand replacement reached 70-80%. These findings add substantially to data from two human subjects with V2 apex bNAbs (PC64 and CAP256) (**fig. S18**) (*23, 46, 61*). Interestingly, unique patterns of C-strand selection corresponded to the structural footprint of both rhesus and human bNAbs: Axe-like bNAb lineages V033 and 41328 selected for mutations primarily at residues 169-171 (**fig. S19, table S2**). Needle-like lineages 6070-a, T646-a, RHA1, 5695-b, 42056-a, 44715-a, and PCT64 selected for mutations primarily at residues 166-169, and bNAbs with combined modes of recognition — V031-a, 40591-a, and CAP256-VRC26 — showed selection throughout the 166-171 span (*28*). Thus, Env escape patterns, which selected for bNAb lineage affinity maturation, reflected structural and chemical recognition patterns shared by rhesus and human V2 apex bNAb paratopes (**fig. S19, table S2**).

To confirm phenotypically that the C-strand selection observed was responsible for virus escape from V2 apex bNAbs, we constructed site-directed mutants in homologous and heterologous Envs bearing these SGS-identified mutations and assessed their sensitivity to neutralization. All mutations tested resulted in diminished neutralization potency by mature V2 apex bNAb lineage members (**Figs. 3C, 5D**) (*27*). These same mutations in heterologous viruses also reduced or abrogated neutralization by corresponding plasma samples (**fig. S1B**) (*27, 28*). In two RMs,

escape also mapped to residues in the V2′ hypervariable loop. For example, in RM V033, partial escape from bNAb neutralization was conferred by mutations at 170/171 or 187, while complete escape resulted from a combination of all three mutations (**Fig. 3C**). In RM 6561, in addition to C-strand selection (**Fig 5**), escape mapped to residue 190 (**fig. S20A**), where a K190E substitution disrupted a salt bridge between the bNAb CDRH3 and the Env V2′ loop (**fig. S20B**). These results thus indicate that few mutations at a limited six residue motif in or near the C-strand, and less commonly in the carboxyterminus of V2, are sufficient to allow for virus escape from autologous neutralization and select for bNAb lineage affinity maturation and the acquisition of neutralization breadth and potency. An important implication of these findings is that a similarly limited set of minimally divergent prime and boost immunogens may be sufficient to guide V2 apex bNAb maturation following vaccination.

C-strand selection is a sensitive and specific indicator of V2 apex bNAb elicitation

To further elucidate the underlying immunobiology of V2 apex bNAb elicitation, we explored the timing of first detection of bNAb lineage members by B cell NGS, first detection of neutralization breadth in plasma, and first detection of epitope-specific Env escape in the evolving plasma viral quasispecies. The question we hoped to answer was this: In monkeys that fail to develop neutralization breadth, is this due to a failure to prime relevant naïve germline B cell precursors or a failure to affinity-mature such cells once primed? In other words, does SHIV infection frequently prime V2 apex bNAb B cell precursors that then go “off-track,” or instead, are precursors simply not primed? To address this question, we asked if C-strand selection might be a sensitive and specific indicator of C-strand targeted NAbs. Because plasma virus has a

lifespan of about an hour, and the cells producing >90% of it, a lifespan of a day (*67-70*), the quasispecies composition of plasma virus serves as an extremely sensitive and dynamic indicator of antiviral selection pressures, including antiretroviral drugs, cytotoxic T cells, or NAbs (*71-76*). We showed previously that epitope-specific mutations in the evolving virus quasispecies can precede the detection of NAbs in the plasma (*30, 64, 72, 73*). Having established C-strand selection at residues 166-171 to be a signature of V2 apex bNAb activity (**Fig. 5**), we calculated Hamming distances of residues 166-171 compared with the infecting SHIV strain in sequential Env gp140 sequences in plasma samples from 101 RMs. In monkeys that developed bNAbs, we plotted longitudinal C-strand Hamming distances against the time of first detection of bNAbs in plasma by the TZM-bl neutralization assay and first detection of bNAb lineage members in circulating blood memory B cells by NGS (**Fig. 6A**). In all ten RMs and two human participants (CAP256 and PC64) with V2 apex bNAbs, a consistent temporal pattern was observed with detection of bNAb lineage B cells by NGS occurring first, C-strand selection in plasma viral RNA detected second, followed by detection of bNAb activity in plasma third (**Fig. 6A**). In only one RM (RM6561) did bNAb activity precede C-strand selection, and in that monkey, we found the early neutralization breadth to be due to a coincident FP-targeted bNAb (**Fig. 1A**, Ce1176). Altogether, the findings confirmed that C-strand selection is an extremely sensitive indicator of V2 apex C-strand targeted bNAbs, and underscored the consistency and rapidity with which C-strand selection occurs following V2 apex bNAb lineage priming.

Heterologous plasma neutralization developed quickly (mean of 17 weeks) after bNAb lineage B cells were first detected by NGS (**Fig. 6A)**. This timing was similar to previous data for the PCT64 and VRC26 lineages that took 12 and 14 weeks, respectively, to acquire heterologous

plasma neutralization (**Fig. 6A)** (*23, 46*). The maximum delay between a lineage being triggered and breadth becoming detectable in plasma was 28 weeks for the V031-a lineage. In this case, breadth appeared just four weeks after the acquisition of a two amino acid CDRH3 insertion. We could thus explain the long delay in breadth acquisition by the requirement for the insertion, which occurred late in lineage maturation (**figs. S9A and S10**). These results suggest that following the priming of V2 apex bNAb UCAs, antibody lineages rapidly acquire somatic hypermutation, which increases binding affinity to the priming virus Env. This exerts strong selection pressure on the autologous viral quasispecies that leads quickly to mutations in the C-strand, which in turn lead to further antibody affinity maturation and tolerance to those mutations resulting in neutralization breadth. The rapid acquisition of neutralization breadth following priming in all ten RMs again highlights the relative simplicity of V2 apex bNAb maturation pathways leading to breadth and potency.

Having established Env escape at residues 166-171 as a highly sensitive indicator or V2 apex bNAb development (sensitivity = 100%), we next sought to determine its specificity by asking what the frequency of C-strand mutations was in RMs that did not develop V2 apex directed plasma breadth. We reasoned that if the bottleneck to V2 apex bNAb elicitation is at the priming stage, we would fail to see C-strand selection in the replicating virus quasispecies in monkeys without bNAbs. On the other hand, if priming of bNAb precursors occurred frequently but these cells eventually went “off-track” prior to the development of neutralization breadth, we would expect to see evidence of C-strand selection from autologous Nab activity. From over 10,000 longitudinal Env gp140 sequences from 83 RMs lacking V2 apex bNAbs, we found few C-strand mutations. SHIVs 191859, 40100, CH694, WITO, CH1012, and BG505, all of which failed to

elicit V2 apex bNAbs, showed virtually no mutations at the C-strand (**Fig. 6B and fig. S21**). In monkeys infected by SHIVs that in some animals elicited V2 apex bNAbs — Q23.17, CAP256SU, T250, Ce1176, and CH505 — C-strand selection was mostly absent in the subset of RMs that did not develop V2 apex bNAbs (**Figs. 6B and fig. S21**), with five exceptions: RMs 45951 (SHIV-Q23.17), 6730 (SHIV-Q23.17), 6734 (SHIV-Q23.17), 6697 (SHIV-CH505), and 6701 (SHIV-CH505). These monkeys developed NAb responses with very limited breadth that mapped phenotypically to the C-strand (**table S1** and **fig. S22**). Other exceptions included macaques infected by SHIV-CH848 and SHIV-B41, which did not develop V2 apex targeted neutralization but nonetheless showed selection in the C-strand due to reversion to global consensus and/or gain of fitness (**figs. S23 and S24**). Overall, 23/23 RMs with phenotypically demonstrable C-strand targeted neutralizing antibody responses showed C-strand selection in the viral quasispecies as opposed to 8/72 RMs without such NAbs, indicating a sensitivity of (100%) and a specificity of (90%) (see Supplemental Text).

Finally, to determine if other mutations in Env, besides C-strand selection, might distinguish monkeys with V2 apex bNAbs from those without, we explored three different Env mutation metrics: (i) mutation frequency at sites spanning the non-hypervariable regions of V1V2 (**Fig. 5C**); (ii) a comparison of the mean Hamming distances for canonical bNAb epitope regions (C-strand residues 166-171; V3-glycan residues 324-344; fusion peptide residues 512-525; MPER residues 660-678) (**Fig. 6C and fig. S25**); and (iii) a sliding window analysis of time-adjusted Hamming distance area under the curve across the full-length Env (**Fig. 6D**). Each analysis showed a highly significant association between the presence of V2 apex bNAbs and detection of mutations in the C-strand but not other Env regions (**Fig. 6 and fig. S25)**. These findings

reinforced C-strand mutations in the evolving virus quasispecies as a sensitive and specific indicator of C-strand targeted NAb responses.

Discussion

The primary goal of this study was to determine why only a small subset of SHIV-infected RMs — and by extension, people living with HIV — develop V2 apex bNAbs and how this information can inform new vaccine design strategies. We established five lines of evidence indicating that the bottleneck to V2 apex bNAb elicitation lies at the B cell priming stage. First, we identified Envs that preferentially induced V2 apex bNAbs (**Fig. 1A)**. Most of these Envs had been reported to bind preferentially to germline-reverted V2 apex bNAbs (*31-35*), suggesting that the primary mechanism behind these Envs' enhanced bNAb elicitation rates is their higher likelihood of engaging V2 apex bNAb UCAs directly (e.g., in RMs V033 and V031) or sometime later when the Env quasispecies had evolved additional changes such N130 or N160 glycan loss (e.g., in RMs T646 and 6070). Second, we found that the frequency of V2 apex bNAb induction was disproportionately high in RMs and was exclusively linked to the expression of the rhesus D3-15*01 gene (**Figure 1A**). In a separate study, we identified structural and biochemical explanations for this preferential D gene usage, including a germline-encoded EDDY motif that binds positively charged C-strand residues (*28*). The combination of a favored D gene and HIV-1 Envs with a propensity for binding such bNAb UCAs, likely explains the high frequency of V2 apex bNAbs in RMs and again points to priming as the rate-limiting step. Third, inference of rhesus UCAs through B cell lineage tracing showed that, from the moment of VDJ recombination, they shared the necessary features of CDRH3 length, charge, and topology to become mature bNAbs. This suggests that priming of such naïve germline B

cells, and not complexities of affinity maturation, is the rate limiting step for bNAb elicitation. Fourth, once primed, V2 apex bNAb precursors evolved rapidly to acquire neutralization breadth and potency, following molecular pathways of affinity maturation guided by only few mutations in the Env C-strand. Affinity maturation generally did not require high levels of somatic hypermutation, indels, or show evidence of epistasis or evolutionary bottlenecks. The average time from UCA priming, as determined by NGS detection of lineage members in memory B cell mRNA, to acquisition of neutralization breadth in plasma was just 17 weeks. Fifth, C-strand selection in the evolving plasma virus quasispecies was found to be a sensitive and specific indicator of V2 apex C-strand targeted antibody responses. Our failure to find C-strand selection in most RMs that lacked V2 apex bNAbs suggested that such B cell precursors were either not primed, or if they were, then they failed to expand and affinity mature even to the point of producing autologous C-strand NAbs. We conclude from these findings that, in the setting of SHIV/HIV infection, V2 apex bNAb elicitation is uncommon because B cell priming is inefficient.

Why then is V2 apex bNAb priming so inefficient during the course of most SHIV/HIV infections? Successful priming requires a sufficient number of suitable B cell precursors and Env ligands with adequate affinity to bind them. Suitable B cell precursors have been defined as those with adequate CDRH3 length (>22aa), aromaticity, negative charge, and in some cases, particular sequence motifs (*28, 35, 64, 66*). Based on such criteria, several studies have estimated the frequency of potential V2 apex bNAb precursors to be in the range of 1 in 10^5-10^7 naïve B cells (*64, 66, 77*). But these features alone are unlikely to be the only requirements for B cell precursors to have the potential to affinity mature to neutralization breadth and potency. Our

findings of special "bNAb imprinting" Envs that exhibit a relatively high frequency of V2 apex bNAb precursor priming and bNAb elicitation (**Fig. 1**, Q23.17 and CH505), combined with results from recent immunization studies with germline-targeted, near-native Env trimers (see below), suggest that authentic V2 apex bNAb precursors circulate at appreciable frequencies. This conclusion is further supported by our findings along with published examples where mutations in the evolving virus quasispecies resulted in subpopulations of Envs with enhanced binding properties for bNAb precursors and the ability to elicit bNAbs (*21, 30, 46, 60-62, 78*). Altogether, the data suggest that stochastic processes associated with the transmission (acquisition) of particular Env variants, the evolution of these variants to acquire enhanced binding affinity to bNAb UCAs (e.g., spontaneous deletion of the glycan at residue N130), and randomness of V(D)J recombination, underlie the variability of V2 apex bNAb induction in SHIV-infected macaques and HIV-infected humans (**fig. S26**). Thus, the rate-limiting step to V2 apex bNAb induction is not a dearth of suitable B cell precursors but the requirement for higher affinity, immunofocused Envs, whether they be in the form of an evolving virus quasispecies variant or an engineered Env trimer immunogen. The key implication of these findings for HIV-1 vaccine design is that if Envs can be engineered to exhibit enhanced binding to V2 apex bNAb UCAs, such precursors are likely to be present in sufficient numbers to generate a bNAb response in most rhesus and humans.

Efficient priming as a rate-limiting step to bNAb induction may not be limited to the V2 apex site. In **Fig. 1**, we show that CD4bs-targeted bNAbs developed in only one of 115 SHIV-infected RMs. Building on studies by Kwong, Wyatt, and Binley (*79-81*), we designed a novel SHIV.CH505 lacking glycans surrounding the CD4bs and found that it induced CD4bs bNAbs in

9 of 11 monkeys within one year of infection ($p<0.0001$, Fisher's Exact Test) (*30*). Likewise, in **Fig. 1** and **Table S1**, we show that V3 glycan bNAbs developed in only four of 115 SHIV-infected RMs and then only after more than a year of infection. By introducing mutations that reduce glycan occupancy near the V3-^{325}GDIR$_{328}$ binding motif in a SHIV.BG505.N332.5MUT platform, we increased the frequency of V3 glycan-targeted bNAbs to 17 of 26 RMs ($p<0.0001$, Fisher's Exact Test) within 40 weeks of infection (A.N.S. and G.M.S., *in preparation*). Similar findings have been reported regarding priming efficiency of fusion peptide targeted bNAbs (*73*). All of these findings thus point to priming as a rate-limiting step to the elicitation of bNAbs targeting other epitope supersites in addition to the V2 apex, and one that is amenable to vaccine engineering.

The finding that B cell priming represents the primary obstacle to V2 apex bNAb elicitation during infection has potentially important implications for new HIV-1 vaccine strategies. A key inference is that if the efficiency of V2 apex bNAb UCA priming can be enhanced, it is likely to lead to more frequent and rapid bNAb elicitation. Recent findings reported in a companion paper (*54*) and elsewhere (*64, 77*) show this to be the case. Ghosh and colleagues found that a stabilized, germline-targeted version of the Q23.17 Env trimer (Q23.Apex.GT1) induced bNAbs in KI mice expressing the V033-a.I1after a single prime and homologous boost (*54*). Andrabi took this a step further with the design of Q23.Apex.GT2 and showed that this immunogen given as a homologous prime and boost could induce V2 apex bNAbs in RMs (*77*). An important feature of both Q23.Apex.GT1 and Q23.Apex.GT2 immunogens is that they are minimally modified from the wildtype Q23.17 Env trimer, which enables them to bind rhesus and human bNAb UCAs with enhanced affinity, and at the same time, allows for affinity maturation to be

driven by a native-like tier-2 HIV-1 Env trimer. This selects for BCRs that remain "on-track" with respect to bNAb development. Wyatt and Kulp also explored Q23.17-derived Envs as immunogens, and both groups observed on-target V2 apex bNAb responses in KI Ig-rearranging mice and RMs (*64*) (R.W., unpublished). Finally, Hahn and colleagues created a novel CAP256-ZM233-T250 V1/V2 chimera in a CAP256SU Env background that showed enhanced binding to multiple rhesus and human V2 apex bNAb UCAs. This germline-targeted Env induced V2 apex bNAbs in RMs when presented as mRNA-LNPs, ferritin nanoparticles or replicating SHIVs (B.H.H., K.W., K.O.S., B. F. H., unpublished). Notably, all of these strategies are based on immunogen platforms derived from Envs previously reported to bind preferentially to V2 apex germline B cell precursors (*31-35*) and reported here to preferentially induce bNAbs as SHIVs. Altogether, the findings highlight priming as the principal obstacle to V2 apex bNAb induction and suggest that effective boosting strategies may be less complicated than previously envisioned.

With respect to new strategies for vaccine development, the current study provides a molecular guide and toolkit of reagents and sequences for designing novel prime and boost immunogens. Previously, there were just two inferred human V2 apex UCAs and no rhesus UCAs (*23, 46*). The current study increases this number by six-fold by providing 12 high confidence rhesus V2 apex UCAs (**Fig. 2B, C**). Already, these have proven to be valuable as screening tools for new germline-targeted immunogens (*54, 77*). Similarly, the HIV-1 Envs identified in **Fig. 1A** as showing a propensity for eliciting V2 apex bNAbs have been incorporated into at least five new vaccine platforms all of which have been shown to induce V2 apex bNAbs in rhesus UCA KI mice, human Ig rearranging KI mice or RMs (*54, 64, 77*). Env sequences from Env-antibody

coevolution analyses have also been used to develop boosting immunogens that have shown success in KI mouse models (*54*). The molecular pathways in Env-Antibody coevolution reported here may thus provide the enabling datasets to investigate shared patterns in V2 apex bNAb induction that can be translated into new vaccine designs.

Limitations of the study

This study represented a prospective analysis of bNAb elicitation in 122 SHIV-infected monkeys with an average observational period of 2 years (range 0.6 to 6 years), as opposed to a retrospective characterization of bNAb development in highly selected individuals culled from much larger human cohorts where the duration of infection was generally much longer (*4, 6, 82-84*). In the latter case, investigators could choose just those individuals with the greatest neutralization breadth and potency for analysis, whereas in our studies, we included all SHIV-infected RMs from infection onward. One prediction, borne out by the results presented here, was that a prospective analysis of bNAb elicitation in rhesus was likely to identify animals with a far wider range of neutralization breadth and potency than might be considered desirable, yet such diverse outcomes are likely to be representative of the spectrum of antibody responses resulting from even the most promising vaccine candidates. Future vaccine trials in humans will need to consider this possibility. A critical question that remains to be answered is whether the neutralization breadth observed in the 18 monkeys with V2 apex bNAbs represented in **Table S1**, which ranged from 11-94% against our 18-member virus panel, was limited by properties inherent to the particular bNAb UCAs that were primed and the particular escape pathways of the homologous viral quasispecies that selected for their affinity maturation. Or, is it possible that the neutralization breadth potential of these UCAs is much greater and could be realized by

boosting with heterologous HIV-1 Envs. This is a question highly relevant to vaccine prime and boost designs and is one that can be addressed in the KI mouse model where individual V2 apex bNAb UCAs can be primed and boosted with homologous and heterologous Env immunogens (*54*).

A second limitation to the study relates to host immunogenetics. The rhesus D3-15*01 gene was expressed by all 12 rhesus V2 apex bNAbs (**Fig. 2C**). This gene is highly favorable for V2 apex bNAb priming and development as it encodes an EDDYG motif that provides negative charge, aromaticity and potential for tyrosine sulfation, each of which contribute to C-strand binding (*28*). There is no human homologue of the rhesus IGHD3-15*01 gene (*28*), although a similar EDDY motif can be generated at appreciable frequencies by non-templated nucleotide addition during V-D-J rearrangement (*64*). Moreover, an EDDY motif can evolve in human D genes under positive selective pressure as exemplified by the PCT64 bNAb lineage (*46*). It remains to be seen whether the priming efficiency of human V2 apex bNAb UCAs can be enhanced as readily as it can be for their rhesus counterparts. It is also not known if affinity maturation of human V2 apex bNAb lineages will be as straightforward as appears to be the case for rhesus V2 apex bNAbs, since many human bNAb germline precursors are unlikely to contain the fortuitous EDDY motif. These considerations notwithstanding, the results presented in this paper suggest that the rhesus model is highly amenable for the iterative design, development and testing of immunogens targeting the V2 apex. If vaccination regimens can be developed in rhesus that consistently elicit V2 apex targeted bNAbs at titers that are clinically protective against heterologous tier 2 SHIV challenge, it would represent an important proof-of-principle advance in the pursuit of an effective HIV-1 vaccine for humans.

Acknowledgements

We thank Dr. James Theiler for statistical advice. We thank the staff at Bioqual for exceptional care and support of nonhuman primates. We thank the University of Pennsylvania flow cytometry core for technical assistance with B cell sorting.

Funding: This work was supported by NIH grants AI160607 and AI165080 (G.M.S.), AI161818 and AI167716 (R.A.), AI150590 (B.H.H.), AI140897 (W.B.W), AI144371 (B.F.H.) and AI045008 (Penn Center for AIDS Research); by the Bill & Melinda Gates Foundation grants INV-041767 and INV-064777 (G.M.S./R.A.). R.H., R.S.R., M.P.H., and A.N.S. were supported by a Training Grant in HIV Pathogenesis (AI007632).

Data and materials availability: V2 apex bNAb UCA sequences are deposited at Genbank under accession numbers PV467379-PV467402. The B cell next-generation sequencing data generated in this study are available under the NCBI Bioproject PRJNA1121265. The atomic model of the V033-a.I1/Q23.MD39 complex generated in this study is available at the Protein Data Bank (PDB, https://www.rcsb.org) under the PDB accession code 9OMG. The corresponding cryo-EM reconstruction is available at the Electron Microscopy Data Bank (EMDB, https://www.ebi.ac.uk/emdb/) under the EMDB access code 70613. Longitudinal Env SGS gp140 sequences are deposited at Genbank under accession numbers XXXX-XXXX.

Author Contributions: R.H., R.S.R., H.L., M.P.H., K.J.S., S.J.P., F.B.R., A.S., C.L.M., J.R., N.C., J.L., W.D., M.S.C., and C.Z. contributed to rhesus plasma and monoclonal antibody neutralization assays. R.S.R., R.J.E., L.S., P.D.K. contributed to structural analyses. J.L., B.L., R.R.C., K.A. contributed to binding assays and affinity measurements. R.H., A.J.C., E.V.I., K.W. (Wiehe) contributed to phylogenetic analyses. R.H., H.L., S.W., J.W.C., K.A., Y.L. contributed to Env single genome sequencing. R.H., R.S.R., M.P.H., L.M., A.N.S., H.L., J.W.C., F.B.R., W.B.W., K.W. (Wiehe), contributed to B cell sorting and next-generation sequencing. Y.P., W.L. contributed to antibody production and synthesis. R.H., A.J.C., M.P.H., K.W. (Wagh), C.J.A., Z.S., B.T.K., contributed to statistical analyses. K.J.S., S.J.P., F.B.R., A.S., C.L.M., J.R., N.C., J.L., W.D., M.S.C., C.Z. M.L. contributed to rhesus macaque sample collection and processing. K.J.B., W.B.W., K.W. (Wiehe), K.O.S., R.J.E., D.W.C., M.L., F.D.B., D.B., R.A., D.W.K., B.F.H., B.T.K., L.S., P.D.K., B.H.H., and G.M.S. supervised the work. K.J.B., W.B.W., R.A., B.F.H., L.S., P.D.K., B.H.H., and G.M.S. contributed to funding acquisition. R.H. and G.M.S. wrote the initial manuscript. All authors contributed to manuscript review and editing.

Methods

Nonhuman primates:

Indian rhesus macaques ages 3-12 years, evenly split male and female, were housed at Bioqual Inc. in accordance with the Association for Assessment and Accreditation of Laboratory Animal Care (AAALAC) guidelines. The study design and all experimental procedures were approved by the University of Pennsylvania and Bioqual Institutional Animal Care and Use Committees. Monkeys were naïve with respect to prior SHIV infections or inoculations. Eight monkeys were

repurposed from prior immunization studies with HIV-1 gp120 monomeric protein or SOSIP Env trimer proteins. None of these animals had HIV-1 nAbs, bNAbs or bNAb lineage precursors detectable at the time of SHIV infection and study initiation. RMs were sedated for procedures including blood draws, anti-CD8 mAb infusions, and SHIV inoculations. A subset of animals received intravenous or subcutaneous infusions of 25 to 50 mg/kg of anti-CD8α mAb (MT807R1) or anti-CD8β mAb (CD8β255R1), administered at the time of SHIV inoculation or two or seven days prior. These anti-CD8 mAbs transiently depleted CD8□ cells for a duration of approximately two months, resulting in elevated peak and set point viral loads compared with monkeys that did not receive anti-CD8 mAbs. Details concerning monkey demographics, study design, and clinical, immunological and virological outcomes are provided in **Table S1**.

Processing and storage of specimens:

RM blood samples were collected in sterile vacutainers containing Anticoagulant Citrate Dextrose Solution A (ACD-A). A total of 40mL of ACD-A-anticoagulated blood was transferred into a sterile 50 mL conical tube and centrifuged at 1000×g for 10 minutes at 20°C. Plasma was carefully collected into a new 50 mL conical tube so as to not disturb the buffy coat and red blood cell pellet. To remove residual platelets and cells, the plasma was centrifuged again at 1500×g for 15 minutes at 20°C. The resulting plasma was aliquoted into 1mL cryovials and stored at –80°C. The remaining pellet was resuspended in an equal volume of Hanks' Balanced Salt Solution (HBSS) without Ca^{2}□ or Mg^{2}□ and supplemented with 2mM EDTA. The mixture was divided into four 50 mL conical tubes, and additional HBSS-EDTA was added to bring each tube to a final volume of 30mL. Each cell suspension was then gently underlaid with 14mL of

96% Ficoll-Paque and centrifuged at 725×g for 15 minutes at 20°C with slow acceleration and deceleration to maintain the Ficoll-cell interface. Mononuclear cells at the interface were collected and suspended in HBSS-EDTA, followed by centrifugation at ~500×g for 15 minutes at 20°C. The pellet was resuspended in HBSS containing Ca^{2+} and Mg^{2+} and supplemented with 1% fetal bovine serum (FBS). To remove additional platelet contamination, the suspension was centrifuged at 200×g for 15 minutes at 20°C, and the supernatant discarded. The resulting pellet was resuspended in 0.1-0.3mL of residual media and brought to 25mL with HBSS + 1% FBS. Cell counts and viability were determined using acridine orange and propidium iodide staining. Cells were then centrifuged at 300×g for 10 minutes at 20°C, resuspended at 5-10×10^{6} cells/mL in CryoStor cell cryopreservation medium, and aliquoted into 1mL cryovials. Cryovials containing PBMCs were stored in Corning CoolCell LX freezing containers at –80°C overnight, followed by transfer to vapor phase liquid nitrogen for long-term storage.

Plasma vRNA quantification

Plasma viral load measurements were performed by the NIH/NIAID-sponsored Nonhuman Primate Virology Core Laboratory at the Duke Human Vaccine Institute. This core facility is CLIAcertified and operates a highly standardized, quality-controlled Applied Biosystems Real-TimeSIV and HIV vRNA PCR assays. QIAsymphony SP and QIAgility automated platforms (QIAGEN) were used for high throughput sample processing and PCR setup. Viral RNA was extracted and purified from plasma, annealed to a target specific primer and reverse transcribed into cDNA. The cDNA was treated with RNase and added to a custom real-time PCR master mix containing target specific primers and a fluorescently labeled hydrolysis probe. Thermal cycling

was performed on a QuantStudio3 (ThermoFisher Scientific) real-time quantitative PCR (qPCR) instrument. Viral RNA cp/reaction was interpolated using quantification cycle data. Raw data were quality-controlled, positive and negative controls are checked, and the mean viral RNA cp/ml wascalculated. The lower limit of quantification (LLOQ) of this assay was 62 RNA copies/mL.

Virus stock generation:

SHIV and pseudovirus stocks were generated by transfection of HEK 293T/17 cells (ATCC, CRL-11268). 4-5 x 10^6 cells were plated in 100mm dishes and grown in DMEM containing 10% FBS and 1% Penicillin/Streptomycin overnight at 37°C. 6µg of SHIV plasmid DNA or was then transfected using FuGENE 6 transfection reagent (Promega, Cat # E2691) according to the manufacturer's instructions. Transfected cells were then incubuated for 48h at 37°C. Supernatants were then centrifuged, aliquoted, and stored at -80°C.

Site-directed mutants were generated using the Q5 Site-Directed Mutagenesis kit (New England BioLabs) according to the manufacturer's instructions, and produced as described above.

Virus titration:

Titration of 293T cell virus stock is performed using TZM-bl cells. TZM-bl cells were grown in cell culture medium (DMEM supplemented with 10% FBS, 1% penicillin/streptomycin) and were plated in 96 well plates at a concentration of 1.5×10^4 cells/well and incubated at 37ºC

overnight. Viruses were diluted five-fold in cell culture media supplemented with 40 ug/ml DEAE-dextran and incubated in quadruplicate with TZM-bl cells at 37º C for 48 hours. Infected cells were then fixed for 10 minutes at room temperature in PBS containing 0.8% glutaraldehyde and 2.2% formaldehyde, washed 3 times with PBS, and stained with PBS containing 4µM Magnesium Chloride, 4µM Potassium Ferricyanide, 4µM Potassium Ferrocyanide, and 400µg/ml X-Gal for 3 hours at 37°C. Stained cells were then washed 3 times with PBS, and imaged on a CTL analyzer (Immunospot). The number of spot counts per virus dilution were then averaged and divided by the volume of viral input to calculate the concentration of infectious viral units.

Neutralization assays:

Neutralizing antibody assays were performed using TZM-bl indicator cells, as previously described (*27*). Briefly, TZM-bl cells were grown in cell culture medium (DMEM supplemented with 10% FBS and 1% penicillin/streptomycin), were plated in 96 well plates at a concentration of 1.5×10^4 cells/well and incubated at 37ºC overnight. Serum samples were heat inactivated at 56°C for 1 hour, and serial 5-fold dilutions, starting at a dilution of 1:20, were made in cell culture media supplemented with 10% normal human serum. For monoclonal antibody neutralization assays, mAbs were serially diluted starting at a concentration of 50µg/ml for mature bNAbs and 200µg/ml for UCAs in cell culture media lacking normal human serum. Viruses were diluted to achieve a multiplicity of infection (MOI) of 0.3 upon addition to TZM-bl cells. Viruses were incubated with serum or antibody dilutions at 37ºC for one hour, after which the virus-serum or virus-antibody mixtures were plated onto adherent TZM-bl cells and incubated at 37ºC for 48 hours. Following incubation, cells were lysed with 0.5% Triton-X 100

in PBS and luciferase activity levels measured using the Promega luciferase assay system (Promega Cat# E1501) on a BioTek Synergy Neo2 plate reader (Agilent Technologies). Neutralization IC_{50}/ID_{50} values were calculated using Prism 10 software.

Antibody production:

To produce select antibodies, paired heavy (VDJ) and light (VJ) chain variable gene sequences were commercially synthesized (GenScript) and cloned into antibody expression plasmids as previously described (*27*). Recombinant antibodies were produced by cotransfecting paired heavy and light chain expression plasmids into Expi293F cells using ExpiFectamine 293 transfection reagents (Gibco), purified from culture supernatants using the Protein A/Protein G GraviTrap kit, and buffer-exchanged into PBS as previously described (*27*).

BLI affinity measurements:

BLI was performed to determine the affinities of V033-a lineage members for Q23 trimers. IgGs (10 µg/ml) were immobilized on Protein A sensors (Sartorius) to a signal of 1.0 nm using an Octet Red96 instrument (ForteBio). The immobilized IgGs were then dipped in running buffer (PBS containing 0.1% bovine serum albumin and 0.02% Tween-20 at pH 7.4). Sensors were then dipped into wells containing Q23 trimers serially diluted in running buffer. Four two-fold dilutions were tested for each trimer, starting at a concentration of 500nM. Following a 120s association period, the tips were dipped into the running buffer and dissociation was measured for 240s.

B cell next-generation sequencing:

B cell NGS was performed as previously described (*27, 85*). Briefly, PBMCs were stained with LIVE/DEAD Aqua, CD3-PerCP-Cy55, CD4-BV785, CD8-BV711, CD14-PE-Cy7, CD20-BV605, IgD-FITC, IgG-AF680, and IgM-BV650. Memory B cells (CD20+, IgG+, IgD-, IgM-) were bulk sorted into RPMI with 10% FBS and 1% Pen-Strep using a BD FACSAria II. RNA was extracted using RNAzol RT according to the manufacturer's guidelines (Molecular Research Center, Inc). cDNA was synthesized using a 5´ rapid amplification of cDNA ends (5´ RACE) approach, with SMARTer cDNA template switching and Superscript II RT. Following synthesis, cDNA was purified using AMPure XP beads (Beckman Coulter). Immunoglobulin transcripts were then selectively PCR amplified using IgG, IgK, or IgL constant region-specific primers and KAPA HiFI HotStart ReadyMix (Roche). Finally, an additional PCR step was used to append Illumina P5 and P7 sequencing adaptors to the libraries. Both heavy and lambda immunoglobulin libraries were sequenced on an Illumina Miseq sequencer with 2 × 300 bp runs using the MiSeq Reagent V3 kit (600-cycle).

Antibody Lineage Tracing Workflow Details

To delineate the ontogeny of each antibody lineage, we analyzed antibody mRNA transcripts from an unbiased sampling of each macaque's B cell receptor repertoire, both for naive antibodies (from IgM+/IgD+ B cells) and mature antibodies (from IgG+ B cells). We used a common amplification and sequencing approach and common early data processing steps,

followed by more specific workflows for the two main aspects of the analysis corresponding to the naive and mature cells.

Sequencing of the naive (IgM+/IgD+) B cells allowed us to indirectly infer the unrearranged, genomic antibody germline gene repertoire for each macaque, primarily using the software IgDiscover (*48, 49*) and MINING-D (*86*). We applied a separate workflow to antibody sequences from IgG+ B cells, using the program SONAR (*47*) to identify sequences belonging to our lineages of interest across longitudinal sampling and to construct phylogenies leading back to the inferred unmutated common ancestor (UCA) of each antibody lineage. The germline sequences derived from the naive repertoire dataset informed this analysis by supplying confident germline gene assignments for each lineage.

In addition to the specific programs and techniques described in more detail below, we used custom code written in Python and Snakemake to coordinate the overall data processing and workflow organization. A final section provides software versions and URLs including for this custom code.

Sequencing and initial data processing for all samples

Library preparation and sequencing was as previously described (*28, 85*). In short, we used 3' primers specific to the applicable rhesus macaque antibody constant regions and a universal 5' RACE primer to amplify the beginning of the antibody transcript including the leader through the J segment to the beginning of the constant region. A second round of PCR incorporated Illumina sequencing adapters and custom sample barcoding. An "inline" barcode was placed at

the start of the forward read (R1), including a varying-length randomized nucleotide prefix for higher nucleotide diversity during sequencing. A second barcode was placed in an index read (I1). To handle this custom barcoding strategy, we performed demultiplexing as part of the data processing after sequencing, using the igseq demux command in our Python program (described below), rather than with default Illumina software. The read layout was 309x8x309 NT for R1, I1, and R2, with the overlapping R1 and R2 sequences merged during processing following adapter trimming.

The output from this step of our workflow was the trimmed and merged antibody reads with adapters and primers removed, spanning from the beginning of each antibody transcript to the end of the J segment.

Establishing individualized antibody germline repertoires

As previously described (*28*) we used the IgM+/IgD+ repertoire sequencing reads (demultiplexed, trimmed, and merged as described above) to develop individualized macaque-specific V and J segment germline references, as well as to check the presence of germline D gene sequences. We used IgDiscover to infer personalized germline sequence sets from a set of generic rhesus macaque starting databases. For the IGH locus, the starting database was KIMDB 1.1 (*87*), a recently published database of rhesus and cynomolgus macaque IGHV, IGHJ, and IGHD sequences. For IGK and IGL, we used an earlier published germline reference (*88*), as KIMDB does not currently include light chain sequences.

In certain instances, we observed large numbers of spurious novel J sequences in IgDiscover's output, particularly for the IGKJ2 family, but at times for heavy chain sequences as well. To exclude these from the final output we applied an additional filtering step for J sequences using IgDiscover's "discoverjd" feature.

As IgDiscover reports evidence of expression of known germline D sequences but does not infer new alleles, we also used the program MINING-D to infer possible D sequences and check for any signs of relevant novel D segments in our lineages of interest. We first annotated, filtered, and clustered the IgM+/IgD+ sequences using the steps described below for lineage tracing for IgG+ sequences, in order to get consensus CDRH3 sequences for each naive antibody repertoire, and gave these sequences as input to MINING-D. We used two p value thresholds (4.5×10^{-36}, labeled "default" in the workflow, and 4.5×10^{-16}, labeled "sensitive") to produce two levels of sensitivity in the output for each macaque. We compared MINING-D's output sequences with IgDiscover's expression tables and with KIMDB's rhesus macaque reference D sequences, as well as other known macaque antibody germline references. As MINING-D is intended as an initial check for possible novel alleles to be confirmed with genomic sequencing, we did not attempt to infer a complete set of germline D sequences per macaque with this approach; instead, we used it to investigate particular established germline D sequences such as those assigned for our lineages of interest.

The output from this step was the inferred V and J allele sequences from IgDiscover and, for heavy chains, inferred D allele sequences from MINING-D with two tiers of sensitivity.

Lineage Tracing

In parallel to the steps described above for investigating per-macaque germline sequences, we used SONAR to analyze IgG reads from longitudinal samples and trace the development of our specific lineages of interest. SONAR's operation is organized in three sequential stages: initial sequence clustering and annotation (module 1), lineage member identification (module 2), and phylogenetic analysis (module 3). The germline information inferred for each macaque was used directly in SONAR's annotation steps, and also informed the final germline assignments for each lineage to determine the most accurate unmutated common ancestor (UCA) inference.

Lineage Tracing: SONAR Module 1 (Annotation)

The IgG+ repertoire sequencing reads (demultiplexed, trimmed, and merged as described above) were supplied to SONAR's module 1 scripts, which uses BLAST+ to assign germline gene segments using each macaque's germline reference and then clustering similar reads (threshold of 99% for clustering and a minimum of 2 identical sequences per cluster). Only productive-looking antibody sequences (those with recognizable junction regions including codons for conserved amino acids, and without frame shifts or stop codons) were included for subsequent analysis.

The output from this step was, for each sample, an AIRR-compatible (*89*) TSV table of annotations for clustered antibody sequences and associated FASTA files corresponding to a representative sequence from each cluster.

Lineage Tracing: SONAR Module 2 (Lineage Member Selection)

Following annotation and clustering, we used SONAR's manually-guided identity/divergence feature for lineage member identification in each sample. This step calculates sequence identity to known antibodies for lineages of interest and divergence from assigned germline V sequences (as defined automatically module 1's annotation and supplied in the AIRR file), for the productive-looking sequence clusters identified in module 1 (SONAR's "goodVJ unique" sequence set).

The identity/divergence file is then supplied to SONAR's "island" selection script to identify groups ("islands") of candidate lineage members on a specialized scatterplot of all sequences for each sample. These plots display divergence from germline V on the x axis and identity to one reference antibody on the y axis, with candidates selected by clicking points to define a boundary polygon on each plot. The final set of candidate lineage members is the combination of all selected repertoire sequences across the known representative lineage members. The list of sequence IDs for candidate lineage members is then supplied to SONAR's getFasta utility script to produce a FASTA file of lineage members for each lineage for each sample.

Our default approach was to use all initial known lineage members as references for the island selection process, with extensive manual review of the candidates afterward to resolve any ambiguous cases (considering evidence such as shared mutations from germline or matching nontemplated nucleotides in the junction region). While relatively labor-intensive compared to automated alternatives, this approach allowed more flexibility in confidently identifying true lineage members than rule-based criteria (e.g., requiring matching germline V and J genes,

junction lengths, and a fixed junction similarity threshold) since it can identify sequences with difficult-to-assign germline genes or with indels relative to known lineage members. While not built into our software workflow directly, candidate UCA sequences and new lineage member sequences identified in the repertoire NGS samples can also be supplied as references for additional rounds of identity calculations and island selection through manual addition to the relevant files.

We found that the default behavior of SONAR's island selection script, using kernel density estimation for a smoothed density visualization, could fail to display individual sequences in certain edge cases. We introduced an alternate plotting approach to instead display sequence counts per binned tile of identity and divergence intervals, which ensures all possible sequences are visible on the plot. This option is now available in SONAR's script as sonar get_island --plotmethod binned, and was used by default in our workflow.

The output from this step was, for each sample and each lineage, a FASTA file with sequences of identified lineage members.

Lineage Tracing: SONAR Module 3 (Phylogeny Analysis)

To investigate the development of each antibody lineage over time, we used SONAR's module 3 features for phylogeny analysis. SONAR includes a specific version of the Immcantation Framework's IgPhyML (*52*, *53*) and an associated script for inferring ancestor sequences for each tree node. SONAR's procedure creates a tree using IgPhyML's antibody-specific HLP19 codon substitution model (*52*) and a nucleotide sequence for each internal node in that tree,

representing an inferred ancestor sequence for the clade beneath that node. The internal node closest to the tree root corresponds to a hypothetical UCA sequence as inferred by the software.

The identified lineage member sequences from module 2 were gathered across time points for each subject and locus and labeled with a prefix for each time point to create a unified set of lineage member sequences discovered from the repertoire over time. For a first-pass phylogenetic analysis, we used SONAR's default behavior, with a MUSCLE alignment of all lineage members including the repertoire-discovered sequences and the "native" mature isolated members, followed by IgPhyML with the tree rooted on our own assigned germline V sequence from that macaque's germline reference.

To refine the tree and inference, we then supplied IgPhyML with a manually adjusted codon alignment of all lineage member sequences and used a draft UCA sequence as the tree root rather than the germline V segment only. To avoid biasing the final tree and inferences, we replaced possible nontemplated nucleotides with N in this root sequence. The earliest inferred ancestor sequence from this final step was compared with all known germline information for the relevant macaque (as described above for IgDiscover and MINING-D) to produce a final inference for the UCA of the lineage. This included any necessary adjustments to revert suspected mutated positions in germline-templated areas to the germline state. For final visualization purposes, we used trees rooted on the full UCA sequence.

Indels in relevant lineages also required extensive manual review, as insertions and deletions are not modeled by HLP19 or the ancestor sequence inference procedure. To account for this, we

reviewed the observed sequences of lineage members in each tree, and attempted to infer the most plausible explanation using qualitative background knowledge on the frequency of indels in lineage maturation and possible specific events such as insertions through duplications of adjacent nucleotide motifs (*9, 30, 57*).

The output from this step, representing the final lineage tracing results for one lineage and chain, was a FASTA file for the alignment used for each tree, the associated Newick-format tree file from IgPhyML, and a FASTA of the inferred sequences for each tree node. This also included our final UCA sequence for heavy and light chains for each lineage.

Software and Configuration

- Custom Python program for common tasks in our workflow such as demultiplexing and adapter trimming: https://github.com/shawhahnlab/igseq
    - cutadapt (*90*): https://github.com/marcelm/cutadapt
    - PEAR (*91*): https://cme.h-its.org/exelixis/web/software/pear/doc.html
- Snakemake-based (*92*) workflow files for ongoing lineage tracing analyses: https://github.com/shawhahnlab/igseqhelper
- Singularity (*93*) for running SONAR's Docker container
- KIMDB 1.1 for IGH germline reference sequences: http://kimdb.gkhlab.se/datasets/ and igseq's data/germ/rhesus/kimdb files
- Ramesh et al. 2017 IGK and IGL as supplied by SONAR's included germDB directory and igseq's data/germ/rhesus/sonarramesh files

- Dedicated code repository for the work presented here: https://github.com/ShawHahnLab/Habib_et_al_2025_igseq

The dedicated repository provides the full detail and commands needed for reproduction of the results reported here.

Env single-genome sequencing:

Using the single genome sequencing (SGS) method described previously (*18, 29*), we amplified SHIV 3′ half genomes from the sequential plasma samples of 103 SHIV-infected animals. Briefly, viral RNA was extracted from plasma using QIAamp Viral RNA kit (Qiagen) and reverse transcribed using SuperScript III Reverse Transcriptase (Invitrogen). Viral cDNA was then endpoint diluted and amplified using nested PCR with primers and conditions as previously reported [ref]. Geneious Prime software was used for sequence analysis. Pixel plots of SGS data were generated using the LANL Pixel plot tools (https://www.hiv.lanl.gov/content/sequence/pixel/pixel.html).

Env SGS Hamming distance analysis

SGS data was analyzed by translating each Env's nucleotide sequence into amino acids and aligning it to the appropriate infecting Env for each individual. Regions of interest such as the C-strand (HXB2 numbering 166-171), V3-glycan (324-334), fusion peptide (512-525), and MPER (656-683) were extracted. The hamming distance between the infecting Env and each sequence was calculated and used to find the mean hamming distance within each timepoint. Mean

hamming distance was then calculated by taking the mean of all timepoints within each individual. These values were then compared between individuals with and without V2-apex bNAbs using a two-tailed Welch's t-test. Additionally, we repeated this process for all continuous 10 amino acid regions of Env (i.e. 1-10, 2-11, 3-12, etc…). Gaps in the alignment were treated as individual differences for the purpose of this analysis. Custom scripts used to perform these calculations can be found here: https://github.com/ShawHahnLab/Habib_et_al_2025_HammingDistance.git

NS-EMPEM:

For negative stain EM polyclonal epitope mapping, 1 mg of polyclonal serum Fab was mixed with 10-20 µg of Env SOSIP, incubated overnight at 4 °C and then fractionated by size exclusion chromotography over a Superose 6 Increase 10/300 column. Running buffer was PBS with 500 mM Na2SO4 added. Fractions corresponding to the presumptive Fab-Env complex were pooled and concentrated in a 0.5-ml, 100-kDa spin concentrator to ~0.2 mg/ml, then applied to a glow-discharged carbon-coated EM grid for 10-12 second, then blotted, and stained with 2 g/dL uranyl formate for 1 min, blotted and air-dried. Grids were examined on a Philips EM420 electron microscope operating at 120 kV and nominal magnification of 49,000x, and **~100-400** images were collected on a 76 Mpix CCD camera at 2.4 Å/pixel. Images were analyzed and 3D refinements obtained using standard protocols with Relion 3.0 (Zivanov et al. 2018. *eLife*. 7:e42166).

Cryo-EM sample preparation and data collection

The structure of V033-a.I1 in complex with Q23.17 MD39 envelope trimer was determined using single-particle cryo-EM. Previous work revealed mature lineage member V033-a.01 to bind multiple Fabs per trimer (ref: Roark 2025). To determine if V033 lineage IgG could engage a single envelope trimer through both antigen-binding arms, V033-a.I1 F(ab)'2 was generated by pepsin digestion and complexed with Q23.17 MD39 at 1.5:1 F(ab)'2-to-trimer molar ratio for a final trimer concentration of 2.5 mg/mL. After incubation for 30 minutes at 4C, the detergent n-Dodecyl β-D-maltoside (DDM) was added to a final concentration of 0.005% (w/v). 3µL of sample was added to copper C-flat Holey carbon-coated grids (CF-1.2/1.3 300 mesh; EMS) that were glow discharged with a PELCO easiGlow. Grids were blotted for 3 seconds at room temperature with 100% humidity and vitrified by liquid ethane using a Vitrobot Mark IV. Single particle cryo-EM datasets were collected on a FEI Titan Krios 300 kV cryo-transmission electron microscope equipped with a Gatan K3 direct electron detector. Movies were collected in counting mode using Leginon (PMID: 15890530) with a total dose of 58 e-/Å2 fractionated over 50 raw frames, with defocus values set to cycle between -0.80 and -2.0 µm. Approximately 7,000 micrographs were collected in 20 hours.

Cryo-EM data processing and model building

All processing was done in cryoSPARC v3.4 (*94*), including micrograph curation, motion correction, CTF estimation, non-templated blob particle picking, 2D classification, ab initio modeling, and iterative 3D refinements. All homogenous and non-uniform 3D refinements of were performed using C1 symmetry. Map resolution was estimated using the 0.143 Fourier shell correlation (FSC) cutoff criterion. Despite using F(ab)'2, the majority of particle complexes contained a single arm bound to trimer without any visible density for the remainder of the

F(ab)’2 molecule; therefore, a final 3D reconstruction with a single Fab domain was used for atomic modeling building. The initial coordinates for the V033-a.I1 complex were obtained by docking the V033-a.01 Fab from PDB-9BNP and the Q23.17 MD39 trimer from PDB-9BNL into the present cryo-EM density using UCSF ChimeraX (*95*). The atomic model was solved by iterative manual rebuilding in Coot (*96*) and real-space refinement in Phenix (*97*). Overall structure quality was assessed using MolProbity (*98*) and EMRinger (*99*).

Supplemental Text

Monte Carlo random sampling analysis of bNAb elicitation rates

For each trial in the Monte-Carlo experiments, the 18 positives for V2 apex and 4 positives for V3-glycan were randomly distributed among the 115 monkeys, with each RM keeping its assigned SHIV. SHIVs were sorted according to the fraction of bNAb positive monkeys associated with that SHIV. The top *n* SHIVs were ranked by the fraction positive, and then a statistic computed for the sum of positives among the top *n* SHIVs. Based on 100,000 trials, the below estimated p-values for different values of n were found for the V2 data:

n	**p**
1	0.03297
2	0.08272
3	0.00073
4	0.00074
5	0.00006

Applied to the V3-glycan data:

n	**p**
1	0.18157
2	0.04934

3	0.41074
4	1.0
5	1.0

These results indicate the restriction of both V2 apex and V3-glycan bNAbers to five and two SHIVs respectively to be significant.

Mapping of early plasma responses in RM V033

Figure **S6** shows sequential Env SGS sequences from RM V033 spanning weeks 0-56 post-infection. At week 8 post-infection, SGS revealed striking positive selection in Env at four sites: an N187S substitution that introduced a glycan to the V2 hypervariable loop at residue 185, an R308H mutation on the V3 loop, several mutations clustered around K460 (K460E, D461G/N, N463H, V464E) at the V5 loop, and a T533A mutation. These mutations were followed at week 12 by additional mutations at Q170R and K171R on the V2 apex C-strand (**Fig. 3B, S6**). To understand which of these mutations constituted escape from NAb lineages, we constructed a series of mutants that incorporated these mutations individually, as well as week 8 and 12 consensus viruses bearing 3 and 5 mutations respectively. All apical mutations (those at residues 170, 171, and 187) as well as R308H conferred decreases in plasma neutralization potency, indicating these to be escape mutations from NAb responses (**fig. S6**). On the other hand, the K460E mutation resulted in no change in neutralization suggesting that this escape arose to escape cytotoxic T cell responses (**fig. S6**). The T533A substitution was not necessary for abrogation of neutralization by week 8 or 12 plasmas, suggesting that it did not arise to escape

Nab responses. Furthermore, the same mutation was identified in all SHIV-Q23.17 infected RMs at the earliest timepoint sequenced (**fig. S27**). A533 is a highly conserved residue, present in >99% of the 10,000+ global HIV-1 Envs in the LANL database (https://www.hiv.lanl.gov). This led us to determine that this mutation was a fitness reversion, rather than an immune escape variant. Overall, these results indicate that the initial immune response in RM V033 consistent of NAbs targeted two epitopes, the V2 apex and linear V3 loop, as well as V5 loop directed cytotoxic T cell responses.

Temporal dynamics of Env escape and breadth acquisition in RM V033

To understand how Env-bNAb coevolution led to breadth development in RM V033, we examined the relationship between Env escape mutations and heterologous virus neutralization. We found that the temporal emergence of within-host V2 apex escape mutations could explain the dynamics of serum breadth acquisition in this macaque. While the Q23.17 T/F Env lacked glycans in the V2 hypervariable loop, the Env quasispecies evolved to acquire a potential N-linked glycan site at 185 through an N187S substitution first detectable at week 4 (**Fig. 3B**). This mutation dominated the quasispecies at week 8 (92%, 34 out of 37) and reached fixation from week 12 onwards. While week 12 serum could neutralize 3 heterologous viruses with one or two glycans in hypervariable V2 loop, week 4 and 8 sera could not, thus indicating that N187S arose to dominance just prior to detection of serum neutralization of heterologous Envs with V2 loop glycans (**Fig. 3A**). A similar trend was also seen for Q170R that dominates the quasispecies beginning week 16 (61%, 17 of 28), preceding the neutralization of R170 containing heterologous viruses MT145K (by week 20 serum, 4 weeks later) and ZM233.6 (by week 24 serum, 8 weeks later). These results suggest that serum neutralization of heterologous

viruses carrying certain V2 apex amino acids could only be detected after those Env features were selected for in the within-host Env quasispecies. N187S provides neutralization escape from the first bNAb intermediate I1 but is sensitive to I2, indicating this mutation was responsible for selecting for maturation from I1 to I2 (**Fig. 3C**). Similarly, Q170R likely was involved in maturation from I6 to the fully mature V033-a.01. These findings suggest a scenario in which within-host Env escape mutations from previous bNAb intermediates select for more matured bNAb lineage members that can neutralize those escape mutations in heterologous viruses, and it is this capacity that confers increasing breadth acquisition as the V033 bNAb lineage matures. Similar patterns were also detected for the other SHIV Q23.17 infected V2 bNAber V031, in which the mutations H130N (which introduces a glycan at N130) and R169K are first detected at week 32 in longitudinal Envs 16 weeks prior to the first detection of serum neutralization of heterologous Envs with either of these amino acids, observed beginning week 48 (**Fig. 5B, Table S1**).

Sensitivity and specificity analysis of C-strand selection in SHIV-infected RMs

Out of the 115 RMs in this study, 18 were found to have V2 apex bNAbs (Fig. 1A), and five were found to have C-strand targeted NAbs responses with limited heterologous neutralization that did not meet our criteria for breadth (**fig. S22**). Nineteen out of 23 RMs with C-strand targeted NAbs showed complete replacement of the WT C-strand, while 23/23 showed at least 50% replacement (**Fig. 5B and fig. S17**). These results established 50% C-strand replacement to have a sensitivity of 1.0 as an indicator of the presence of a C-strand targeted NAb. To probe the specificity of C-strand selection, we looked for the frequency of C-strand selection among RMs that did not make C-strand targeted NAbs. No RMs infected with SHIVs CH694, 40100, WITO,

191859, CH1012, or BG505 achieved 50% replacement of the C-strand (**Fig. 6B and fig. S21**). Two out of three RMs infected with SHIV-ZM233 showed no C-strand selection (**fig. S21)**. Amongst SHIVs that reproducibly elicited V2 apex bNAbs — Q23.17, CAP256SU, T250, Ce1176, and CH505 — C-strand selection was absent in the majority of RMs that did not develop C-strand-targeted responses, indicating this selection was specifically the result of antibody escape (**Fig. 6B and fig. S21**). Only one RM, 6927 (SHIV-T250), showed over 50% C-strand replacement that was not associated with a C-strand targeted NAb response.

SHIVs B41 and CH848, and Ce1086 represented outliers. Six out of six SHIV-B41 infected RMs showed rapid C-strand selection as early as week 12 post-infection (**fig. S21 and S24**), however this selection only reached 50% replacement in three out of six RMs. Three out of six RMs infected with SHIV-CH848 acquired an E169K reversion to group M consensus also detectable in the initial trial participant CH848 (**Fig. S23**). However, this mutation is expected to sensitize the V2 apex to neutralization by V2 apex bNAbs (*100*), suggesting that it was acquired to increase viral replicative capacity rather than as escape from an antibody lineage. C-strand selection in SHIV Ce1086-infected RMs was transient, reverted to the T/F sequence following acquisition of a K160N mutation introducing a glycan at residue 160, and only one RM (T683) reached 50% C-strand replacement (**fig. S28**). Genetic linkage between acquisition of the N160 glycan and C-strand selection suggest that C-strand escape in those RMs was the result of a 2909-like N160 glycan hole-specific antibody response (*50, 101*). Despite the frequency of selection, none of the SHIV-B41, Ce1086, or CH848 infected RMs showed any evidence of V2 apex-directed breadth.

Overall, 17/23 RMs with C-strand targeted responses showed complete T/F loss at the C-strand, while 23/23 RMs had at least 50% replacement of the WT C-strand. Analysis of RMs without V2 apex-directed NAbs yielded a final number of 3/78 RMs showing complete replacement of the WT C-strand, and 8/78 showing at least 50% T/F loss. These results identify 50% C-strand replacement as a highly significant, sensitive, and specific indicator of C-strand targeted responses ($p < 0.0001$, Fischer's Exact Test; Sensitivity = 1.000; Specificity = 0.897).

Figure Legends

Fig. 1. HIV-1 Envs with a predilection for V2 apex bNAb induction. (**A**) Numbers of RMs infected with SHIV strains expressing different primary HIV-1 Envs that elicited V2 apex, V3 glycan, fusion peptide, CD4-binding site, or silent face bNAbs. RMs with bNAbs were defined as RMs with ID_{50} titers of ≥1:80 against two or more members of an 18-strain tier 1B/2 heterologous virus panel (**B**) SHIV strains expressing HIV-1 Envs that were previously shown to be sensitive to neutralization by V2 apex bNAb inferred germline (iGL) precursor antibodies or iGL-intermediate antibodies were significantly more likely to elicit V2 apex bNAbs compared with other strains ($p = 0.0002$; Fisher's Exact test). (**C**) Maximum plasma neutralization breadth (defined as percent of viruses neutralized at an ID_{50} titer of ≥1:20) achieved by RMs on an 18-strain heterologous tier 1B/2 virus panel, grouped by bNAb specificity. (**D**) Geometric means of heterologous plasma ID_{50} neutralization titers of RMs at the timepoint at which they showed maximum breadth. (**E**) Time (in weeks post-infection) until the first detection of any heterologous plasma neutralization by RMs, grouped by bNAb specificity. (**F**) Time (in weeks post-infection) until the acquisition of breadth that met our predermined criteria for breadth descried in **A**. RMs are grouped by infecting SHIV strain. Significance in panels C-F was determined by Kruskal-Wallis test followed by Dunn's multiple comparisons test. Error bars in C-F indicate one standard deviation from the mean.

Fig. 2. Features of V2 apex bNAb lineage UCAs. (A) Overview of V2 apex bNAb lineage tracing. (**B**) Nucleotide and translation alignment of the V033-a.UCA with assigned VDJ genes and B cell NGS-derived lineage members from weeks 4 and 8. Mismatches to the UCA are

highlighted. (**C**) Table describing immunogenetic features of rhesus and human V2 apex bNAb UCAs and iGLs. Underlined residues in CDRH3 sequences indicate nontemplated residues. Previous estimates of SHM for the rhesus bNAbs reported still lower values based on V_H gene analysis only (*27, 28*); determinations here included mutations across the entire antibody heavy chain, including the CDRH3, which is under strong positive selection in V2 apex bNAbs. (**D**) Frequency histogram of naïve B cell receptor CDRH3 lengths in the rhesus repertoire. CDRH3 lengths of rhesus and human UCAs and iGLs are indicated. (**E**) Frequency histogram of naïve B cell receptor CDRH3 charges in the rhesus repertoire. CDRH3 charges of rhesus and human UCAs and iGLs are indicated.

Fig. 3. Env-antibody coevolution in RM V033. (**A**) (Left) Longitudinal autologous and heterologous reciprocal plasma neutralization ID_{50} values in SHIV-Q23.17-infected RM V033. Data are adapted from Roark et al. bioRxiv 2024. (Middle) Neutralization IC50 values of V033-a lineage intermediates and UCA against a panel of heterologous viruses. Increasing intermediate numbers indicate more mature antibodies. (Right) Sequence features of viruses included in the neutralization panel. Residues 130, 166-171, and the number of glycans on the V2 hypervariable loops are shown. Dots indicate sequence identity, and N-linked glycans are denoted by “O”. (**B**) Longitudinal Env V1V2 sequences from RM V033. Sequences are grouped by timepoint indicated on the left. Dashes indicate identity, and colored residues indicate escape mutations from the V033-a lineage. (**C**) Neutralization IC50 values of mature V033-a bNAb mAbs against Q23.17 Envs incorporating escape mutations from B. (**D**) Neutralization IC50 values of V033-a lineage intermediates against Q23.17 Envs incorporating escape mutations from (B). (**E**)

Neutralization IC50 values of the V033-a.UCA and UCA site-directed mutants singly incorporating mutations from the mature V033-a bNAbs against Q23.17 Env variants.

Fig. 4. Independent mutational trajectories leading to V2 apex bNAb maturation. (**A**) Radial IgPhyML trees of V2 apex bNAb lineage heavy chains. All trees are rooted on the lineage's inferred UCA. Grey, yellow, orange, red, and black dots indicate mature bNAb lineage members, colored by their neutralization breadth on our 18-virus panel as previously reported (*28*). Neutralization breadth values for PCT64 lineage are represented as reported in Landais et al. Immunity 2017 (*46*). Cyan dots indicate the most recent common ancestor (MRCA) of all broadly neutralizing members of the lineage. Different clades branching off from the MRCA and independently acquiring breadth are colored indigo and lilac. CDRH3 insertions in the 6561-a lineage are indicated by arrows. Scale bars are represented internally, with each concentric circle indicating 10 nucleotide mutations from the UCA. (**B**) Protein alignments of the lineages shown in A. UCA heavy chains are aligned with representative mature bNAb lineage members from each independent clade. Mismatches to the UCA are highlighted. Red highlights indicate mutations in common between the two clades.

Fig. 5. Limited and convergent Env mutations guide V2 apex bNAb maturation. (A) Protein topology diagram of the Env V2 apex, highlighting positions of key escape residues and glycans. **(B)** Amino acid alignments of longitudinal Env sequences obtained by SGS of circulating plasma virion RNA in RMs with V2 apex bNAbs. Sequences show residues 130 and 156-177 (HXB2 numbering). Sequences are grouped by timepoint indicated on the left in weeks. Dashes indicate identity to the T/F sequence. Mutations at residues 166-171, mutations that

delete glycans at N156 or N160, or mutations that introduce a glycan to residue 130 are highlighted. Glycan sequons are denoted by “O”. Highlighter plots for RMs 5695, 6070, 40591, and 42056 are adapted with permission from Roark et al. Science 2021 (*27*). **(C)** Mutation frequencies of RMs with (top) versus without (middle) V2 apex bNAbs at residues 130 and comparison of mutation incidence of these sites between the two groups (bottom, Wilcoxon matched-paired signed rank test, $p < 0.0001$) **(D)** Neutralization IC50 values of V2 apex bNAb lineage members against autologous Env mutants incorporating mutations identified in **B**.

Fig. 6. C-strand selection is detectable soon after a V2 apex lineage is triggered but rarely occurs in RMs without V2 apex bNAbs. (**A**) Mean longitudinal Hamming distances of Env residues 166-171 from the T/F sequence in RMs with V2 apex bNAbs. Values for participant CAP256 indicate the distance from the superinfecting strain CAP256SU. Dotted lines indicate the timepoint where the V2 apex bNAb lineage was first detected by B cell NGS. Shaded regions indicate timepoints where heterologous tier-2 plasma neutralization are observed. (**B**) Mean longitudinal Hamming distances of Env residues 166-171 from the T/F sequence in 101 SHIV-infected rhesus macaques. Data from human trial participants from which the SHIV Envs were isolated are included where available. Data for the remaining SHIVs are shown in fig. S18. (**C**) Comparison of the mean C-strand Hamming distances between RMs with and without V2 apex bNAbs at the bNAb epitopes indicated. Significance was determined by Welch’s t-test. (**D**) Test for significantly different mean longitudinal hamming distances for moving regions of 10 amino acids across the envelope gene. P values shown are from two-tailed Welch’s t-tests. The significance threshold was adjusted using a Bonferroni correction for multiple comparisons. For all panels, RMs with V2 apex bNAbs are colored red while those without are colored teal. RMs

with C-strand targeted antibody responses that did not meet our criteria for breadth are colored orange. All error bars indicate 95% confidence intervals.

Fig. S1. Mapping sites of heterologous neutralization in SHIV-infected RMs. (**A**) Neutralization mapping against heterologous wild type and FP-epitope mutant viruses by plasma from RM6561. (**B**) Neutralization mapping against heterologous wild type and V2 apex-epitope mutant viruses by plasma from eight RMs. (**C-D**) Negative-stain electron microscopy polyclonal epitope mapping (NS-EMPEM) of polyclonal Fabs from RMs with silent face bNAbs 41712 (**C**) and 6727 (**D**) against soluble heterologous Env trimers.

Fig. S2. Inference of V2 apex bNAb UCAs. Nucleotide and translation alignments of (**A**) newly inferred rhesus and (**B**) re-inferred human V2 apex bNAb UCAs with assigned VDJ genes and early B cell NGS-derived lineage members. Mismatches to the UCA are highlighted. Data in panel B are re-analyzed from Doria-Rose et al. Nature 2014 and Landais et al. Immunity 2017 (*23*, *46*). Both previously published and revised inferences of the VRC26 UCA are shown.

Fig. S3. Longitudinal somatic hypermutation of V2 apex bNAb lineages. Percent somatic hypermutation of rhesus V2 apex bNAb lineages members at timepoints where lineages were detectable by B cell NGS**.** Error bars represent the range of values.

Fig. S4. Longitudinal V033-a lineage heavy chain sequences. Sequence alignment of B cell NGS-derived V033-a lineage members from weeks 4, 8, and 12 post-infection, and mature bNAb

sequences isolated at week 24 post-infection. Mismatches to the UCA are highlighted. Residue 100j is indicated by a red arrow.

Fig. S5. Env-Antibody Coevolution in RM V033. (**A**) A pixel plot of longitudinal Env sequences from RM V033. Mismatches to the T/F sequence are colored red, and major mutations are indicated below. (**B**) Neutralization of wild type and mutant Q23.17 pseudoviruses by plasma from RM V033 at weeks 8 and 12 post-infection. Q23.17 pseudoviruses contained mutations identified from week 8 and week 12 SGS sequences.

Fig. S6. Affinity changes during V033-a lineage maturation. BLI measurements of the apparent affinities, on-rates, and off-rates of V033-a lineage mAbs for a stabilized WT Q23 trimer and trimer mutants incorporating SGS-derived escape mutations.

Fig. S7. Env sensitivity and resistance signatures to the V033-a bNAb lineage. (**A**) The number of viruses sensitive and resistant to neutralization by the V033-a lineage that contain or lack a glycan at N130 ($p < 0.0001$; Fischer's Exact test). (**B**) The number of N130-glycan containing viruses sensitive and resistant to neutralization by the V033-a lineage grouped by the presence or absence of Q170 ($p < 0.0001$; Fischer's Exact test).

Fig. S8. Structural maturation of the V033-a lineage (A) Cryo-EM structure of the V033-a.I1 antibody in complex with a stabilized Q23.MD39 trimer aligned to the structure of the mature V033-a.01 bNAb (PDB: 9BNP). **(B)** Maturation of CDRH3 contacts with the V2 apex C-strand during V033-a lineage affinity maturation. **(C)** Maturation of CDRH3 interactions with Env K168 during V033-a lineage affinity maturation.

Fig. S9. Heavy chain phylogenetic trees of V2 apex bNAb lineages. Radial IgPhyML trees of V2 apex bNAb lineage heavy chains showing (**A**) intermediate and (**B**) late phylogenetic divergence. All trees are rooted on the lineage's inferred UCA. Gray, yellow, orange, red, and black dots indicate mature bNAb lineage members, colored by their neutralization breadth on our 19-virus panel reported in Roark et al. bioRxiv 2024. Blue dots indicate the most recent common ancestor (MRCA) of all broadly neutralizing members of the lineage. Different clades branching off from the MRCA and independently acquiring breadth are colored indigo and lilac. A CDRH3 insertion in the V031-a lineage is indicated by an arrow. Scale bars are represented internally, with each concentric circle indicating 10 nucleotide mutations from the UCA.

Fig. S10. A two-residue insertion in necessary for heterologous neutralization by the V031-a.01 mAb. Neutralization of a pseudovirus panel by the bNAb from RM V031 (V031-a.01) and a V031-a.01 mutant lacking a two residue CDRH3 insertion (V031-a.01del).

Fig S11. Mutational Bottleneck in the 42056-a lineage. (**A**) The mutation probabilities of the amino acid mutations computed with ARMADiLLO for the mAbs and nineteen representative

sequences. Only the V segment region is shown for clarity. Three highly improbable mutations (black arrows) that are shared only by the isolated bNAb mAbs from the 42056-a lineage (42056-a.01, 42056-a.02, 42056-a.03) and some members of their clade (colored blue). (**B**) An IgPhyML tree of the 42056-a lineage heavy chain showing the positions of sequences from **A**.

Fig. S12. Neutralization phenotype of inferred V2 apex bNAb UCAs. (**A**) Neutralization IC50 values of all rhesus V2 apex bNAb UCAs against a panel of Envs previously described to be sensitive to neutralization by V2 apex bNAb precursors. (**B**) Neutralization IC50 values of the 6070-a.UCA and T646-a.UCA against a panel of autologous and heterologous N160 glycan-deficient viruses.

Fig. S13. T/F V1V2 sequences are usually absent preceding bNAb initiation. Highlighter plots showing alignments of Env SGS V1V2 sequences (residues 130-199) at the timepoint prior to when V2 apex bNAbs lineage first became detectable by B cell NGS. In each plot, the top sequence represents the T/F Env sequence, and mismatches to the T/F Env sequence are highlighted.

Fig. S14. N130 glycan deletion precedes V2 apex bNAb elicitation in SHIV-CH505-infected RMs. Longitudinal glycan sequon frequencies at residue 130 in SHIV-CH505-infected RMs that developed V2 apex bNAbs. RMs where sufficient sequences were available for analysis are

shown. Dotted lines indicate the timepoint where the V2 apex bNAb lineage was first detected by B cell NGS. Shaded regions indicate timepoints where heterologous tier-2 plasma neutralization are observed. Longitudinal glycan sequon frequencies at residue 130 in human participant CH505 are included for comparison.

Fig. S15. V1V2 sequence evolution in RM 6070. Amino acid alignments of longitudinal Env sequences obtained by SGS of circulating plasma virion RNA from RM 6070. Sequences show residues 130-199 (HXB2 numbering). Sequences are grouped by timepoint indicated on the left in weeks. Dashes indicate identity to the T/F sequence. C-strand residues 166-171 are shaded red. Mutations that delete the glycan at N160 are shaded green. A red box indicates the timepoint when the bNAb lineage was first detected is highlighted.

Fig. S16. V1V2 sequence evolution in RM T646. Amino acid alignments of longitudinal Env sequences obtained by SGS of circulating plasma virion RNA from RM T646. Sequences show residues 130-199 (HXB2 numbering). Sequences are grouped by timepoint indicated on the left in weeks. Dashes indicate identity to the T/F sequence. C-strand residues 166-171 are shaded red. Mutations that delete the glycan at N160 are shaded green. A red box indicates the timepoint when the bNAb lineage was first detected is highlighted.

Fig. S17. Limited and convergent Env mutations guide rhesus V2 apex bNAb maturation. Amino acid alignments of longitudinal Env sequences obtained by SGS of circulating plasma virion RNA in RMs with V2 apex bNAbs. Sequences show residues 130 and 156-177 (HXB2 numbering). Sequences are grouped by timepoint indicated on the left in weeks. Dashes indicate identity to the T/F sequence. Mutations at residues 166-171, mutations that delete glycans at N156 or N160, or mutations that introduce a glycan to residue 130 are highlighted. Glycan sequons are denoted by "O".

Fig. S18. Limited and convergent Env mutations guide human V2 apex bNAb maturation. Longitudinal Env SGS in human participants (**A**) CAP256 and (**B**) and PC64 who made V2 apex bNAbs. Mismatches in (**A**) are shown against the superinfecting strain CAP256SU. Dashes indicate sequence identity. Mutations at residues 166-171, mutations that delete glycans at N156 or N160, or mutations that insert glycans at residue 130 are highlighted. Sequences are grouped by timepoint indicated on the left in months. Data in this figure are re-analyzed from Doria-Rose et al. Nature 2014 and Landais et al. Immunity 2017 (*23, 46*).

Fig. S19. Env selection correlates with bNAb structural footprints. Heatmap of the percent replacement of Env C-strand residues 166-171 in SGS sequences from humans and RMs with V2 apex bNAbs at the timepoint indicated. The structural class of each V2 apex bNAb is indicated on the left.

Fig. S20. A K190E V2 hypervariable loop mutation mediates initial escape from the 6561-a bNAb lineage. (**A**) Neutralization of Ce1176 wild-type and K190E mutant viruses by the 6561-a.01 mAb. (**B**) Inset from cryo-EM structure of 6561-a.01 in complex with an autologous Ce1176-SOSIP (PDB: 9BTJ) to highlight electrostatic contact between HCDR3 residue E100 and Env hypervariable V2 residue K190.

Fig. S21. Longitudinal C-strand Hamming distances in SHIV-infected RMs. Mean longitudinal Hamming distances of Env residues 166-171 from the T/F sequence in 101 SHIV-infected rhesus macaques. Data from human trial participants from which the SHIV strains were isolated are included where available. For all panels, RMs with V2 apex bNAbs are colored red and RMs without are colored teal. Data for the remaining SHIVs are shown in Figure 6B. RMs with C-strand targeted antibody responses that did not meet our criteria for breadth are colored orange. All error bars indicate 95% confidence intervals.

Fig. S22. Evidence of C-strand targeted NAbs in five RMs. Neutralization mapping against Q23.17 wild-type and V2 apex-epitope mutant pseudoviruses by plasma from SHIV-Q23.17 infected RMs 45951, 6734, 6730, and SHIV-CH505 infected RMs 6697 and 6701.

Fig. S23. C-strand selection in SHIV CH848-infected RMs usually consists of an E169K reversion to group M consensus. Longitudinal Env SGS alignments of V2 apex strands B and

C from SHIV-CH848-infected RMs. Dots indicate identical residues. Residue 169 is highlighted red.

Fig. S24. C-strand selection in SHIV B41-infected RMs. Longitudinal Env SGS alignments of the V1V2 region from SHIV-B41-infected RMs 41949 (left), 42534 (middle), and 42579 (right). Dots indicate identical residues, while dashes represent gaps in the alignment. C-strand residues 166-171 are highlighted red, while V1/V2 hypervariable loop deletions are highlighted teal.

Fig. S25. Selection at other bNAb epitopes is not significantly associated with the development of V2 apex bNAbs. Comparison of the mean C-strand Hamming distances between RMs with and without V2 apex bNAbs at the bNAb epitopes indicated. Epitopes analyzed include the V3-glycan (residues 324-334), fusion peptide (residues 512-525) and MPER (residues 660-678). Significance was determined by Welch's t-test. ns = not significant.

Fig. S26. Model of V2 apex bNAb priming

Fig. S27. An early fitness reversion in SHIV-Q23.17 infected RMs. A pixel plot of Env sequences from the first sequenced timepoint from each SHIV-Q23.17 infected RM. Mismatches to the T/F sequence are colored. A universally detected T533A reversion to HIV-1 group M consensus is indicated below.

Fig. S28. Transient C-strand selection in SHIV-Ce1086 infected RMs reverts after replacement of the N160 glycan. Longitudinal Env SGS alignments of V2 apex strands B and C

from SHIV-CH1086-infected RMs that exhibited C-strand selection. Dots indicate identical residues. N160 glycan additions are highlighted green.

References

1. E. S. Gray, M. C. Madiga, T. Hermanus, P. L. Moore, C. K. Wibmer, N. L. Tumba, L. Werner, K. Mlisana, S. Sibeko, C. Williamson, S. S. A. Karim, L. Morris, The CAPRISA002 Study Team, The Neutralization Breadth of HIV-1 Develops Incrementally over Four Years and Is Associated with CD4+ T Cell Decline and High Viral Load during Acute Infection. *Journal of Virology* **85 (10)**, 4828-4840 (2011).
2. N. A. Doria-Rose, R. M. Klein, M. G. Daniels, S. O'Dell, M. Nason, A. Lapedes, T. Bhattacharya, S. A. Migueles, R. T. Wyatt, B. T. Korber, J. R. Mascola, M. Connors, Breadth of Human Immunodeficiency Virus-Specific Neutralizing Activity in Sera: Clustering Analysis and Association with Clinical Variables. *Journal of Virology* **84 (3)**, 1631-1636 (2010).
3. I. Mikell, D. N. Sather, S. A. Kalams, M. Altfeld, G. Alter, L. Stamatatos, Characteristics of the Earliest Cross-Neutralizing Antibody Response to HIV-1. *PLoS Pathogens* **7 (1)**, e1001251 (2011).
4. E. Landais, X. Huang, C. Havenar-Daughton, B. Murrell, M. A. Price, L. Wickramasinghe, A. Ramos, C. B. Bian, M. Simek, S. Allen, E. Karita, W. Kilembe, S. Lakhi, M. Inambao, A. Kamali, E. J. Sanders, O. Anzala, V. Edward, L.-G. Bekker, J. Tang, J. Gilmour, S. L. Kosakovsky-Pond, P. Phung, T. Wrin, S. Crotty, A. Godzik, P. Poignard, Broadly Neutralizing Antibody Responses in a Large Longitudinal Sub-Saharan HIV Primary Infection Cohort. *PLOS Pathogens* **12 (1)**, e1005369 (2016).
5. G. D. Tomaras, J. M. Binley, E. S. Gray, E. T. Crooks, K. Osawa, P. L. Moore, N. Tumba, T. Tong, X. Shen, N. L. Yates, J. Decker, C. K. Wibmer, F. Gao, S. M. Alam, P. Easterbrook, S. A. Karim, G. Kamanga, J. A. Crump, M. Cohen, G. M. Shaw, J. R. Mascola, B. F. Haynes, D. C. Montefiori, L. Morris, Polyclonal B Cell Responses to Conserved Neutralization Epitopes in a Subset of HIV-1-Infected Individuals. *Journal of Virology* **85 (21)**, 11502-11519 (2011).
6. P. Rusert, R. D. Kouyos, C. Kadelka, H. Ebner, M. Schanz, M. Huber, D. L. Braun, N. Hozé, A. Scherrer, C. Magnus, J. Weber, T. Uhr, V. Cippa, C. W. Thorball, H. Kuster, M. Cavassini, E. Bernasconi, M. Hoffmann, A. Calmy, M. Battegay, A. Rauch, S. Yerly, V. Aubert, T. Klimkait, J. Böni, J. Fellay, R. R. Regoes, H. F. Günthard, A. Trkola, P. Rusert, R. D. Kouyos, C. Kadelka, H. Ebner, M. Schanz, M. Huber, D. L. Braun, N. Hozé, A. Scherrer, C. Magnus, J. Weber, T. Uhr, V. Cippa, C. W. Thorball, H. Kuster, M. Cavassini, E. Bernasconi, M. Hoffmann, A. Calmy, M. Battegay, A. Rauch, S. Yerly, V. Aubert, T. Klimkait, J. Böni, J. Fellay, R. R. Regoes, H. F. Günthard, A. Trkola, Determinants of HIV-1 broadly neutralizing antibody induction. *Nature Medicine* **22 (11)**, 1260-1267 (2016).
7. R. D. Kouyos, P. Rusert, C. Kadelka, M. Huber, A. Marzel, H. Ebner, M. Schanz, T. Liechti, N. Friedrich, D. L. Braun, A. U. Scherrer, J. Weber, T. Uhr, N. S. Baumann, C. Leemann, H. Kuster, J.-P. Chave, M. Cavassini, E. Bernasconi, M. Hoffmann, A. Calmy, M. Battegay, A. Rauch, S. Yerly, V. Aubert, T. Klimkait, J. Böni, K. J. Metzner, H. F. Günthard, A. Trkola, R. D. Kouyos, P. Rusert, C. Kadelka, M. Huber, A. Marzel, H. Ebner, M. Schanz, T. Liechti, N. Friedrich, D. L. Braun, A. U. Scherrer, J. Weber, T. Uhr, N. S. Baumann, C. Leemann, H. Kuster, J.-P. Chave, M. Cavassini, E. Bernasconi, M. Hoffmann, A. Calmy, M. Battegay, A. Rauch, S. Yerly, V. Aubert, T. Klimkait, J. Böni, K. J. Metzner, H. F. Günthard, A. Trkola,

1516 Tracing HIV-1 strains that imprint broadly neutralizing antibody responses. *Nature* **561**
1517 **(7723)**, 406–410 (2018).
1518 8. P. L. Moore, C. Williamson, L. Morris, Virological features associated with the
1519 development of broadly neutralizing antibodies to HIV-1. *Trends in Microbiology* **23 (4)**,
1520 204-211 (2015).
1521 9. C. Joyce, S. Murrell, B. Murrell, O. Omorodion, L. S. Ver, N. Carrico, R. Bastidas, R.
1522 Nedellec, M. Bick, J. Woehl, F. Zhao, A. Burns, S. Barman, M. Appel, A. Ramos, L.
1523 Wickramasinghe, K. Eren, T. Vollbrecht, D. M. Smith, S. L. K. Pond, R. McBride, C. Worth,
1524 F. Batista, D. Sok, The IAVI Protocol C Investigators & The IAVI African HIV Research
1525 Network, P. Poignard, B. Briney, I. A. Wilson, E. Landais, D. R. Burton, Antigen pressure
1526 from two founder viruses induces multiple insertions at a single antibody position to
1527 generate broadly neutralizing HIV antibodies. *PLOS Pathogens* **19 (6)**, e1011416 (2023).
1528 10. V. Cortez, K. Odem-Davis, R. S. McClelland, W. Jaoko, J. Overbaugh, HIV-1 Superinfection
1529 in Women Broadens and Strengthens the Neutralizing Antibody Response. *PLOS*
1530 *Pathogens* **8 (3)**, e1002611 (2012).
1531 11. D. N. Sather, J. Armann, L. K. Ching, A. Mavrantoni, G. Sellhorn, Z. Caldwell, X. Yu, B.
1532 Wood, S. Self, S. Kalams, L. Stamatatos, Factors Associated with the Development of
1533 Cross-Reactive Neutralizing Antibodies during Human Immunodeficiency Virus Type 1
1534 Infection. *Journal of Virology* **83 (2)**, 757-769 (2009).
1535 12. K. Wagh, E. F. Kreider, Y. Li, H. J. Barbian, G. H. Learn, E. Giorgi, P. T. Hraber, T. G.
1536 Decker, A. G. Smith, M. V. Gondim, L. Gillis, J. Wandzilak, G.-Y. Chuang, R. Rawi, F. Cai, P.
1537 Pellegrino, I. Williams, J. Overbaugh, F. Gao, P. D. Kwong, B. F. Haynes, G. M. Shaw, P.
1538 Borrow, M. S. Seaman, B. H. Hahn, B. Korber, Completeness of HIV-1 Envelope Glycan
1539 Shield at Transmission Determines Neutralization Breadth. *Cell Reports* **25 (4)**, 893–
1540 908.e897 (2018).
1541 13. B. F. Haynes, K. Wiehe, P. Borrow, K. O. Saunders, B. Korber, K. Wagh, A. J. McMichael,
1542 G. Kelsoe, B. H. Hahn, F. Alt, G. M. Shaw, B. F. Haynes, K. Wiehe, P. Borrow, K. O.
1543 Saunders, B. Korber, K. Wagh, A. J. McMichael, G. Kelsoe, B. H. Hahn, F. Alt, G. M. Shaw,
1544 Strategies for HIV-1 vaccines that induce broadly neutralizing antibodies. *Nature*
1545 *Reviews Immunology* **23 (3)**, 142–158 (2022).
1546 14. D. Sok, D. R. Burton, Recent progress in broadly neutralizing antibodies to HIV. *Nature*
1547 *Immunology* **19 (11)**, 1179-1188 (2018).
1548 15. P. D. Kwong, J. R. Mascola, HIV-1 Vaccines Based on Antibody Identification, B Cell
1549 Ontogeny, and Epitope Structure. *Immunity* **48 (5)**, 855-871 (2018).
1550 16. G. Y. Chuang, J. Zhou, P. Acharya, R. Rawi, C. H. Shen, Z. Sheng, B. Zhang, T. Zhou, R. T.
1551 Bailer, V. P. Dandey, N. A. Doria-Rose, M. K. Louder, K. McKee, J. R. Mascola, L. Shapiro,
1552 P. D. Kwong, Structural Survey of Broadly Neutralizing Antibodies Targeting the HIV-1
1553 Env Trimer Delineates Epitope Categories and Characteristics of Recognition. *Structure*
1554 **27 (1)**, 196-206.e196 (2019).
1555 17. L. M. Walker, M. D. Simek, F. Priddy, J. S. Gach, D. Wagner, M. B. Zwick, S. K. Phogat, P.
1556 Poignard, D. R. Burton, A Limited Number of Antibody Specificities Mediate Broad and
1557 Potent Serum Neutralization in Selected HIV-1 Infected Individuals. *PLoS Pathogens* **6**
1558 **(8)**, e1001028 (2010).

18. H. Li, S. Wang, R. Kong, W. Ding, F. H. Lee, Z. Parker, E. Kim, G. H. Learn, P. Hahn, B. Policicchio, E. Brocca-Cofano, C. Deleage, X. Hao, G. Y. Chuang, J. Gorman, M. Gardner, M. G. Lewis, T. Hatziioannou, S. Santra, C. Apetrei, I. Pandrea, S. M. Alam, H. X. Liao, X. Shen, G. D. Tomaras, M. Farzan, E. Chertova, B. F. Keele, J. D. Estes, J. D. Lifson, R. W. Doms, D. C. Montefiori, B. F. Haynes, J. G. Sodroski, P. D. Kwong, B. H. Hahn, G. M. Shaw, Envelope residue 375 substitutions in simian-human immunodeficiency viruses enhance CD4 binding and replication in rhesus macaques. *Proceedings of the National Academy of Sciences* **113 (24)**, E3413-E3422 (2016).
19. H. Li, S. Wang, F.-H. Lee, R. S. Roark, A. I. Murphy, J. Smith, C. Zhao, J. Rando, N. Chohan, Y. Ding, E. Kim, E. Lindemuth, K. J. Bar, I. Pandrea, C. Apetrei, B. F. Keele, J. D. Lifson, M. G. Lewis, T. N. Denny, B. F. Haynes, B. H. Hahn, G. M. Shaw, New SHIVs and Improved Design Strategy for Modeling HIV-1 Transmission, Immunopathogenesis, Prevention and Cure. *Journal of Virology* **95 (11)**, e00071-00021 (2021).
20. B. F. Haynes, G. Kelsoe, S. C. Harrison, T. B. Kepler, B-cell–lineage immunogen design in vaccine development with HIV-1 as a case study. *Nature biotechnology* **30 (5)**, 423-433 (2012).
21. M. Bonsignori, E. F. Kreider, D. Fera, R. R. Meyerhoff, T. Bradley, K. Wiehe, S. M. Alam, B. Aussedat, W. E. Walkowicz, K. K. Hwang, K. O. Saunders, R. Zhang, M. A. Gladden, A. Monroe, A. Kumar, S. M. Xia, M. Cooper, M. K. Louder, K. McKee, R. T. Bailer, B. W. Pier, C. A. Jette, G. Kelsoe, W. B. Williams, L. Morris, J. Kappes, K. Wagh, G. Kamanga, M. S. Cohen, P. T. Hraber, D. C. Montefiori, A. Trama, H. X. Liao, T. B. Kepler, M. A. Moody, F. Gao, S. J. Danishefsky, J. R. Mascola, G. M. Shaw, B. H. Hahn, S. C. Harrison, B. T. Korber, B. F. Haynes, Staged induction of HIV-1 glycan-dependent broadly neutralizing antibodies. *Science Translational Medicine* **9 (381)**, eaai7514 (2017).
22. M. Bonsignori, T. Zhou, Z. Sheng, L. Chen, F. Gao, M. G. Joyce, G. Ozorowski, G.-Y. Chuang, Chaim A. Schramm, K. Wiehe, S. M. Alam, T. Bradley, Morgan A. Gladden, K.-K. Hwang, S. Iyengar, A. Kumar, X. Lu, K. Luo, Michael C. Mangiapani, Robert J. Parks, H. Song, P. Acharya, Robert T. Bailer, A. Cao, A. Druz, Ivelin S. Georgiev, Young D. Kwon, Mark K. Louder, B. Zhang, A. Zheng, Brenna J. Hill, R. Kong, C. Soto, James C. Mullikin, Daniel C. Douek, David C. Montefiori, Michael A. Moody, George M. Shaw, Beatrice H. Hahn, G. Kelsoe, Peter T. Hraber, Bette T. Korber, Scott D. Boyd, Andrew Z. Fire, Thomas B. Kepler, L. Shapiro, Andrew B. Ward, John R. Mascola, H.-X. Liao, Peter D. Kwong, Barton F. Haynes, Maturation Pathway from Germline to Broad HIV-1 Neutralizer of a CD4-Mimic Antibody. *Cell* **165 (2)**, 449-463 (2016).
23. N. A. Doria-Rose, C. A. Schramm, J. Gorman, P. L. Moore, J. N. Bhiman, B. J. DeKosky, M. J. Ernandes, I. S. Georgiev, H. J. Kim, M. Pancera, R. P. Staupe, H. R. Altae-Tran, R. T. Bailer, E. T. Crooks, A. Cupo, A. Druz, N. J. Garrett, K. H. Hoi, R. Kong, M. K. Louder, N. S. Longo, K. McKee, M. Nonyane, S. O'Dell, R. S. Roark, R. S. Rudicell, S. D. Schmidt, D. J. Sheward, C. Soto, C. K. Wibmer, Y. Yang, Z. Zhang, J. C. Mullikin, J. M. Binley, R. W. Sanders, I. A. Wilson, J. P. Moore, A. B. Ward, G. Georgiou, C. Williamson, S. S. A. Karim, L. Morris, P. D. Kwong, L. Shapiro, J. R. Mascola, Developmental pathway for potent V1V2-directed HIV-neutralizing antibodies. *Nature* **508 (7498)**, 55-62 (2014).
24. H. X. Liao, R. Lynch, T. Zhou, F. Gao, S. Munir Alam, S. D. Boyd, A. Z. Fire, K. M. Roskin, C. A. Schramm, Z. Zhang, J. Zhu, L. Shapiro, J. C. Mullikin, S. Gnanakaran, P. Hraber, K.

1603 Wiehe, G. Kelsoe, G. Yang, S. M. Xia, D. C. Montefiori, R. Parks, K. E. Lloyd, R. M. Scearce,
1604 K. A. Soderberg, M. Cohen, G. Kamanga, M. K. Louder, L. M. Tran, Y. Chen, F. Cai, S.
1605 Chen, S. Moquin, X. Du, M. Gordon Joyce, S. Srivatsan, B. Zhang, A. Zheng, G. M. Shaw,
1606 B. H. Hahn, T. B. Kepler, B. T. M. Korber, P. D. Kwong, J. R. Mascola, B. F. Haynes, J.
1607 Becker, B. Benjamin, R. Blakesley, G. Bouffard, S. Brooks, H. Coleman, M. Dekhtyar, M.
1608 Gregory, X. Guan, J. Gupta, J. Han, A. Hargrove, S. L. Ho, T. Johnson, R. Legaspi, S. Lovett,
1609 Q. Maduro, C. Masiello, B. Maskeri, J. McDowell, C. Montemayor, J. Mulliki, M. Park, N.
1610 Riebow, K. Schandler, B. Schmidt, C. Sison, M. Stantripop, J. Thomas, P. Thomas, M.
1611 Vemulapalli, A. Young, Co-evolution of a broadly neutralizing HIV-1 antibody and
1612 founder virus. *Nature* **496 (7446)**, 469-476 (2013).
1613 25. N. A. Doria-Rose, E. Landais, Coevolution of HIV-1 and broadly neutralizing antibodies.
1614 *Current Opinion in HIV and AIDS* **14 (4)**, 286-293 (2019).
1615 26. F. Gao, M. Bonsignori, H.-X. Liao, A. Kumar, S.-M. Xia, X. Lu, F. Cai, K.-K. Hwang, H. Song,
1616 T. Zhou, Rebecca M. Lynch, S. M. Alam, M. A. Moody, G. Ferrari, M. Berrong, G. Kelsoe,
1617 George M. Shaw, Beatrice H. Hahn, David C. Montefiori, G. Kamanga, Myron S. Cohen, P.
1618 Hraber, Peter D. Kwong, Bette T. Korber, John R. Mascola, Thomas B. Kepler, Barton F.
1619 Haynes, Cooperation of B Cell Lineages in Induction of HIV-1-Broadly Neutralizing
1620 Antibodies. *Cell* **158 (3)**, 481-491 (2014).
1621 27. R. S. Roark, H. Li, W. B. Williams, H. Chug, R. D. Mason, J. Gorman, S. Wang, F. H. Lee, J.
1622 Rando, M. Bonsignori, K. K. Hwang, K. O. Saunders, K. Wiehe, M. A. Moody, P. T. Hraber,
1623 K. Wagh, E. E. Giorgi, R. M. Russell, F. Bibollet-Ruche, W. Liu, J. Connel, A. G. Smith, J.
1624 DeVoto, A. I. Murphy, J. Smith, W. Ding, C. Zhao, N. Chohan, M. Okumura, C. Rosario, Y.
1625 Ding, E. Lindemuth, A. M. Bauer, K. J. Bar, D. Ambrozak, C. W. Chao, G. Y. Chuang, H.
1626 Geng, B. C. Lin, M. K. Louder, R. Nguyen, B. Zhang, M. G. Lewis, D. D. Raymond, N. A.
1627 Doria-Rose, C. A. Schramm, D. C. Douek, M. Roederer, T. B. Kepler, G. Kelsoe, J. R.
1628 Mascola, P. D. Kwong, B. T. Korber, S. C. Harrison, B. F. Haynes, B. H. Hahn, G. M. Shaw,
1629 Recapitulation of HIV-1 Env-antibody coevolution in macaques leading to neutralization
1630 breadth. *Science* **371 (6525)**, eabd2638 (2021).
1631 28. R. S. Roark, R. Habib, J. Gorman, H. Li, A. J. Connell, M. Bonsignori, Y. Guo, M. P. Hogarty,
1632 A. S. Olia, K. Sowers, B. Zhang, F. Bibollet-Ruche, S. Callaghan, J. W. Carey, G. Cerutti, D.
1633 R. Harris, W. He, E. Lewis, T. Liu, R. D. Mason, Y. Park, J. M. Rando, A. Singh, J. Wolff, Q.
1634 P. Lei, M. K. Louder, N. A. Doria-Rose, R. Andrabi, K. O. Saunders, M. S. Seaman, B. F.
1635 Haynes, D. W. Kulp, J. R. Mascola, M. Roederer, Z. Sheng, B. H. Hahn, G. M. Shaw, P. D.
1636 Kwong, L. Shapiro, HIV-1 neutralizing antibodies in SHIV-infected macaques recapitulate
1637 structurally divergent modes of human V2 apex recognition with a single D gene. *The*
1638 *Journal of Experimental Medicine (in press)*, (bioRxiv doi:
1639 https://doi.org/10.1101/2024.1106.1111.598384) (2024).
1640 29. B. F. Keele, E. E. Giorgi, J. F. Salazar-Gonzalez, J. M. Decker, K. T. Pham, M. G. Salazar, C.
1641 Sun, T. Grayson, S. Wang, H. Li, X. Wei, C. Jiang, J. L. Kirchherr, F. Gao, J. A. Anderson, L.
1642 H. Ping, R. Swanstrom, G. D. Tomaras, W. A. Blattner, P. A. Goepfert, J. M. Kilby, M. S.
1643 Saag, E. L. Delwart, M. P. Busch, M. S. Cohen, D. C. Montefiori, B. F. Haynes, B. Gaschen,
1644 G. S. Athreya, H. Y. Lee, N. Wood, C. Seoighe, A. S. Perelson, T. Bhattacharya, B. T.
1645 Korber, B. H. Hahn, G. M. Shaw, Identification and characterization of transmitted and

1646 early founder virus envelopes in primary HIV-1 infection. *Proceedings of the National*
1647 *Academy of Sciences* **105 (21)**, 7552-7557 (2008).
1648 30. D. J. Morris, J. Gorman, T. Zhou, J. Lora, A. J. Connell, H. Li, W. Liu, R. S. Roark, M. S.
1649 Campion, J. W. Carey, R. Habib, Y. Li, C. L. Martella, Y. Park, A. Singh, K. J. Sowers, I.-T.
1650 Teng, S. Wang, N. Chohan, W. Ding, C. Lauer, E. Lewis, R. D. Mason, J. M. Rando, L.
1651 Peyton, C. A. Schramm, K. Wagh, B. Korber, M. S. Seaman, D. C. Douek, B. F. Haynes, D.
1652 W. Kulp, M. Roederer, B. H. Hahn, P. D. Kwong, G. M. Shaw, Transient glycan-shield
1653 reduction induces CD4-binding site broadly neutralizing antibodies in SHIV-infected
1654 macaques. *Cell Reports, in press*, (bioRxiv doi:
1655 https://doi.org/10.1101/2024.1112.1130.630768) (2024).
1656 31. J. Gorman, C. Soto, M. M. Yang, T. M. Davenport, M. Guttman, R. T. Bailer, M.
1657 Chambers, G. Y. Chuang, B. J. Dekosky, N. A. Doria-Rose, A. Druz, M. J. Ernandes, I. S.
1658 Georgiev, M. C. Jarosinski, M. G. Joyce, T. M. Lemmin, S. Leung, M. K. Louder, J. R.
1659 McDaniel, S. Narpala, M. Pancera, J. Stuckey, X. Wu, Y. Yang, B. Zhang, T. Zhou, J. C.
1660 Mullikin, U. Baxa, G. Georgiou, A. B. McDermott, M. Bonsignori, B. F. Haynes, P. L.
1661 Moore, L. Morris, K. K. Lee, L. Shapiro, J. R. Mascola, P. D. Kwong, Structures of HIV-1
1662 Env V1V2 with broadly neutralizing antibodies reveal commonalities that enable vaccine
1663 design. *Nature Structural and Molecular Biology* **23 (1)**, 81-90 (2016).
1664 32. J. E. Voss, R. Andrabi, L. E. McCoy, N. de Val, R. P. Fuller, T. Messmer, C. Y. Su, D. Sok, S.
1665 N. Khan, F. Garces, L. K. Pritchard, R. T. Wyatt, A. B. Ward, M. Crispin, I. A. Wilson, D. R.
1666 Burton, Elicitation of Neutralizing Antibodies Targeting the V2 Apex of the HIV Envelope
1667 Trimer in a Wild-Type Animal Model. *Cell Reports* **21 (1)**, 222-235 (2017).
1668 33. M. Bonsignori, K. K. Hwang, X. Chen, C. Y. Tsao, L. Morris, E. Gray, D. J. Marshall, J. A.
1669 Crump, S. H. Kapiga, N. E. Sam, F. Sinangil, M. Pancera, Y. Yongping, B. Zhang, J. Zhu, P.
1670 D. Kwong, S. O'Dell, J. R. Mascola, L. Wu, G. J. Nabel, S. Phogat, M. S. Seaman, J. F.
1671 Whitesides, M. A. Moody, G. Kelsoe, X. Yang, J. Sodroski, G. M. Shaw, D. C. Montefiori, T.
1672 B. Kepler, G. D. Tomaras, S. M. Alam, H. X. Liao, B. F. Haynes, Analysis of a Clonal Lineage
1673 of HIV-1 Envelope V2/V3 Conformational Epitope-Specific Broadly Neutralizing
1674 Antibodies and Their Inferred Unmutated Common Ancestors. *Journal of Virology* **85**
1675 **(19)**, 9998-10009 (2011).
1676 34. K. O. Saunders, L. K. Verkoczy, C. Jiang, J. Zhang, R. Parks, H. Chen, M. Housman, H.
1677 Bouton-Verville, X. Shen, A. M. Trama, R. Scearce, L. Sutherland, S. Santra, A. Newman,
1678 A. Eaton, K. Xu, I. S. Georgiev, M. G. Joyce, G. D. Tomaras, M. Bonsignori, S. G. Reed, A.
1679 Salazar, J. R. Mascola, M. A. Moody, D. W. Cain, M. Centlivre, S. Zurawski, G. Zurawski,
1680 H. P. Erickson, P. D. Kwong, S. M. Alam, Y. Levy, D. C. Montefiori, B. F. Haynes, Vaccine
1681 induction of heterologous tier 2 HIV-1 neutralizing antibodies in animal models. *Cell*
1682 *Reports* **21 (13)**, 3681-3690 (2017).
1683 35. R. Andrabi, J. E. Voss, C. H. Liang, B. Briney, L. E. McCoy, C. Y. Wu, C. H. Wong, P.
1684 Poignard, D. R. Burton, Identification of Common Features in Prototype Broadly
1685 Neutralizing Antibodies to HIV Envelope V2 Apex to Facilitate Vaccine Design. *Immunity*
1686 **43 (5)**, 959-973 (2015).
1687 36. C. R. Brown, M. Czapiga, J. Kabat, Q. Dang, I. Ourmanov, Y. Nishimura, M. A. Martin, V.
1688 M. Hirsch, Unique Pathology in Simian Immunodeficiency Virus-Infected Rapid

Progressor Macaques Is Consistent with a Pathogenesis Distinct from That of Classical AIDS. *Journal of Virology* **81 (11)**, 5594-5606 (2007).

37. V. M. Hirsch, S. Santra, S. Goldstein, R. Plishka, A. Buckler-White, A. Seth, I. Ourmanov, C. R. Brown, R. Engle, D. Montefiori, J. Glowczwskie, K. Kunstman, S. Wolinsky, N. L. Letvin, Immune Failure in the Absence of Profound CD4+ T-Lymphocyte Depletion in Simian Immunodeficiency Virus-Infected Rapid Progressor Macaques. *Journal of Virology* **78 (1)**, 275-284 (2004).

38. M. G. Pauthner, J. P. Nkolola, C. Havenar-Daughton, B. Murrell, S. M. Reiss, R. Bastidas, J. Prévost, R. Nedellec, B. v. Bredow, P. Abbink, C. A. Cottrell, D. W. Kulp, T. Tokatlian, B. Nogal, M. Bianchi, H. Li, J. H. Lee, S. T. Butera, D. T. Evans, L. Hangartner, A. Finzi, I. A. Wilson, R. T. Wyatt, D. J. Irvine, W. R. Schief, A. B. Ward, R. W. Sanders, S. Crotty, G. M. Shaw, D. H. Barouch, D. R. Burton, Vaccine-Induced Protection from Homologous Tier 2 SHIV Challenge in Nonhuman Primates Depends on Serum-Neutralizing Antibody Titers. *Immunity* **50 (1)**, 241-252.e246 (2019).

39. A. Pegu, B. Borate, Y. Huang, M. G. Pauthner, A. J. Hessell, B. Julg, N. A. Doria-Rose, S. D. Schmidt, L. N. Carpp, M. D. Cully, X. Chen, G. M. Shaw, D. H. Barouch, N. L. Haigwood, L. Corey, D. R. Burton, M. Roederer, P. B. Gilbert, J. R. Mascola, Y. Huang, A meta-analysis of passive immunization studies shows an association of serum neutralizing antibody titer with protection against SHIV challenge. *Cell Host & Microbe* **26 (3)**, 336-346.e333 (2019).

40. B. K. Felber, Z. Lu, X. Hu, A. Valentin, M. Rosati, C. A. Remmel, J. A. Weiner, M. C. Carpenter, K. Faircloth, S. Stanfield-Oakley, W. B. Williams, X. Shen, G. D. Tomaras, C. C. LaBranche, D. Montefiori, H. V. Trinh, M. Rao, M. S. Alam, N. A. Vandergrift, K. O. Saunders, Y. Wang, W. Rountree, J. Das, G. Alter, S. G. Reed, P. P. Aye, F. Schiro, B. Pahar, J. P. Dufour, R. S. Veazey, P. A. Marx, D. J. Venzon, G. M. Shaw, G. Ferrari, M. E. Ackerman, B. F. Haynes, G. N. Pavlakis, Co-immunization of DNA and Protein in the Same Anatomical Sites Induces Superior Protective Immune Responses against SHIV Challenge. *Cell Reports* **31 (6)**, 107624 (2020).

41. K. O. Saunders, L. Wang, M. G. Joyce, Z.-Y. Yang, A. B. Balazs, C. Cheng, S.-Y. Ko, W.-P. Kong, R. S. Rudicell, I. S. Georgiev, L. Duan, K. E. Foulds, M. Donaldson, L. Xu, S. D. Schmidt, J.-P. Todd, D. Baltimore, M. Roederer, A. T. Haase, P. D. Kwong, S. S. Rao, J. R. Mascola, G. J. Nabel, Broadly Neutralizing Human Immunodeficiency Virus Type 1 Antibody Gene Transfer Protects Nonhuman Primates from Mucosal Simian-Human Immunodeficiency Virus Infection. *Journal of Virology* **89 (16)**, 8334–8345 (2015).

42. J.-P. Julien, J. H. Lee, A. Cupo, C. D. Murin, R. Derking, S. Hoffenberg, M. J. Caulfield, C. R. King, A. J. Marozsan, P. J. Klasse, R. W. Sanders, J. P. Moore, I. A. Wilson, A. B. Ward, Asymmetric recognition of the HIV-1 trimer by broadly neutralizing antibody PG9. *Proceedings of the National Academy of Sciences* **110 (11)**, 4351-4356 (2013).

43. J. S. McLellan, M. Pancera, C. Carrico, J. Gorman, J. P. Julien, R. Khayat, R. Louder, R. Pejchal, M. Sastry, K. Dai, S. O'Dell, N. Patel, S. Shahzad-Ul-Hussan, Y. Yang, B. Zhang, T. Zhou, J. Zhu, J. C. Boyington, G. Y. Chuang, D. Diwanji, I. Georgiev, Y. Do Kwon, D. Lee, M. K. Louder, S. Moquin, S. D. Schmidt, Z. Y. Yang, M. Bonsignori, J. A. Crump, S. H. Kapiga, N. E. Sam, B. F. Haynes, D. R. Burton, W. C. Koff, L. M. Walker, S. Phogat, R. Wyatt, J. Orwenyo, L. X. Wang, J. Arthos, C. A. Bewley, J. R. Mascola, G. J. Nabel, W. R. Schief, A. B.

Ward, I. A. Wilson, P. D. Kwong, Structure of HIV-1 gp120 V1/V2 domain with broadly neutralizing antibody PG9. *Nature* **480 (7377)**, 336-343 (2011).

44. R. Pejchal, L. M. Walker, R. L. Stanfield, S. K. Phogat, W. C. Koff, P. Poignard, D. R. Burton, I. A. Wilson, R. Pejchal, L. M. Walker, R. L. Stanfield, S. K. Phogat, W. C. Koff, P. Poignard, D. R. Burton, I. A. Wilson, Structure and function of broadly reactive antibody PG16 reveal an H3 subdomain that mediates potent neutralization of HIV-1. *Proceedings of the National Academy of Sciences* **107 (25)**, (2010).

45. J. Gorman, G.-Y. Chuang, Y.-T. Lai, C.-H. Shen, J. C. Boyington, A. Druz, H. Geng, M. K. Louder, K. McKee, R. Rawi, R. Verardi, Y. Yang, B. Zhang, N. A. Doria-Rose, B. Lin, P. L. Moore, L. Morris, L. Shapiro, J. R. Mascola, P. D. Kwong, Structure of Super-Potent Antibody CAP256-VRC26.25 in Complex with HIV-1 Envelope Reveals a Combined Mode of Trimer-Apex Recognition. *Cell Reports* **31 (1)**, 107488 (2020).

46. E. Landais, B. Murrell, B. Briney, S. Murrell, K. Rantalainen, Z. T. Berndsen, A. Ramos, L. Wickramasinghe, M. L. Smith, K. Eren, N. de Val, M. Wu, A. Cappelletti, J. Umotoy, Y. Lie, T. Wrin, P. Algate, P. Y. Chan-Hui, E. Karita, A. B. Ward, I. A. Wilson, D. R. Burton, D. Smith, S. L. K. Pond, P. Poignard, HIV Envelope Glycoform Heterogeneity and Localized Diversity Govern the Initiation and Maturation of a V2 Apex Broadly Neutralizing Antibody Lineage. *Immunity* **47 (5)**, 990-1003.e1009 (2017).

47. C. A. Schramm, Z. Sheng, Z. Zhang, J. R. Mascola, P. D. Kwong, L. Shapiro, SONAR: A high-throughput pipeline for inferring antibody ontogenies from longitudinal sequencing of B cell transcripts. *Frontiers in Immunology* **7**, 372 (2016).

48. M. M. Corcoran, G. E. Phad, N. V. Bernat, C. Stahl-Hennig, N. Sumida, M. A. A. Persson, M. Martin, G. B. K. Hedestam, Production of individualized v gene databases reveals high levels of immunoglobulin genetic diversity. *Nature Communications* **7 (1)**, 1-14 (2016).

49. N. Vázquez Bernat, M. Corcoran, U. Hardt, M. Kaduk, G. E. Phad, M. Martin, G. B. Karlsson Hedestam, High-Quality Library Preparation for NGS-Based Immunoglobulin Germline Gene Inference and Repertoire Expression Analysis. *Frontiers in Immunology* **10**, 660 (2019).

50. M. Lee, A. Changela, J. Gorman, R. Rawi, T. Bylund, C. W. Chao, B. C. Lin, M. K. Louder, A. S. Olia, B. Zhang, N. A. Doria-Rose, S. Zolla-Pazner, L. Shapiro, G.-Y. Chuang, P. D. Kwong, M. Lee, A. Changela, J. Gorman, R. Rawi, T. Bylund, C. W. Chao, B. C. Lin, M. K. Louder, A. S. Olia, B. Zhang, N. A. Doria-Rose, S. Zolla-Pazner, L. Shapiro, G.-Y. Chuang, P. D. Kwong, Extended antibody-framework-to-antigen distance observed exclusively with broad HIV-1-neutralizing antibodies recognizing glycan-dense surfaces. *Nature Communications* **12 (1)**, 6470 (2021).

51. B. Briney, A. Inderbitzin, C. Joyce, D. R. Burton, B. Briney, A. Inderbitzin, C. Joyce, D. R. Burton, Commonality despite exceptional diversity in the baseline human antibody repertoire. *Nature* **566 (7744)**, 393–397 (2019).

52. K. B. Hoehn, J. A. V. Heiden, J. Q. Zhou, G. Lunter, O. G. Pybus, S. H. Kleinstein, K. B. Hoehn, J. A. Vander Heiden, J. Q. Zhou, G. Lunter, O. G. Pybus, S. H. Kleinstein, Repertoire-wide phylogenetic models of B cell molecular evolution reveal evolutionary signatures of aging and vaccination. *Proceedings of the National Academy of Sciences* **116 (45)**, 22664-22672 (2019).

53. K. B. Hoehn, G. Lunter, O. G. Pybus, A Phylogenetic Codon Substitution Model for Antibody Lineages. *Genetics* **206 (1)**, 417-427 (2017).
54. A. Ghosh, Companion Manuscript.
55. B. T. Grenfell, O. G. Pybus, J. R. Gog, J. L. N. Wood, J. M. Daly, J. A. Mumford, E. C. Holmes, Unifying the Epidemiological and Evolutionary Dynamics of Pathogens. *Science* **303 (5656)**, 327-332 (2004).
56. D. T. MacLeod, N. M. Choi, B. Briney, F. Garces, L. S. Ver, E. Landais, B. Murrell, T. Wrin, W. Kilembe, C. H. Liang, A. Ramos, C. B. Bian, L. Wickramasinghe, L. Kong, K. Eren, C. Y. Wu, C. H. Wong, S. L. Kosakovsky Pond, I. A. Wilson, D. R. Burton, P. Poignard, The IAVI Protocol C. Investigators, Early Antibody Lineage Diversification and Independent Limb Maturation Lead to Broad HIV-1 Neutralization Targeting the Env High-Mannose Patch. *Immunity* **44 (5)**, 1215-1226 (2016).
57. Thomas B. Kepler, H.-X. Liao, S. M. Alam, R. Bhaskarabhatla, R. Zhang, C. Yandava, S. Stewart, K. Anasti, G. Kelsoe, R. Parks, Krissey E. Lloyd, C. Stolarchuk, J. Pritchett, E. Solomon, E. Friberg, L. Morris, Salim S. A. Karim, Myron S. Cohen, E. Walter, M. A. Moody, Barton F. Haynes, Immunoglobulin Gene Insertions and Deletions in the Affinity Maturation of HIV-1 Broadly Reactive Neutralizing Antibodies. *Cell Host & Microbe* **16 (3)**, 304–313 (2014).
58. K. Wiehe, T. Bradley, R. R. Meyerhoff, C. Hart, W. B. Williams, D. Easterhoff, W. J. Faison, T. B. Kepler, K. O. Saunders, S. M. Alam, M. Bonsignori, B. F. Haynes, Functional Relevance of Improbable Antibody Mutations for HIV Broadly Neutralizing Antibody Development. *Cell Host & Microbe* **23 (6)**, 759-765.e756 (2018).
59. J. van Schooten, E. Farokhi, A. Schorcht, T. L. G. M. van den Kerkhof, H. Gao, P. v. d. Woude, J. A. Burger, T. G. R. Meesters, T. Bijl, R. Ghalaiyini, H. L. Turner, J. Dorning, B. D. C. van Schaik, A. H. C. van Kampen, C. C. Labranche, R. L. Stanfield, D. Sok, D. C. Montefiori, D. R. Burton, M. S. Seaman, G. Ozorowski, I. A. Wilson, R. W. Sanders, A. B. Ward, M. J. van Gils, Identification of IOMA-class neutralizing antibodies targeting the CD4-binding site on the HIV-1 envelope glycoprotein. *Nature Communications* **13 (1)**, 4515 (2022).
60. R. M. Lynch, P. Wong, L. Tran, S. O'Dell, M. C. Nason, Y. Li, X. Wu, J. R. Mascola, HIV-1 Fitness Cost Associated with Escape from the VRC01 Class of CD4 Binding Site Neutralizing Antibodies. *Journal of Virology* **89 (8)**, 4201-4213 (2015).
61. J. N. Bhiman, C. Anthony, N. A. Doria-Rose, O. Karimanzira, C. A. Schramm, T. Khoza, D. Kitchin, G. Botha, J. Gorman, N. J. Garrett, S. S. A. Karim, L. Shapiro, C. Williamson, P. D. Kwong, J. R. Mascola, L. Morris, P. L. Moore, Viral variants that initiate and drive maturation of V1V2-directed HIV-1 broadly neutralizing antibodies. *Nature Medicine* **21 (11)**, 1332-1336 (2015).
62. C. K. Wibmer, J. N. Bhiman, E. S. Gray, N. Tumba, S. S. Abdool Karim, C. Williamson, L. Morris, P. L. Moore, Viral Escape from HIV-1 Neutralizing Antibodies Drives Increased Plasma Neutralization Breadth through Sequential Recognition of Multiple Epitopes and Immunotypes. *PLoS Pathogens* **9 (10)**, e1003738 (2013).
63. F. A. Schleich, S. Bale, J. Guenaga, G. Ozorowski, M. Adori, X. Lin, X. Castro Dopico, R. Wilson, M. Chernyshev, A. T. Cotgreave, M. Mandolesi, J. Cluff, E. D. Doyle, L. M. Sewall, W. H. Lee, S. Zhang, S. O'Dell, B. S. Healy, D. Lim, V. R. Lewis, E. Ben-Akiva, D. J. Irvine, N.

A. Doria-Rose, M. Corcoran, D. Carnathan, G. Silvestri, I. A. Wilson, A. B. Ward, G. B. Karlsson Hedestam, R. T. Wyatt, Vaccination of nonhuman primates elicits a broadly neutralizing antibody lineage targeting a quaternary epitope on the HIV-1 Env trimer. *Immunity*, https://doi.org/10.1016/j.immuni.2025.1004.1010 (2025).

64. R. Habib, S. O. Solieva, Z. J. Lin, S. Ghosh, K. Bayruns, M. Singh, C. J. Agostino, N. J. Tursi, K. J. Sowers, J. Huang, R. S. Roark, M. Purwar, Y. Park, K. Ayyanathan, H. Li, J. W. Carey, A. Kim, J. Park, M. E. McCanna, A. N. Skelly, N. Chokkalingam, S. Kriete, N. Shupin, A. Huynh, S. Walker, N. Laenger, J. Du, J. Cui, B. H. Hahn, A. Patel, A. Escolano, P. D. Kwong, L. Shapiro, G. R. Bowman, G. M. Shaw, D. B. Weiner, J. Pallesen, D. W. Kulp, Deep Mining of the Human Antibody Repertoire Identifies Frequent and Immunogenetically Diverse CDRH3 Topologies Targetable by Vaccination. *Nature Communications, in review*, (bioRxiv doi: https://doi.org/10.1101/2024.1110.1104.616739) (2024).

65. J. H. Lee, R. Andrabi, C. Y. Su, A. Yasmeen, J. P. Julien, L. Kong, N. C. Wu, R. McBride, D. Sok, M. Pauthner, C. A. Cottrell, T. Nieusma, C. Blattner, J. C. Paulson, P. J. Klasse, I. A. Wilson, D. R. Burton, A. B. Ward, A Broadly Neutralizing Antibody Targets the Dynamic HIV Envelope Trimer Apex via a Long, Rigidified, and Anionic β-Hairpin Structure. *Immunity* **46 (4)**, 690-702 (2017).

66. J. R. Willis, Z. T. Berndsen, K. M. Ma, J. M. Steichen, T. Schiffner, E. Landais, A. Liguori, O. Kalyuzhniy, J. D. Allen, S. Baboo, O. Omorodion, J. K. Diedrich, X. Hu, E. Georgeson, N. Phelps, S. Eskandarzadeh, B. Groschel, M. Kubitz, Y. Adachi, T.-M. Mullin, N. B. Alavi, S. Falcone, S. Himansu, A. Carfi, I. A. Wilson, J. R. Yates, J. C. Paulson, M. Crispin, A. B. Ward, W. R. Schief, Human immunoglobulin repertoire analysis guides design of vaccine priming immunogens targeting HIV V2-apex broadly neutralizing antibody precursors. *Immunity* **55 (11)**, 2149-2167.e2149 (2022).

67. X. Wei, S. K. Ghosh, M. E. Taylor, V. A. Johnson, E. A. Emini, P. Deutsch, J. D. Lifson, S. Bonhoeffer, M. A. Nowak, B. H. Hahn, M. S. Saag, G. M. Shaw, X. Wei, S. K. Ghosh, M. E. Taylor, V. A. Johnson, E. A. Emini, P. Deutsch, J. D. Lifson, S. Bonhoeffer, M. A. Nowak, B. H. Hahn, M. S. Saag, G. M. Shaw, Viral dynamics in human immunodeficiency virus type 1 infection. *Nature* **373 (6510)**, 117-122 (1995).

68. D. D. Ho, A. U. Neumann, A. S. Perelson, W. Chen, J. M. Leonard, M. Markowitz, D. D. Ho, A. U. Neumann, A. S. Perelson, W. Chen, J. M. Leonard, M. Markowitz, Rapid turnover of plasma virions and CD4 lymphocytes in HIV-1 infection. *Nature* **373 (6510)**, 123-126 (1995).

69. M. Markowitz, M. Louie, A. Hurley, E. Sun, M. Di Mascio, A. S. Perelson, D. D. Ho, A Novel Antiviral Intervention Results in More Accurate Assessment of Human Immunodeficiency Virus Type 1 Replication Dynamics and T-Cell Decay In Vivo. *Journal of Virology* **77 (8)**, 5037-5038 (2003).

70. V. Simon, D. D. Ho, HIV-1 dynamics in vivo: implications for therapy. *Nature Reviews Microbiology* **1 (3)**, 181-190 (2003).

71. X. Wei, J. M. Decker, S. Wang, H. Hui, J. C. Kappes, X. Wu, J. F. Salazar-Gonzalez, M. G. Salazar, J. M. Kilby, M. S. Saag, N. L. Komarova, M. A. Nowak, B. H. Hahn, P. D. Kwong, G. M. Shaw, Antibody neutralization and escape by HIV-1. *Nature* **422 (6929)**, 307-312 (2003).

72. K. J. Bar, C.-y. Tsao, S. S. Iyer, J. M. Decker, Y. Yang, M. Bonsignori, X. Chen, K.-K. Hwang, D. C. Montefiori, H.-X. Liao, P. Hraber, W. Fischer, H. Li, S. Wang, S. Sterrett, B. F. Keele, V. V. Ganusov, A. S. Perelson, B. T. Korber, I. Georgiev, J. S. McLellan, J. W. Pavlicek, F. Gao, B. F. Haynes, B. H. Hahn, P. D. Kwong, G. M. Shaw, Early Low-Titer Neutralizing Antibodies Impede HIV-1 Replication and Select for Virus Escape. *PLoS Pathogens* **8 (5)**, e1002721 (2012).

73. H. Wang, C. Cheng, J. L. D. Santo, C.-H. Shen, T. Bylund, A. R. Henry, C. A. Howe, J. Hwang, N. C. Morano, D. J. Morris, S. Pletnev, R. S. Roark, T. Zhou, B. T. Hansen, F. H. Hoyt, T. S. Johnston, S. Wang, B. Zhang, D. R. Ambrozak, J. E. Becker, M. F. Bender, A. Changela, R. Chaudhary, M. Corcoran, A. R. Corrigan, K. E. Foulds, Y. Guo, M. Lee, Y. Li, B. C. Lin, T. Liu, M. K. Louder, M. Mandolesi, R. D. Mason, K. McKee, V. Nair, S. O'Dell, A. S. Olia, L. Ou, A. Pegu, N. Raju, R. Rawi, J. Roberts-Torres, E. K. Sarfo, M. Sastry, A. J. Schaub, S. D. Schmidt, C. A. Schramm, C. L. Schwartz, S. C. Smith, T. Stephens, J. Stuckey, I.-T. Teng, J.-P. Todd, Y. Tsybovsky, D. J. V. Wazer, S. Wang, N. A. Doria-Rose, E. R. Fischer, I. S. Georgiev, G. B. K. Hedestam, Z. Sheng, R. A. Woodward, D. C. Douek, R. A. Koup, T. C. Pierson, L. Shapiro, G. M. Shaw, J. R. Mascola, P. D. Kwong, Potent and broad HIV-1 neutralization in fusion peptide-primed SHIV-infected macaques. *Cell* **187 (25)**, 7214-7231.e7223 (2024).

74. N. Goonetilleke, M. K. Liu, J. F. Salazar-Gonzalez, G. Ferrari, E. Giorgi, V. V. Ganusov, B. F. Keele, G. H. Learn, E. L. Turnbull, M. G. Salazar, K. J. Weinhold, S. Moore, CHAVI Clinical Core B, N. Letvin, B. F. Haynes, M. S. Cohen, P. Hraber, T. Bhattacharya, P. Borrow, A. S. Perelson, B. H. Hahn, G. M. Shaw, B. T. Korber, A. J. McMichael, The first T cell response to transmitted/founder virus contributes to the control of acute viremia in HIV-1 infection. *The Journal of Experimental Medicine* **206 (6)**, 1253-1272 (2009).

75. J. F. Salazar-Gonzalez, M. G. Salazar, B. F. Keele, G. H. Learn, E. E. Giorgi, H. Li, J. M. Decker, S. Wang, J. Baalwa, M. H. Kraus, N. F. Parrish, K. S. Shaw, M. B. Guffey, K. J. Bar, K. L. Davis, C. Ochsenbauer-Jambor, J. C. Kappes, M. S. Saag, M. S. Cohen, J. Mulenga, C. A. Derdeyn, S. Allen, E. Hunter, M. Markowitz, P. Hraber, A. S. Perelson, T. Bhattacharya, B. F. Haynes, B. T. Korber, B. H. Hahn, G. M. Shaw, Genetic identity, biological phenotype, and evolutionary pathways of transmitted/founder viruses in acute and early HIV-1 infection. *The Journal of Experimental Medicine* **206 (6)**, 1273-1289 (2009).

76. H. Song, J. W. Pavlicek, F. Cai, T. Bhattacharya, H. Li, S. S. Iyer, K. J. Bar, J. M. Decker, N. Goonetilleke, M. K. Liu, A. Berg, B. Hora, M. S. Drinker, J. Eudailey, J. Pickeral, M. A. Moody, G. Ferrari, A. McMichael, A. S. Perelson, G. M. Shaw, B. H. Hahn, B. F. Haynes, F. Gao, Impact of immune escape mutations on HIV-1 fitness in the context of the cognate transmitted/founder genome. *Retrovirology* **9**, 89 (2012).

77. R. Andrabi, Germline-targeting HIV immunogen induces cross-neutralizing antibodies in outbred macaques. *Submitted*, (2025).

78. P. L. Moore, E. S. Gray, C. K. Wibmer, J. N. Bhiman, M. Nonyane, D. J. Sheward, T. Hermanus, S. Bajimaya, N. L. Tumba, M.-R. Abrahams, B. E. Lambson, N. Ranchobe, L. Ping, N. Ngandu, Q. A. Karim, S. S. A. Karim, R. I. Swanstrom, M. S. Seaman, C. Williamson, L. Morris, P. L. Moore, E. S. Gray, C. K. Wibmer, J. N. Bhiman, M. Nonyane, D. J. Sheward, T. Hermanus, S. Bajimaya, N. L. Tumba, M.-R. Abrahams, B. E. Lambson, N. Ranchobe, L. Ping, N. Ngandu, Q. A. Karim, S. S. A. Karim, R. I. Swanstrom, M. S.

Seaman, C. Williamson, L. Morris, Evolution of an HIV glycan–dependent broadly neutralizing antibody epitope through immune escape. *Nature Medicine* **18 (11)**, 1688-1692 (2012).

79. V. Dubrovskaya, J. Guenaga, N. d. Val, R. Wilson, Y. Feng, A. Movsesyan, G. B. K. Hedestam, A. B. Ward, R. T. Wyatt, c. *PLoS Pathogens* **13 (9)**, e1006614 (2017).

80. T. Zhou, N. A. Doria-Rose, C. Cheng, G. B. E. Stewart-Jones, G.-Y. Chuang, M. Chambers, A. Druz, H. Geng, K. McKee, Y. D. Kwon, S. O'Dell, M. Sastry, S. D. Schmidt, K. Xu, L. Chen, R. E. Chen, M. K. Louder, M. Pancera, T. G. Wanninger, B. Zhang, P. D. Kwong, Quantification of the Impact of the HIV-1-Glycan Shield on Antibody Elicitation. *Cell Reports* **19 (4)**, 719-732 (2017).

81. E. T. Crooks, K. Osawa, T. Tong, S. L. Grimley, Y. D. Dai, R. G. Whalen, D. W. Kulp, S. Menis, W. R. Schief, J. M. Binley, Effects of Partially Dismantling the CD4 Binding Site Glycan Fence of HIV-1 Envelope Glycoprotein Trimers on Neutralizing Antibody Induction. *Virology* **505**, (2017).

82. L. M. Walker, S. K. Phogat, P.-Y. Chan-Hui, D. Wagner, P. Phung, J. L. Goss, T. Wrin, M. D. Simek, S. Fling, J. L. Mitcham, J. K. Lehrman, F. H. Priddy, O. A. Olsen, S. M. Frey, P. W. Hammond, Protocol G Principal Investigators, S. Kaminsky, T. Zamb, M. Moyle, W. C. Koff, P. Poignard, D. R. Burton, Broad and Potent Neutralizing Antibodies from an African Donor Reveal a New HIV-1 Vaccine Target. *Science* **326 (5950)**, 285-289 (2009).

83. M. D. Simek, W. Rida, F. H. Priddy, P. Pung, E. Carrow, D. S. Laufer, J. K. Lehrman, M. Boaz, T. Tarragona-Fiol, G. Miiro, J. Birungi, A. Pozniak, D. A. McPhee, O. Manigart, E. Karita, A. Inwoley, W. Jaoko, J. DeHovitz, L.-G. Bekker, P. Pitisuttithum, R. Paris, L. M. Walker, P. Poignard, T. Wrin, P. E. Fast, D. R. Burton, W. C. Koff, Human Immunodeficiency Virus Type 1 Elite Neutralizers: Individuals with Broad and Potent Neutralizing Activity Identified by Using a High-Throughput Neutralization Assay together with an Analytical Selection Algorithm. *Journal of Virology* **83 (14)**, 7337-7348 (2009).

84. M. A. Moody, I. Pedroza-Pacheco, N. A. Vandergrift, C. Chui, K. E. Lloyd, R. Parks, K. A. Soderberg, A. T. Ogbe, M. S. Cohen, H.-X. Liao, F. Gao, A. J. McMichael, D. C. Montefiori, L. Verkoczy, G. Kelsoe, J. Huang, P. R. Shea, M. Connors, P. Borrow, B. F. Haynes, Immune perturbations in HIV-1–infected individuals who make broadly neutralizing antibodies. *Science Immunology* **1 (1)**, aag0851 (2016).

85. S. J. Krebs, Y. D. Kwon, C. A. Schramm, W. H. Law, G. Donofrio, K. H. Zhou, S. Gift, V. Dussupt, I. S. Georgiev, S. Schätzle, J. R. McDaniel, Y. T. Lai, M. Sastry, B. Zhang, M. C. Jarosinski, A. Ransier, A. L. Chenine, M. Asokan, R. T. Bailer, M. Bose, A. Cagigi, E. M. Cale, G. Y. Chuang, S. Darko, J. I. Driscoll, A. Druz, J. Gorman, F. Laboune, M. K. Louder, K. McKee, L. Mendez, M. A. Moody, A. M. O'Sullivan, C. Owen, D. Peng, R. Rawi, E. Sanders-Buell, C. H. Shen, A. R. Shiakolas, T. Stephens, Y. Tsybovsky, C. Tucker, R. Verardi, K. Wang, J. Zhou, T. Zhou, G. Georgiou, S. M. Alam, B. F. Haynes, M. Rolland, G. R. Matyas, V. R. Polonis, A. B. McDermott, D. C. Douek, L. Shapiro, S. Tovanabutra, N. L. Michael, J. R. Mascola, M. L. Robb, P. D. Kwong, N. A. Doria-Rose, Longitudinal Analysis Reveals Early Development of Three MPER-Directed Neutralizing Antibody Lineages from an HIV-1-Infected Individual. *Immunity* **50 (3)**, 677-691.e613 (2019).

86. V. Bhardwaj, M. Franceschetti, R. Rao, P. A. Pevzner, Y. Safonova, Automated analysis of immunosequencing datasets reveals novel immunoglobulin D genes across diverse species. *PLOS Computational Biology* **16 (4)**, e1007837 (2020).
87. N. Vázquez Bernat, M. Corcoran, I. Nowak, M. Kaduk, X. Castro Dopico, S. Narang, P. Maisonasse, N. Dereuddre-Bosquet, B. Murrell, G. B. Karlsson Hedestam, Rhesus and cynomolgus macaque immunoglobulin heavy-chain genotyping yields comprehensive databases of germline VDJ alleles. *Immunity* **54 (2)**, 355-366.e354 (2021).
88. A. Ramesh, S. Darko, A. Hua, G. Overman, A. Ransier, J. R. Francica, A. Trama, G. D. Tomaras, B. F. Haynes, D. C. Douek, T. B. Kepler, Structure and diversity of the rhesus macaque immunoglobulin loci through multiple de novo genome assemblies. *Frontiers in Immunology* **8**, 1407 (2017).
89. F. Breden, E. T. Luning Prak, B. Peters, F. Rubelt, C. A. Schramm, C. E. Busse, J. A. Vander Heiden, S. Christley, S. A. C. Bukhari, A. Thorogood, F. A. Matsen IV, Y. Wine, U. Laserson, D. Klatzmann, D. C. Douek, M.-P. Lefranc, A. M. Collins, T. Bubela, S. H. Kleinstein, C. T. Watson, L. G. Cowell, J. K. Scott, T. B. Kepler, Reproducibility and Reuse of Adaptive Immune Receptor Repertoire Data. *Frontiers in Immunology* **8**, 1418 (2017).
90. M. Martin, Cutadapt removes adapter sequences from high-throughput sequencing reads. *EMBnet Journal* **17**, 10-12 (2011).
91. J. Zhang, K. Kobert, T. Flouri, A. Stamatakis, PEAR: a fast and accurate Illumina Paired-End reAd mergeR. *Bioinformatics* **30 (5)**, 614-620 (2014).
92. F. Mölder, K. P. Jablonski, B. Letcher, M. B. Hall, C. H. Tomkins-Tinch, V. Sochat, J. Forster, S. Lee, S. O. Twardziok, A. Kanitz, A. Wilm, M. Holtgrewe, S. Rahmann, S. Nahnsen, J. Köster, F. Mölder, K. P. Jablonski, B. Letcher, M. B. Hall, C. H. Tomkins-Tinch, V. Sochat, J. Forster, S. Lee, S. O. Twardziok, A. Kanitz, A. Wilm, M. Holtgrewe, S. Rahmann, S. Nahnsen, J. Köster, Sustainable data analysis with Snakemake. *F1000Research* **10**, 33 (2021).
93. D. Trudgian, G. M. Kurtzer, cclerget, M. Bauer, I. Kaneshiro, D. Godlove, Vanessasaurus, Y. Cote, C. E. A. Gutierrez, G. Vallee, DrDaveD, J. Cook, A. Hughes, J. Stover, B. P. Bockelman, M. Magallon, J. Chappell, M. Frisch, D. Tamino, C. Madison, S. Yakovtseva, A. Duffy, S. Ghosh, VP, T. Huynh, M. Gray, Y. Halchenko, F. Abecassis, sylabs/singularity: SingularityCE 4.3.1. *Zenodo*, (2015).
94. A. Punjani, J. L. Rubinstein, D. J. Fleet, M. A. Brubaker, A. Punjani, J. L. Rubinstein, D. J. Fleet, M. A. Brubaker, cryoSPARC: algorithms for rapid unsupervised cryo-EM structure determination. *Nature Methods* **14 (3)**, 290-296 (2017).
95. E. F. Pettersen, T. D. Goddard, C. C. Huang, E. C. Meng, G. S. Couch, T. I. Croll, J. H. Morris, T. E. Ferrin, UCSF ChimeraX: Structure visualization for researchers, educators, and developers. *Protein Science* **30 (1)**, 70-82 (2021).
96. P. Emsley, K. Cowtan, Coot: model-building tools for molecular graphics. *Acta Crystallographica Section D* **60 (Pt 12 Pt 1)**, 2126-2132 (2004).
97. P. D. Adams, K. Gopal, R. W. Grosse-Kunstleve, L.-W. Hung, T. R. Ioerger, A. J. McCoy, N. W. Moriarty, R. K. Pai, R. J. Read, T. D. Romo, J. C. Sacchettini, N. K. Sauter, L. C. Storoni, T. C. Terwilliger, Recent developments in the PHENIX software for automated crystallographic structure determination. *Journal of Synchrotron Radiation* **11 (Pt 1)**, 53-55 (2004).

98. I. W. Davis, L. W. Murray, J. S. Richardson, D. C. Richardson, MolProbity: structure validation and all-atom contact analysis for nucleic acids and their complexes. *Nucleic Acids Research* **35 (suppl_2)**, W375–W383 (2004).

99. B. A. Barad, N. Echols, R. Y.-R. Wang, Y. Cheng, F. DiMaio, P. D. Adams, J. S. Fraser, B. A. Barad, N. Echols, R. Y.-R. Wang, Y. Cheng, F. DiMaio, P. D. Adams, J. S. Fraser, EMRinger: side chain–directed model and map validation for 3D cryo-electron microscopy. *Nature Methods* **12 (10)**, 943-946 (2015).

100. C. A. Bricault, K. Yusim, M. S. Seaman, H. Yoon, J. Theiler, E. E. Giorgi, K. Wagh, M. Theiler, P. Hraber, J. P. Macke, E. F. Kreider, G. H. Learn, B. H. Hahn, J. F. Scheid, J. M. Kovacs, J. L. Shields, C. L. Lavine, F. Ghantous, M. Rist, M. G. Bayne, G. H. Neubauer, K. McMahan, H. Peng, C. Chéneau, J. J. Jones, J. Zeng, C. Ochsenbauer, J. P. Nkolola, K. E. Stephenson, B. Chen, S. Gnanakaran, M. Bonsignori, L. D. Williams, B. F. Haynes, N. Doria-Rose, J. R. Mascola, D. C. Montefiori, D. H. Barouch, B. Korber, HIV-1 Neutralizing Antibody Signatures and Application to Epitope-Targeted Vaccine Design. *Cell Host & Microbe* **25 (1)**, 59-72.e58 (2019).

101. A. Changela, X. Wu, Y. Yang, B. Zhang, J. Zhu, G. A. Nardone, S. O'Dell, M. Pancera, M. K. Gorny, S. Phogat, J. E. Robinson, L. Stamatatos, S. Zolla-Pazner, J. R. Mascola, P. D. Kwong, Crystal Structure of Human Antibody 2909 Reveals Conserved Features of Quaternary Structure-Specific Antibodies That Potently Neutralize HIV-1. *Journal of Virology* **85 (6)**, 2524-2535. (2010).

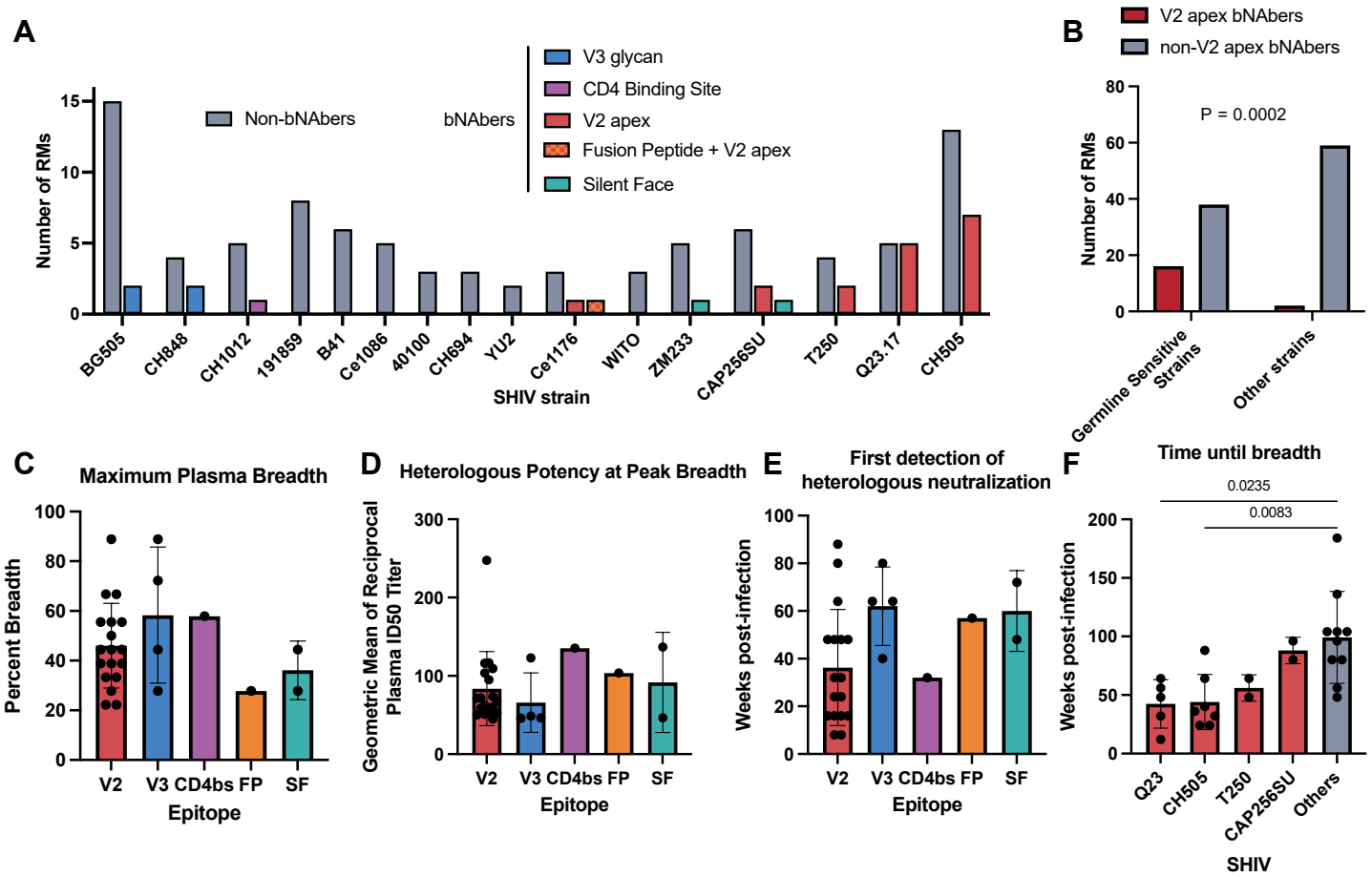

Fig. 1. HIV-1 Envs with a predilection for V2 apex bNAb induction. (**A**) Numbers of RMs infected with SHIV strains expressing different primary HIV-1 Envs that elicited V2 apex, V3 glycan, fusion peptide, CD4-binding site, or silent face bNAbs. RMs with bNAbs were defined as RMs with ID_{50} titers of ≥1:80 against two or more members of an 18-strain tier 1B/2 heterologous virus panel (**B**) SHIV strains expressing HIV-1 Envs that were previously shown to be sensitive to neutralization by V2 apex bNAb inferred germline (iGL) precursor antibodies or iGL-intermediate antibodies were significantly more likely to elicit V2 apex bNAbs compared with other strains (p = 0.0002; Fisher's Exact test). (**C**) Maximum plasma neutralization breadth (defined as percent of viruses neutralized at an ID_{50} titer of ≥1:20) achieved by RMs on an 18-strain heterologous tier 1B/2 virus panel, grouped by bNAb specificity. (**D**) Geometric means of heterologous plasma ID_{50} neutralization titers of RMs at the timepoint at which they showed maximum breadth. (**E**) Time (in weeks post-infection) until the first detection of any heterologous plasma neutralization by RMs, grouped by bNAb specificity. (**F**) Time (in weeks post-infection) until the acquisition of breadth that met our predermined criteria for breadth descried in **A**. RMs are grouped by infecting SHIV strain. Significance in panels C-F was determined by Kruskal-Wallis test followed by Dunn's multiple comparisons test. Error bars in C-F indicate one standard deviation from the mean.

A

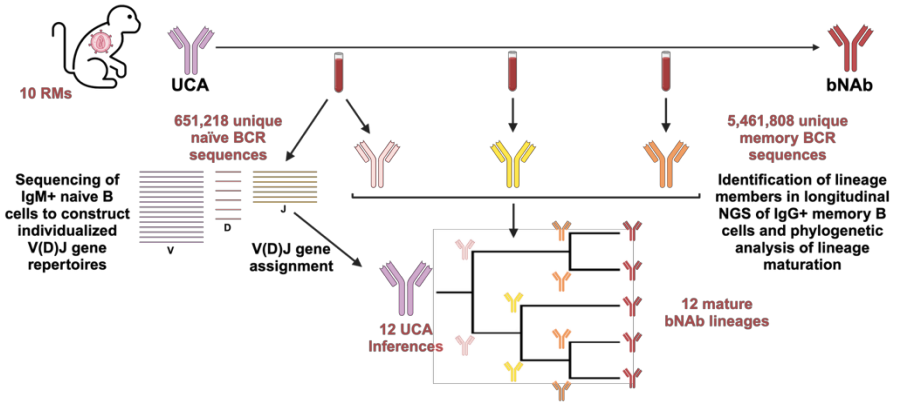

B

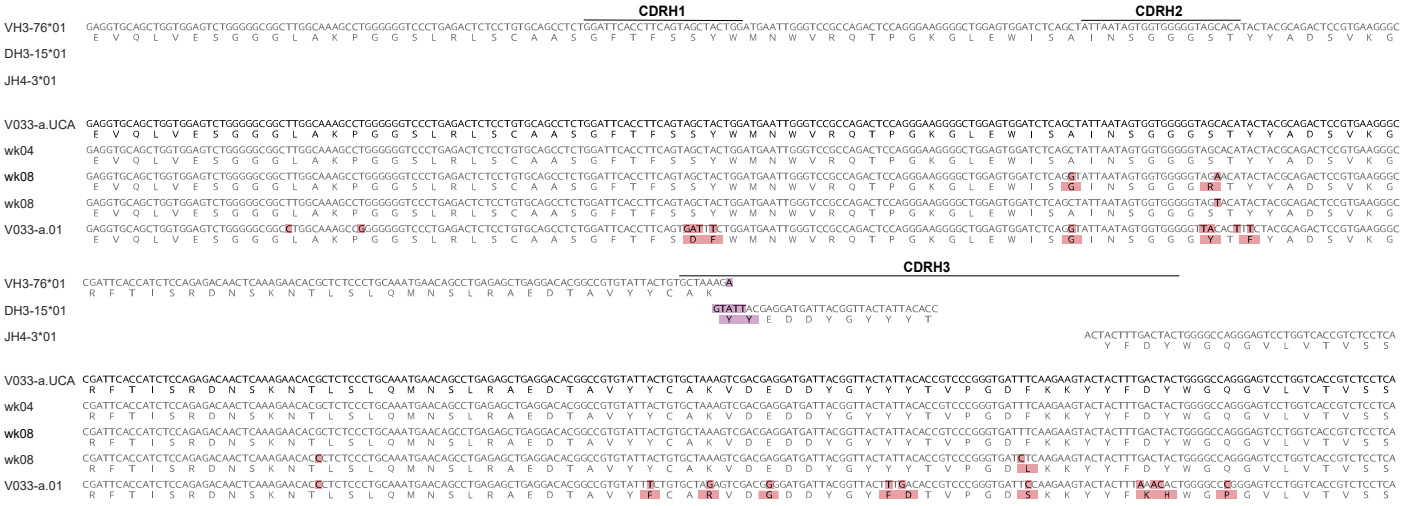

C

Rhesus Lineage	IGVH Gene	Heavy chain affinity maturation (%nt)	IGDH Gene	IGJH Gene	UCA CDRH3 Length	UCA CDRH3 Sequence	IGVL/ IGVK Gene	IGVL/VK affinity maturation (%nt)	IGJL/IGJK Gene	Indels	UCA CDRH3 Charge
RHA1	VH4-NL_36*01_S8200	6.1-10.8%	D3-15*01	JH2*01	24	CARKGEEYYEDDYGYYYTEDWYFDLW	VL1-ACN*02	6%	JL2*01	+2 CDRH1, -4 CDRL3	-6
5695-b	IGHV3-88*01	8.8-10.5%	D3-15*01	JH6-6*01	24	CAREVTWYYEDDYGQIRGRSYGLDSW	VL2-ABU*01_S3471	4%	JL1*01	None	-3
6561-a	VH4-NL_38*01_S9244	9.5-17.9%	D3-15*01	JH5-5*01	25	CARDRLVGEYYEDDYGYYRVFDSLDVW	VL4-ACF*02	7%	JL6*01_S7212	+1 CDRH3	-4
40591-a	VH3-NL_1*01_S9854	10.3-13.5%	D3-15*01	JH5-4*03	26	CTSQGPDPYYEDDYGYYYEVLSNRFDVW	VK1-ACE*01_S9604	10%	JK4*01	None	-5
42056-a	VH4-NL_17*01_S2469	15.0-16.5%	D3-15*01	JH6-6*01	23	CAREREFYYEDDYGLETGRVGLDSW	VK2-AEB*01	9%	JK2*01	None	-4
42056-b	VH4-NL_17*01_S2469	13.0%	D3-15*01	JH5-5*01	27	CARDAPFDLPYYEDDYGYYYTEGGSLDVW	VL1-ADA*01	8%	JL2*01	None	-6
T646-a	VH4-79*01	7.3-9.5%	D3-15*01	JH4-3*01	25	CARAPRSFLYEDDYGYYYTESDYFDYW	VL1-ABN*01	2%	JL6*01_S7212	None	-4
6070-a	VH2-173*01	4.1-5.6%	D3-15*01	JH3-2*01	23	CARGEESYYEDDYGLIEWLHAFDFW	VK1-ABR*01	5%	JK4*01	None	-5
V033-a	VH3-76*01	3.5-7.8%	D3-15*01	JH4-3*01	25	CAKVDEDDYGYYYTVPGDFKKYYFDYW	VK1-ACI-S*01	5%	JK2*01	None	-3
41328-a	VH4-144*01_S8155	3.5-9.0%	D3-15*01	JH6-6*01	25	CARGFTYYEDDYGYYYTEPTYLFLDSW	VL1-ABN*02	5%	JL1*01	None	-4
V031-a	VH2-7*02_S1732	12.3-14.7%	D3-15*01	JH6-6*01	26	CARSQRYYYEDDYGYYYTNSRDYGLDSW	VK2-AAO*01_S5152	7%	JK2*01	+2 CDRH3	-2
44715-a	VH3-NL_17*01_S9589	8.0-12.3%	D3-15*01	JH5-4*03	25	CTTYGSIVEDDYGYYYIERIENRFDVW	VK2-ACL*01_S1827	6%	JK3*01	-1 CDRH2, -1 CDRL3	-4

Human Lineage	IGVH Gene	IGVH affinity maturation (%nt)	IGDH Gene	IGJH Gene	UCA/iGL CDRH3 Length	UCA/iGL CDRH3 Sequence	IGVL/ IGVK Gene	IGVL/VK affinity maturation (%nt)	IGJL/IGJK Gene	Indels	UCA/iGL CDRH3 Charge
PG9	VH3-33*05	14%	DH3-3*01	JH6*03	30	CAREAGGPDYRNGYNYYDFWSGYYYYYYMDVW	VL2-14*01	8%	JL3*02	None	-2
VRC26	VH3-30*18	12%	DH3-3*01	JH3*01	37	CAKDLGESENEEWATDYYDFWSGYPGQDPRGVVGAFDIW	VL1-51*02	10%	JL1*02	+1 CDRH3	-7
PCT64	VH3-15*01	13%	DH3-3*01	JH6*03	25	CTTGVETYDFWSGYYDHYYYYYYMDVW	VK3-20*01	8%	JK3*01	None	-4
PGT145	VH1-8*01	17%	DH4-17*01	JH6*02	33	CARGSKHRLRDYFDYGDYGPNYEEWGDYYYGMDVW	VK2-28*01	17%	JK1*01	None	-2
CH01	VH3-20*01	16%	DH3-10*01	JH2*01	26	CARGTDYTIDDQGIHYYGSGTYWYFDLW	VK3-20*01	11%	JK1*01	None	-2

D

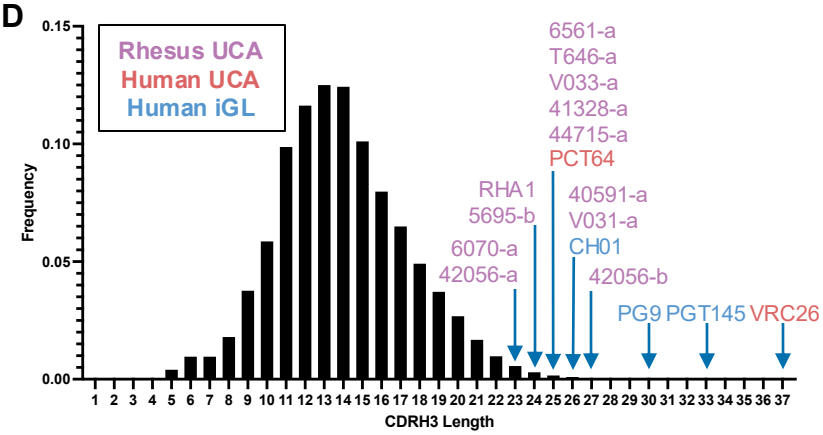

E

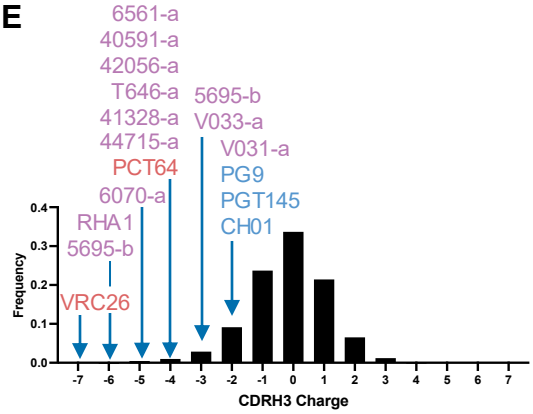

Fig. 2. Features of V2 apex bNAb lineage UCAs. (A) Overview of V2 apex bNAb lineage tracing. (**B**) Nucleotide and translation alignment of the V033-a.UCA with assigned VDJ genes and B cell NGS-derived lineage members from weeks 4 and 8. Mismatches to the UCA are highlighted. (**C**) Table describing immunogenetic features of rhesus and human V2 apex bNAb UCAs and iGLs. Underlined residues in CDRH3 sequences indicate nontemplated residues. Previous estimates of SHM for the rhesus bNAbs reported still lower values based on V_H gene analysis only (*26, 27*); determinations here included mutations across the entire antibody heavy chain, including the CDRH3, which is under strong positive selection in V2 apex bNAbs. (**D**) Frequency histogram of naïve B cell receptor CDRH3 lengths in the rhesus repertoire. CDRH3 lengths of rhesus and human UCAs and iGLs are indicated. (**E**) Frequency histogram of naïve B cell receptor CDRH3 charges in the rhesus repertoire. CDRH3 charges of rhesus and human UCAs and iGLs are indicated.

A

Week	V033 Plasma 0	4	8	12	16	20	24	V033 UCA and Intermediates: V033 UCA	V033 I2	V033 I4	V033 I6	V033-a.01	130	166	167	168	169	170	171	V2	glycans
Q23.17	<20	<20	3376	13380	10718	16297	35026	106	0.38	0.02	0.01	0.002	H	R	D	K	R	Q	K	-	-
BG505	<20	<20	<20	163	205	365	882	>50	12	0.51	0.12	0.02	Q	.	.	.	K	.	.	O	O
BJOX002000	<20	<20	<20	213	267	407	234	>50	37	0.73	0.15	0.04	E	.	.	R	K	.	.	O	-
25710	<20	<20	<20	89	152	426	927	>50	>50	0.75	0.12	0.03	E	.	.	.	K	.	.	O	O
WITO.33	<20	<20	<20	<20	179	1153	2845	>50	>50	2.11	0.03	0.01	H	.	.	.	I	.	.	-	-
246F3	<20	<20	<20	<20	28	101	506	>50	>50	6.31	0.20	0.03	D	.	.	.	.	.	.	O	O
CE0217	<20	<20	<20	<20	30	241	1014	>50	>50	43	0.19	0.01	N	K	.	.	K	K	.	O	O
MT145K	<20	<20	<20	<20	<20	95	567	>50	>50	50	0.24	0.04	T	.	.	.	K	R	.	O	-
T250-4	<20	<20	<20	<20	<20	61	298	>50	>50	>50	3.74	0.23	D	.	.	.	K	K	.	-	-
CH119.10	<20	<20	<20	<20	<20	45	96	>50	>50	>50	3.38	0.11	E	.	.	R	Q	.	.	O	O
X2278	<20	<20	<20	<20	<20	32	23	>50	>50	>50	>50	0.73	D	.	.	.	V	K	.	O	-
ZM233.6	<20	<20	<20	<20	<20	<20	25	>50	>50	>50	>50	>50	D	.	.	.	K	R	.	O	-
TRO.11	<20	<20	<20	<20	<20	<20	<20	>50	>50	>50	>50	>50	O	.	.	.	V	K	.	O	-
X1632	<20	<20	<20	<20	<20	<20	<20	>50	>50	>50	>50	>50	T	.	.	.	K	K	Q	O	-
CE1176.A3	<20	<20	<20	<20	<20	<20	<20	>50	>50	>50	>50	>50	T	K	.	.	K	K	N	O	-
CNE55	<20	<20	<20	<20	<20	<20	<20	>50	>50	>50	>50	>50	O	.	.	.	K	.	R	O	-
CAP256SU	<20	<20	<20	<20	<20	<20	<20	>50	>50	>50	>50	>50	O	.	.	.	K	K	.	O	-
CH848 T/F	<20	<20	<20	<20	<20	<20	<20	>50	>50	>50	>50	>50	O	.	.	.	E	K	.	O	-
CH505 TF	<20	<20	<20	<20	<20	<20	<20	>50	>50	>50	>50	>50	O	.	.	.	.	E	.	O	-

B

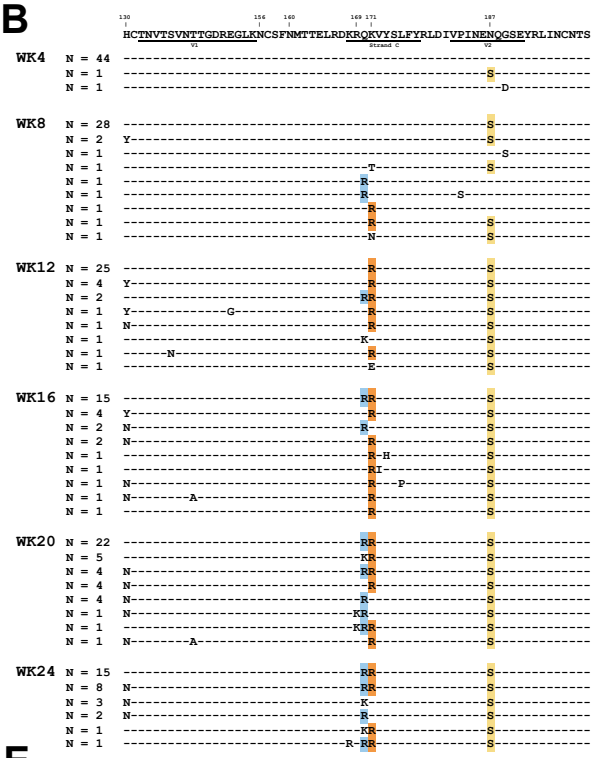

Plasma ID50: 20-100 | 100-1000 | >1000

mAb IC50 (ug/mL): <0.1 | 0.1-1.0 | 1.0-10 | 10-50

C

HIV-Q23 *in vivo* immunotype

	Wild Type	K171R	Q170R/K171R	N187S	170R/171R/187S
V033-a.01	0.002	0.002	1.9	0.018	>25
V033-a.02	0.003	0.003	2.2	0.034	>25
V033-a.03	0.006	0.15	>25	0.093	>25
V033-a.04	0.002	5.5	>25	0.038	>25
V033-a.05	0.002	0.002	3.0	0.018	>25
V033-a.06	0.002	0.004	24	0.047	>25
V033-a.07	0.002	0.008	>25	0.035	>25

D

V033 mAb

	UCA	I1	I2	I3	I4	I5	I6	a.01
MLV	>200	>50	>50	>50	>50	>50	>50	>50
WT	106	5.6	0.21	0.15	0.023	0.023	0.006	0.002
N187S	>200	>50	44	18	0.38	0.28	0.057	0.018
K171R.N187S	>200	>50	>50	>50	>50	>50	0.87	0.40
Q170R.K171R.N187S	>200	>50	>50	>50	>50	>50	>50	>50
N160K	>200	>50	2.6	2.0	0.060	0.005	0.001	0.002

E

Heavy Chain

	UCA	S31D	Y32F	A50G	S57R	S57Y	K98R	E101G	Y107F	Y108D	F114L (I1)	F114S	D120K	Y121H	a.01
MLV	>200	>200	>200	>200	>200	>200	>200	>200	>200	>200	>200	>200	>200	>200	>50
Q23 WT	106	3.3	24	10	16	26	74	25	21	18	5.6	8.8	22	32	0.011
Q23 N187S	>200	>200	>200	>200	>200	>200	>200	>200	>200	>200	>200	>200	>200	>200	0.23
Q23 K171R	>200	>200	>200	>200	>200	>200	>200	>200	>200	>200	>200	>200	>200	>200	0.019

Kappa Chain

	UCA	S30N	P46S	S76N	Y87F	N92Y	V104L	a.01
MLV	>200	>200	>200	>200	>200	>200	>200	>50
Q23 WT	106	42	38	25	22	30	50	0.011
Q23 N187S	>200	>200	>200	>200	>200	>200	>200	0.23
Q23 K171R	>200	>200	>200	>200	>200	>200	>200	0.019

Fig. 3. Env-antibody coevolution in RM V033. (**A**) (Left) Longitudinal autologous and heterologous reciprocal plasma neutralization ID_{50} values in SHIV-Q23.17-infected RM V033. Data are adapted from Roark et al. bioRxiv 2024. (Middle) Neutralization IC50 values of V033-a lineage intermediates and UCA against a panel of heterologous viruses. Increasing intermediate numbers indicate more mature antibodies. (Right) Sequence features of viruses included in the neutralization panel. Residues 130, 166-171, and the number of glycans on the V2 hypervariable loops are shown. Dots indicate sequence identity, and N-linked glycans are denoted by "O". (**B**) Longitudinal Env V1V2 sequences from RM V033. Sequences are grouped by timepoint indicated on the left. Dashes indicate identity, and colored residues indicate escape mutations from the V033-a lineage. (**C**) Neutralization IC50 values of mature V033-a bNAb mAbs against Q23.17 Envs incorporating escape mutations from B. (**D**) Neutralization IC50 values of V033-a lineage intermediates against Q23.17 Envs incorporating escape mutations from (B). (**E**) Neutralization IC50 values of the V033-a.UCA and UCA site-directed mutants singly incorporating mutations from the mature V033-a bNAbs against Q23.17 Env variants.

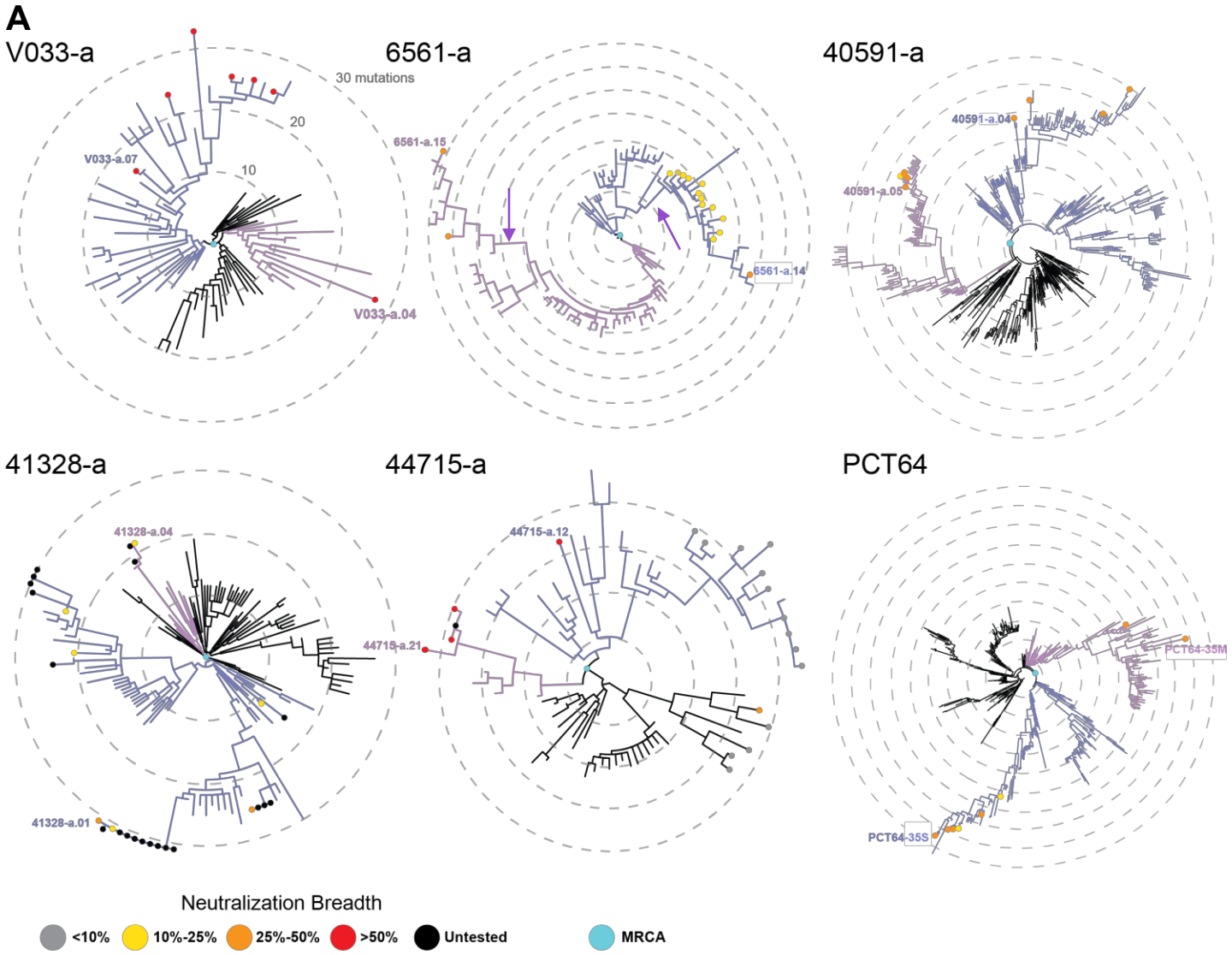

B

```
                                   CDRH1                                   CDRH2                                                                   CDRH3
V033-a.UCA HC EVQLVESGGGLAKPGGSLRLSCAASGFTFSSYWMNWVRQTPGKGLEWISAINSGGGSTYYADSVKGRFTISRDNSKNTLSLQMNSLRAEDTAVYYCAKVDEDDYGYYTVPGDFKKYYFDYWGQGVLVTVSS
V033-a.07  HC EVQLVESGGGLAKPGGSLRLSCAASGFTFSNYWMNWVRQTPGKGLEWISGINSGGGRTYYADSVKGRFTISRDNSKNTLSLQMNSLRAEDTAVYHCARVDADDYGYYTTVPGDLKEYYFKHWGQGVLVEVSS
V033-a.04  HC EVQLVESGGGLAKPGGSLRLSCAVSGFTFHDYWMNWVRQTPGKGLEWISGINSDGGYSFYADSVKGRFTISRDNSKNTVSLQMNVLRQEDTAVYECVRVDGDDYGSYTTVPGDLKKYYFKEWGQGVLVTVSS

                                   CDRH1                                   CDRH2                                                                   CDRH3
6561-a.UCA HC QVQLQESGPGLVKPSETLSLTCAVSGGSISDSYYWNWIRQPPGKGLEWIGNIYGNSASTYYNPSLKSRVTISKDTSKNQFFLKLSSVTAADTAVYYCARDRLVGEYYEDDY-GYYRVFDSLDVWGRGVLVTVSS
6561-a.14  HC QVQLQESGPGLVKPSETLSVTCSVSGGSISDRYYWNWIRQPGKALEWIGNIYGFSDRTYHNPSLKSRVTISKDTSKNQFFLSLESVTAADTAVYYCVRDRLLEEYYEEDYDNWYRALDAMEVWGRGILVTVSS
6561-a.15  HC QVQLQESGPGLVKPSETLSLTCNVSGGSISSGHYWSWIRQSPGKGLEWIGCIYGFSSRSYPNPSLRSRVTISKDTSKNQLLLNLSSVTAADTAIYYCARDLFLGEYKEEDYDSWYRLFDALEVWGRGVMVTVSS

                                   CDRH1                                   CDRH2                                                                   CDRH3
40591-a.UCA HC EVQLVESGGGLVQPGGSLRLSCAASGFTFSSYGMSWVRQAPGKGLEWVSSISSASSYIYYADSVKGRFTISRDNAKNSLSLQMNSLRAEDTAVYYCTSQGPDPYYEDDYGYYYEVLSNRFDVWGPGVLVTVSS
40591-a.04  HC EVQVVESGGGLVQPGGSLRLSCKASGLSFNDYGMGWVRQAPGKGLEWVSSISSCSSYTDYADSVKGRFTISRDNVKNSVFLQMNSLTTEDTAVYECVSQGPDPWYEADEGYIYEILSNRFDVWGPGVLVTVSA
40591-a.05  HC EVQLVESGGGLVQPGGSLRLSCKGSGFTFRNYAMSWVRQAPGKGLEWVSSISSESSDIEYADSVKGRFTISRDNYRTSLSLQMNSLRVEDTAVYYCTTQGPDPWSDNDYGYEYEALSNRFHDWGPGVLVTVSS

                                   CDRH1                                   CDRH2                                                                   CDRH3
41328-a.UCA HC QVKLQQWGEGLVKPSETLSLTCAVYGGSISGYYYWSWIRQAPGKGLEWIGNIDGNSASTNYNPSLKNRVTISKDTSKNQFSLKLSSVTAADTAVYYCARGFTYYEDDYGYYYTEPTYLFLDSWGQGVVVTVSS
41328-a.01  HC QVQLQQWGEGLVKPSETLSLSCAVYGGSISGHYYWSWIRQAPGKGLEWIGKIDANSASTNYNPSFKNRVSISKDTSKKQFYLNLESVTAADTAVYYCARGSIYYEDDEGYYYSPATYLHLILWGQGVVVTVSS
41328-a.04  HC QVQLQQWGEGLVKPSETLSLTCAVYGGSISGYYFLTWIRQAPGKGLEWIGNIAGNIASTNYSPSLKNRVTISKDTSKNQFSLRLESVTAADTAVYYCARGSTYYEDDEGYYYTEPTYLFLCEWGQGVVVTVSS

                                   CDRH1                                   CDRH2                                                                   CDRH3
44715-a.UCA HC EVQLVESGGGLVQPGGSLRLSCAASGFTFSNVWMNWVRQAPGKGLEWVARIKSKADG-GTADYAASVKGRFTISRDDSKNTLYLQMNSLKTEDTAVYYCTTDGSIVEDDYGYYYTERIENRFDVWGPGVLVTVS
44715-a.12  HC EVQLVESGGGLVQPGGSLRLSCTVSGFTFSTYVWMNWVRQAPGKGLEWIARVKTKCDG-GTFDYAASVKGRFSISRDDSKNVASLQMNSLKIEDTAVYYCTADGSIVEDEGFYYYIDFIESRFDVWGPGVLVTVSS
44715-a.21  HC EVQVVESGGGLVQPGGSLRLSCAASGFTFSHYWMNWVRQAPGKGLEWVARIKTKGEGGGGTAHYAASVKDRFSVSRDEGTNTAHLQMNSLKTEDTAVYHCKTDGSIVVDEGFDFYIDAIEKGFVWGPGVLVTVSS

                                   CDRH1                                   CDRH2                                                                   CDRH3
PCT64-UCA HC EVQLVESGGGLVKPGGSLRLSCAASGFTFSNAWMSWVRQAPGKGLEWVGRIKSKTDGGTTDYAAPVKGRFTISRDDSKNTLYLQMNSLKTEDTAVYYCTTGVETYDFWSGYYDHYYYYYYMDVWGKGTTVTVSS
PCT64-35S  HC EVQLVESGGGLVKPGGSLRLACVGSGFTFSDAWMTWVRQAPGKGLEWVGHMRPTTEGGAKDYAAAVEGRFTIERDDSKSTLYLQMNSLKIEDTGVYYCYTGVERGDFWSDDYSQHYNTYLIDVWGKGTTVTVSS
PCT64-35M  HC EVQLVESGGGLVKPGGSVRLSCSASGFKFSDAWMTWVRQAPGKGLEWVGHVRTQADGGTTEYAAPVKGRFTISRDDSKNILYLQMNGLKTEDTAKYYCYTGVEWYDFWSDDYSQEETKYFKDVWGKGTTVTVSS
```

Fig. 4. Independent mutational trajectories leading to V2 apex bNAb maturation. (**A**) Radial IgPhyML trees of V2 apex bNAb lineage heavy chains. All trees are rooted on the lineage's inferred UCA. Grey, yellow, orange, red, and black dots indicate mature bNAb lineage members, colored by their neutralization breadth on our 18-virus panel as previously reported (*27*). Neutralization breadth values for PCT64 lineage are represented as reported in Landais et al. Immunity 2017 (*45*). Cyan dots indicate the most recent common ancestor (MRCA) of all broadly neutralizing members of the lineage. Different clades branching off from the MRCA and independently acquiring breadth are colored indigo and lilac. CDRH3 insertions in the 6561-a lineage are indicated by arrows. Scale bars are represented internally, with each concentric circle indicating 10 nucleotide mutations from the UCA. (**B**) Protein alignments of the lineages shown in A. UCA heavy chains are aligned with representative mature bNAb lineage members from each independent clade. Mismatches to the UCA are highlighted. Red highlights indicate mutations in common between the two clades.

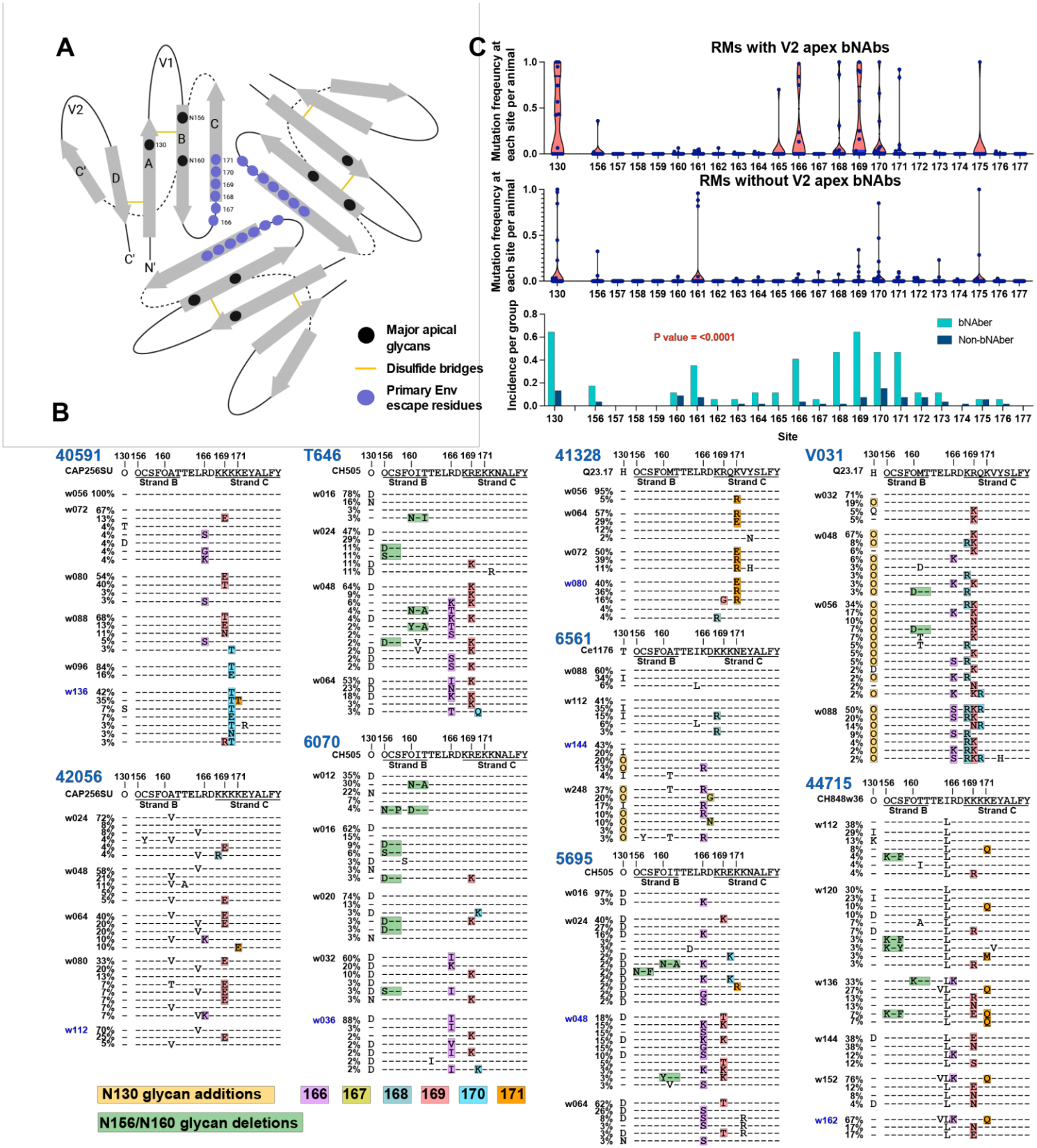

D

CAP256SU in vivo immunotype

	WT	R169E	R166K	R166S	K169T	K169N
40591-a.02	0.006	>50	0.016	3.9	5.3	36
40591-a.03	0.078	>50	1.1	>50	1.9	7.5
40591-a.08	0.008	>50	0.12	>50	>50	>50

Q23.17 in vivo immunotype

	WT	K171R	K171E	R169G	N187S
41328-a.01	0.002	0.012	>50	0.88	0.054
41328-a.02	0.004	0.018	>50	4.2	7.6
41328-a.03	0.004	0.068	>50	>50	1.00

CAP256SU in vivo immunotype

	WT	K169E	R166K
42056-a.01	0.007	>50	9.136
42056-a.02	0.162	>50	>50
42056-a.03	0.197	>50	>50

CH505 in vivo immunotype

	WT	N130D R166S	N130D R166G	N130D R166K/R169K	N130D R169K	N130D R169T
RHA1.V2.01	0.29	>50	>50	5.8	0.21	>50
5695-b.05	>50	>50	>50	>50	1.2	>50

CH505 in vivo immunotype

	WT	R166K	R169K	R166I
6070-a.01	8.6	>50	>50	>50
6070-a.02	33	>50	>50	>50
6070-a.05	34	>50	>50	>50

CH505 in vivo immunotype

	WT	R166K	R169K	R166I
T646-a.01	0.66	>50	>50	>50
T646-a.03	0.40	>50	>50	>50

Fig. 5. Limited and convergent Env mutations guide V2 apex bNAb maturation. (A) Protein topology diagram of the Env V2 apex, highlighting positions of key escape residues and glycans. **(B)** Amino acid alignments of longitudinal Env sequences obtained by SGS of circulating plasma virion RNA in RMs with V2 apex bNAbs. Sequences show residues 130 and 156-177 (HXB2 numbering). Sequences are grouped by timepoint indicated on the left in weeks. Dashes indicate identity to the T/F sequence. Mutations at residues 166-171, mutations that delete glycans at N156 or N160, or mutations that introduce a glycan to residue 130 are highlighted. Glycan sequons are denoted by "O". Highlighter plots for RMs 5695, 6070, 40591, and 42056 are adapted with permission from Roark et al. Science 2021 (*26*). **(C)** Mutation frequencies of RMs with (top) versus without (middle) V2 apex bNAbs at residues 130 and comparison of mutation incidence of these sites between the two groups (bottom, Wilcoxon matched-paired signed rank test, $p < 0.0001$) **(D)** Neutralization IC50 values of V2 apex bNAb lineage members against autologous Env mutants incorporating mutations identified in **B**.

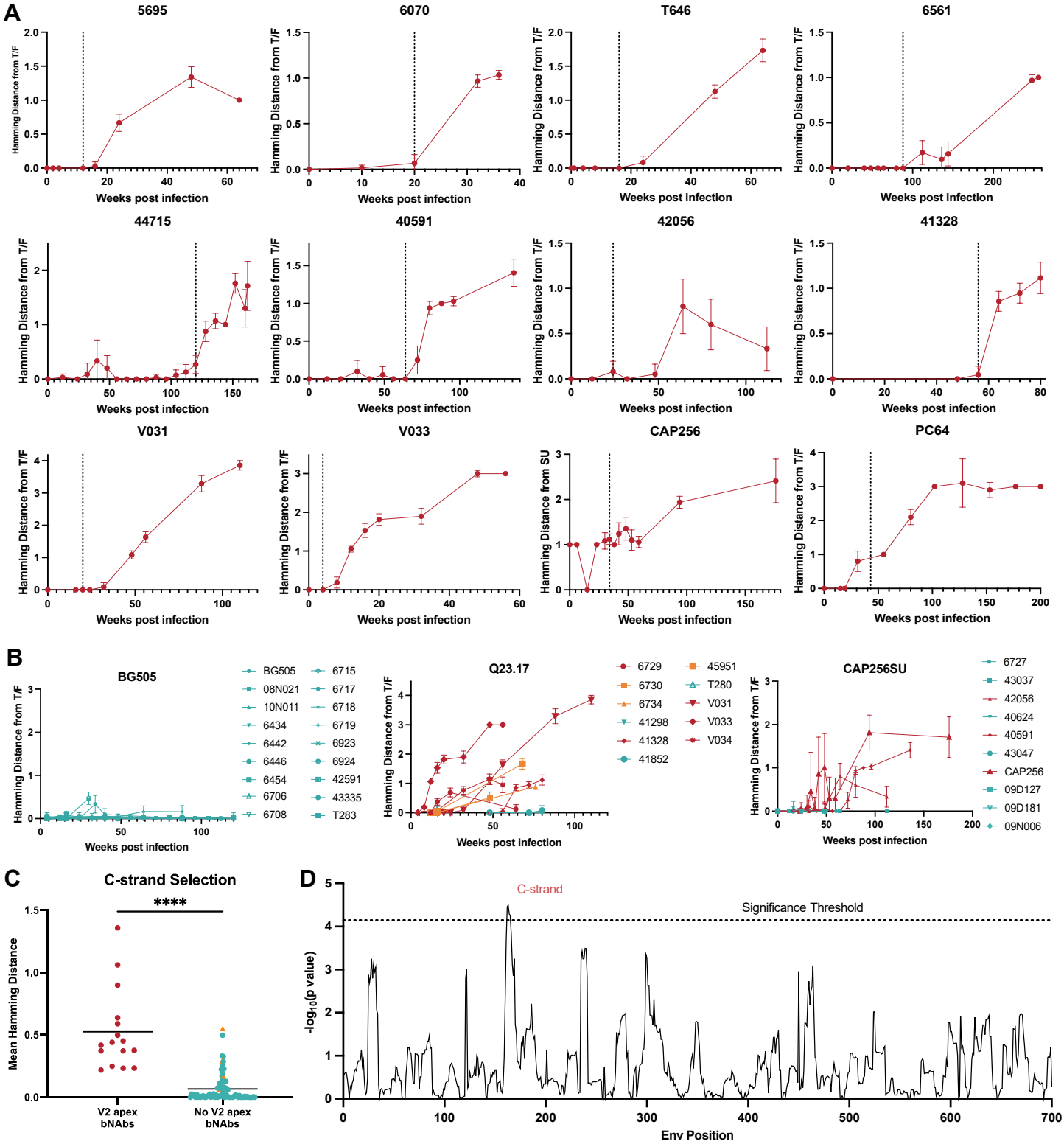
A
5695
6070
T646
6561
44715
40591
42056
41328
V031
V033
CAP256
PC64
Hamming Distance from T/F
Hamming Distance from SU
Weeks post infection
B
BG505
Q23.17
CAP256SU
BG505
08N021
10N011
6434
6442
6446
6454
6706
6708
6715
6717
6718
6719
6923
6924
42591
43335
T283
6729
6730
6734
41298
41328
41852
45951
T280
V031
V033
V034
6727
43037
42056
40624
40591
43047
CAP256
09D127
09D181
09N006
C
C-strand Selection
****
Mean Hamming Distance
V2 apex bNAbs
No V2 apex bNAbs
D
C-strand
Significance Threshold
-log10(p value)
Env Position

Fig. 6. C-strand selection is detectable soon after a V2 apex lineage is triggered but rarely occurs in RMs without V2 apex bNAbs. (**A**) Mean longitudinal Hamming distances of Env residues 166-171 from the T/F sequence in RMs with V2 apex bNAbs. Values for participant CAP256 indicate the distance from the superinfecting strain CAP256SU. Dotted lines indicate the timepoint where the V2 apex bNAb lineage was first detected by B cell NGS. Shaded regions indicate timepoints where heterologous tier-2 plasma neutralization are observed. (**B**) Mean longitudinal Hamming distances of Env residues 166-171 from the T/F sequence in 101 SHIV-infected rhesus macaques. Data from human trial participants from which the SHIV Envs were isolated are included where available. Data for the remaining SHIVs are shown in fig. S18. (**C**) Comparison of the mean C-strand Hamming distances between RMs with and without V2 apex bNAbs at the bNAb epitopes indicated. Significance was determined by Welch's t-test. (**D**) Test for significantly different mean longitudinal hamming distances for moving regions of 10 amino acids across the envelope gene. P values shown are from two-tailed Welch's t-tests. The significance threshold was adjusted using a Bonferroni correction for multiple comparisons. For all panels, RMs with V2 apex bNAbs are colored red while those without are colored teal. RMs with C-strand targeted antibody responses that did not meet our criteria for breadth are colored orange. All error bars indicate 95% confidence intervals.